Department of Precision and Microsystems Engineering

Ferrofluid Rotary Seal with Replenishment System for Sealing Liquids

K. van der Wal

Report no	: 2019.041
Coach	: ir. S. G. E. Lampaert
Professor	: dr. ir. R. A. J. van Ostayen
Specialisation	: Mechatronic System Design
Type of report	: Master of Science Thesis
Date	: 12 December 2019

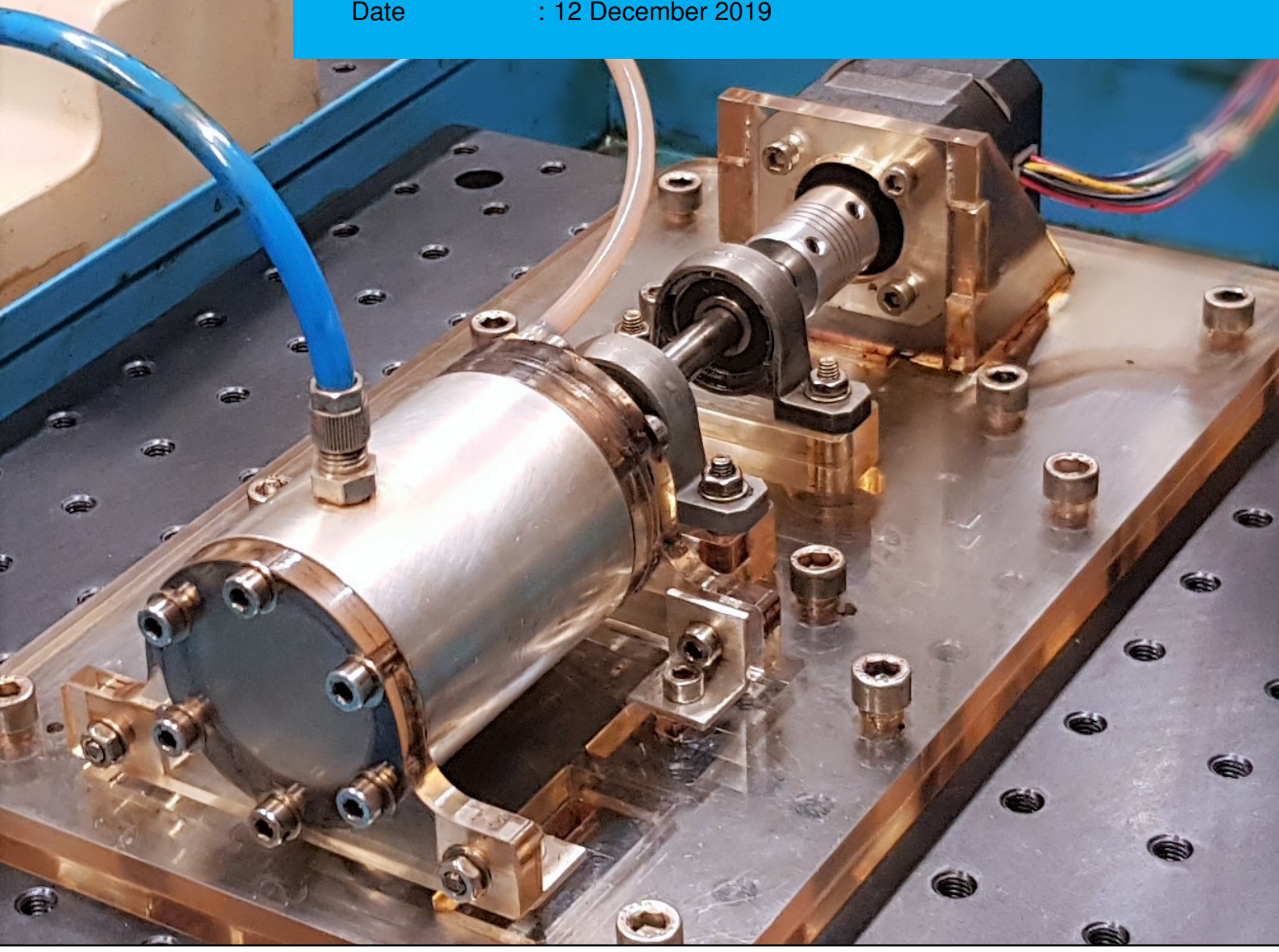

TU Delft Delft University of Technology

Challenge the future

Ferrofluid Rotary Seal with Replenishment System for Sealing Liquids

by

K. van der Wal

to obtain the degree of Master of Science in Mechanical Engineering
at Delft University of Technology,
to be defended publicly on Thursday December 12, 2019 at 13:30.

Student number:	4286774	
Thesis committee:	dr. ir. R.A.J. van Ostayen,	TU Delft
	ir. S.G.E. Lampaert,	TU Delft, supervisor
	dr. ir. W. P. Breugem,	TU Delft

An electronic version of this thesis is available at https://repository.tudelft.nl.

Faculty of Mechanical, Maritime and Materials Engineering (3mE) · Delft University of Technology

The work in this thesis was supported by AEGIR Marine.

Department of Precision and Microsystems Engineering (PME)

Acknowledgements

This document presents the research that I have done to ferrofluid rotary sealing technology for liquids. During this research I have received a lot of help from many people, to whom I would like to express my gratitude.

First and foremost, I want to thank Stefan Lampaert for coaching me during this project. Our several meetings and interesting discussions proved to be crucial for the results of this research. I really appreciate the time and effort you have put in this project and coaching me.

I want to thank Ron van Ostayen for his useful insights, supervision and weekly student meetings. The meetings were always very interesting and I have learned a lot of them. Also I want to thank my fellow PME students for their input and insights during and outside of these meetings.

The company AEGIR Marine has supported this research as an industrial partner. I want to thank them for their interest, insights from an industrial point of view and effort for making this project a success.

I want to thank the entire technical support staff of PME, especially Patrick van Holst, Harry Jansen and Rob Lutjeboer, for their help with my experiments and experimental setup. Jos van Driel for his help on the sensors and programming and the staff of the student workshop, Gerard van Vliet and René van Ommen, for their help and instructions during the manufacturing of the experimental setup.

Finally, I would like to thank my parents, brother and friends for their support not only during this project, but also my entire study.

Karoen van der Wal
Delft, 12 December 2019

Abstract

Seals are an important class of structural components used in machines to prevent leakage, contain pressure or exclude contamination. The relative motion between the surfaces of a rotating shaft and machine housing makes the design of durable rotary seals complex. Since the 1930's radial lip seals are industry standard, consisting of an elastomer ring compressed around the rotating shaft. This contact-based rotary seal is inherently subjected to wear, which limits its service life and causes leaks. Ferrofluid rotary seals are contact-free magnetic liquid seals and are characterised by their simple structure, low friction and ability to hermetically seal. Usually ferrofluids consist of an oil carrier liquid that has suspended iron oxide mineral nanoparticles, giving the oil magnetic properties. A basic ferrofluid rotary seal is created by locating ferrofluid in the seal gap between the shaft and machine housing using a magnet. Ferrofluid rotary seals that perform in vacuum and gas environments already have proven themselves in industry. However, literature learns that ferrofluid rotary seals fail prematurely when they are used for sealing liquids. Because the limited service life of the seal is preventing current implementation of the sealing technology in for example the marine industry, the main objective of this thesis project is to the improve the service life of a ferrofluid rotary seal that seals liquids.

Analysis of the literature showed that premature failure of the ferrofluid rotary seal that seals a liquid is mainly caused by two important phenomena. Firstly, interfacial instability between the ferrofluid seal and the liquid that is sealed can cause instant seal failure. By adding a shielding structure in front of the seal which minimises the relative velocity between the two fluids this problem can be solved. Secondly, the degradation of a ferrofluid seal that is in contact with a liquid which decreases its sealing capacity over time and therefore limits its service life. In order to solve this problem, this thesis presents a new type of ferrofluid rotary seal for sealing liquids that implements a ferrofluid replenishment system. A mathematical model and FEM analysis are used to design the seal and predict its sealing capacity. Within the ferrofluid sealing device that has been designed two ferrofluid seals are formed by the magnetic field distribution. The replenishment system generates an axial flow of ferrofluid through these seals during operation. By doing so, the ferrofluid seals are constantly being renewed. Theoretically, this means service life of this new ferrofluid rotary seal could be extended towards infinity if the seals are replaced at sufficient rate.

An experimental test setup has been built in order to measure the performance of the ferrofluid sealing device and to validate that its service life is improved by the ferrofluid replenishment system. Results of the experiments have shown that the service life of the ferrofluid rotary

sealing device while dynamically sealing pressurised water is successfully improved and controlled by the ferrofluid replenishment system. The seal has not been observed to fail while the ferrofluid replenishment system was active. When the ferrofluid replenishment system is deactivated, the seal will fail shortly after. Both ferrofluid seals in the sealing device continued to function while ferrofluid was transported from one seal to another. The static sealing capacity of the ferrofluid sealing device when it sealed water was 75.9 kPa. The analytical model and FEM analysis overestimated the static sealing capacity by approximately 20 %. During the experiments it was observed that the static sealing capacity of the device increased over time at zero shaft speeds. This could partially be attributed to the migration of the magnetic particles in the carrier liquid of the ferrofluid to higher magnetic field intensities. The sealing capacity of the device decreased when the shaft speed increased, which has also has been found in other studies. At higher shaft speeds the sealing capacity stabilises.

Overall, the main objective of this thesis project has successfully been achieved by introducing a ferrofluid replenishment system in the design of a ferrofluid rotary seal that seals a liquid. It has been demonstrated that the ferrofluid seals of the rotary sealing device are renewed by the replenishment system without losing their sealing capacity and while they are dynamically sealing pressurised water. Additional research and experiments can validate if this new method can be used to prolong service life of a ferrofluid rotary seal that seals liquids towards infinity.

Table of Contents

Chapter 1

Introduction

1-1 Background

Designs of machines can be dated back to various ancient and medieval societies, allowing humans to exceed the limitations of their bodies. An important class of structural components of these machines are seals. Seals prevent leakage, contain pressure or exclude contamination in a machine. Sealing between two stationary mating surfaces is done by using static sealing devices. An example is the gasket that can be found between the engine block and cylinder heads of an internal combustion engine. Challenge is increased when it is necessary to seal against a dynamic surface. The need for innovative dynamic sealing solutions has increased since the Industrial Revolution spawned the development of engines, transmissions and gearboxes.

Rotary shaft seals are dynamic sealing devices which are used for sealing the gap between the surfaces of a rotary shaft and housing of a machine. Since the 1930's radial lip seals are widely used to retain lubricant and exclude contamination in rotating shaft and bearing applications [1]. Important applications of these seals are in rotary pumps and propeller shafts of ships. Currently used seal structures mostly consists of a main elastomer sealing lip having mechanical contact with the rotating shaft. Often a garter spring is added to help compensate for lip wear and elastomer material changes. At first glance this rotary shaft seal appears to be a device with only relatively simple functions. However, in reality requirements like demands for increased service life and reliability are not easy to fulfil. Due to its mechanical contact with the rotating shaft it inherently is subjected to wear, which limits its service life and causes leaks. The elastomer rotary shaft seals used in for example ships are reported to leak lots of oil into the marine environment [2]. A promising new rotary sealing technology that operates without mechanical contact is a rotary seal that is based on magnetic liquid instead of elastomer material [3, 4, 5].

In the 1960's space agency NASA tasked Steven Papell with the controlling and directing of liquid rocket fuel in outer space. Papell converted non-magnetic rocket fuel into fuel having magnetic properties, enabling control of the fluid under zero gravity using magnets. In 1965

a US patent was obtained by Papell for the first magnetic fluid based on kerosene [6]. Funded by NASA Ronald E. Rosensweig led the development of a wide variety of magnetic fluids for commercial use and conducted research to the fluid mechanics of magnetic liquids [7, 8]. The branch of physics that is concerned with the fluid mechanics of magnetic fluids is called Ferrohydrodynamics. Ferrofluid is a magnetic liquid that consists of a carrier liquid with suspended ferromagnetic particles that are usually smaller than 10 nm [9]. The three main application areas of ferrofluids are sealing, damping and heat transfer [10]. In most of these applications ferrofluid is positioned magnetically and secondary properties of the fluid are then exploited. An example of application is a planar ferrofluid bearing, where absence of both stick slip and mechanical contact result in respectively a potential high precision and high lifetime [11, 12]. Dynamic manipulation of ferrofluids shows a lot of future potential for new technologies, however sophistication is preventing current application. Ferrofluid rotary seals are a promising class of contact-free rotary shaft seals and are characterised by their simple structure, low friction and ability to hermetically seal. The most commonly known ferrofluid seals are ferrofluid rotary vacuum seals in machinery operating in a vacuum chamber. Ferrofluid rotary seals performing in vacuum and gas environments already have proven themselves in industry [13, 14, 15]. Ferrofluid sealing is also considered to be very important in preserving the environment, since ferrofluid is able to create hermetic sealing for hazardous gases [16].

However, while ferrofluid rotary seals are successfully operating in vacuum and gas environments, literature learns that a ferrofluid rotary seal fails prematurely when it is used to seal liquids [17, 18, 19, 20, 21]. The driving mechanisms that cause premature failure of the seal when liquids instead of vacuum or gasses are sealed are still not fully understood. Kurfess and Muller have investigated the stability of the interface between the liquid that is contained and ferrofluid of the seal [3]. It is suggested that at this interface the ferrofluid may start to dissolve or emulsify when this interface becomes unstable. Also magnetic properties of ferrofluid in contact with water are reported to decrease [22]. Degradation of the ferrofluid decreases the sealing capacity of the seal and therefore shortens its service life. Jarno et al. considered gradual removal of ferrofluid due to shear forces also as possible cause of performance drop of the seal [23]. Wang et al. state the existence of shearing forces at the interface causes poor performance of the seal when sealing liquids [24]. Research to the application of ferrofluid rotary seals for sealing water in marine industry has been done by Matuszewski and concludes that ferrofluid sealing in ships is very promising [25, 26]. Experimental investigations showed that a ferrofluid seal effectively could seal water pressurised at 0.1 MPa at a shaft speed of 3000 rpm ($\varnothing$ 50 mm). This diameter corresponds with the propeller shaft diameter of a small boat or fish cutter. Mitamura et al. have investigated the application of ferrofluid seals in rotary blood pumps [5] and stated that its low friction and no wear makes it an interesting sealing technology. However, at the moment ferrofluid rotary seals for sealing liquids are not implemented in industry due to its unpredictable and limited service life.

1-2 Project Objective

Literature learns that ferrofluid rotary seals have a very limited and unpredictable service life when they are used to to seal liquids. It is not fully understood which phenomena cause premature failure of the seal when it is used to seal liquids. Also no clear methods for the

design of a ferrofluid rotary seal can be found in literature which impedes the development of the sealing technology.

The performance of a ferrofluid rotary seal can be indicated in terms of its sealing capacity and service life for a certain sealing condition. The sealing capacity of a ferrofluid rotary seal is the maximum pressure difference it is able to maintain between the medium that is sealed and the atmosphere (gauge pressure) before it fails. This is also been called the critical pressure. When the seal is subjected to a pressure difference that is higher than its sealing capacity, the ferrofluid seals will burst and leakage occurs. Service life of a ferrofluid rotary seal is the amount of time the seal is successfully able to seal the medium until sudden seal failure occurs. Since the limited service life of the ferrofluid rotary seal is preventing current implementation of the sealing technology for the sealing of liquids, the main objective of this thesis project is set as follows:
Improve the service life of a ferrofluid rotary seal that seals liquids.

In order to improve the service life of a ferrofluid rotary seal that seals liquids first knowledge on its fundamental working principles has to be obtained. Next, the failure mechanisms mentioned in literature have to be analysed and understood. Finally, a solution for these failure mechanisms has to be introduced into the design of a ferrofluid rotary seal in order to improve its service life. An experimental setup has to be built and experiments have to be conducted in order to validate if premature failure of the new designed ferrofluid rotary seal indeed is prevented and therefore its service life is improved.

1-3 Thesis Outline

This thesis starts by describing the fundamental theory behind the working principles of a ferrofluid rotary seal in chapter 2. Chapter 3 elaborates the dynamic operation of ferrofluid rotary sealing devices in aqueous environments. Chapter 4 discusses designs and patents of ferrofluid seals found in literature in order to provide inspiration and insight in the state-of-the-art.

The main part of this thesis is the paper "*Ferrofluid Rotary Seal with Replenishment System for Sealing Liquids*" that is presented in chapter 5 and can be read independently from the rest of this thesis. The paper presents the design of a new type of ferrofluid rotary seal which implements a ferrofluid replenishment system in order to prevent premature failure of the seal. Additional information that supports the paper can be found in the appendices. Appendix A elaborates the experimental test setup, appendix B the measurements of the experiments, appendix C some calculations that are made for the test setup and appendix D provides some useful data-sheets.

Chapter 6 contains a discussion on the results of the literature study, results of the research presented in the paper and some additional results provided by the appendices. Finally, the main conclusions drawn from the results of this thesis project and some recommendations for further research are presented in chapter 7.

Chapter 2

Fundamentals of a Ferrofluid Rotary Seal

A ferrofluid seal for rotating shaft configurations consists of a few standard elements. The cross section of the most basic version of the sealing device can be seen in figure 2-1. Ferrofluid is a magnetic fluid which seals the gap between the annular magnet and the rotating shaft. Ferrofluid is kept in place by the magnetic field generated by the annular magnet and is able to maintain a pressure difference $\Delta p = p_{high} - p_{low}$. This chapter will discuss the fundamental theory behind the working principles of such a ferrofluid seal.

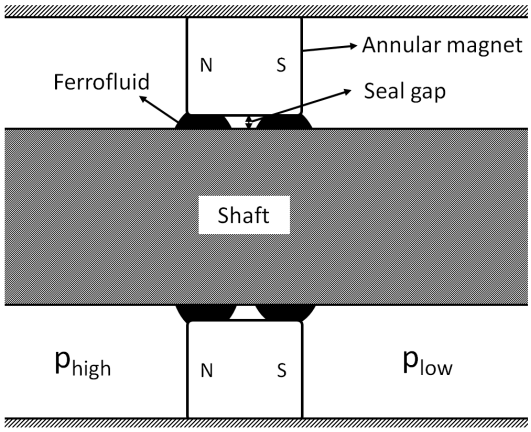

Figure 2-1: This figure presents the cross section of a basic ferrofluid seal for a rotating ferromagnetic shaft. The device consists of an annular magnet which is placed around the shaft. Ferrofluid is kept in place by this magnet and seals the gap between the magnet and shaft.

2-1 Magnetic Fluid and Circuit

This section will discuss fundamental theory of the magnetic circuit and fluid of a ferrofluid rotary seal. The magnetic field is generated by a permanent ring magnet which can be seen in figure 2-1. Permanent magnets are preferred over electromagnets due to their constant magnetic field generation and lack of power input. This makes the device relatively easy to implement in current sealing configurations. Also for remote locations such passive system can be preferred over an active system.

The magnetic fluid (ferrofluid) inside of the ferrofluid rotary seal consists of a carrier liquid with suspended magnetic particles. The behaviour of magnetic fluids depends on the size of these particles and based on this behaviour two main groups magnetic liquids can be distinguished. The first group are the so-called ferrofluids, having a particle size up to 10 nm. Second group are the magnetorheological fluids containing particle size larger than 10 nm. In this section it will become clear why ferrofluids are preferred in a rotary seal based on magnetic fluid.

2-1-1 Modelling the Magnetic Circuit

The permanent ring magnet presented in figure 2-1 contains magnetic dipoles creating a force field which can be represented by a vector field. Inside the ring magnet a remanent magnetic field $\mathbf{B_r}$ is present. The poles of the ring magnet are oriented in axial direction instead of radial orientation, making sure the magnetic fluid will be contained in the annular gap between the shaft and magnet. The magnetic field lines will travel from the ring magnet through the surrounding material back to the ring magnet. It can be concluded that the magnetic properties of the material surrounding the ring magnet are important for the magnetic field distribution inside the system. The magnetic field distribution can be defined by magnetic flux density $\mathbf{B}$, which can be calculated using equation 2-1.

$$\mathbf{B} = \mu_0(\mathbf{H} + \mathbf{M}) \tag{2-1}$$

where $\mathbf{B}$ is the magnetic field [T], $\mathbf{H}$ magnetic field strength [A/m], μ_0 the permeability of vacuum [H/m] and $\mathbf{M}$ the magnetisation of the material [A/m]. The magnetisation $\mathbf{M}$ can be interpreted as the local value of the magnetic moment per unit volume of a certain material. The magnetic field strength $\mathbf{H}$ can be understood as the driving magnetic influence independent of the material's magnetic response ($\mathbf{M}$).

Electromagnetic fields such as magnetic and electric fields can be described using the four Maxwell equations. The fourth Maxwell equation, also known as Ampere's law with Maxwell's correction, written using the $\mathbf{H}$-field definition in differential form can be seen in equation 2-2. $\mathbf{J_f}$ [Am^{-2}] is defined as the free current density, $\mathbf{D}$ [Cm^{-2}] as the electric displacement field. This equation relates magnetic field generation and electric current. No electromagnets are considered for magnetic field generation in the ferrofluid seal, therefore no currents are present in the system. Free current density $\mathbf{J_f}$ and time varying electric field $\frac{\partial \mathbf{D}}{\partial t}$ are thus equal to zero. Equation 2-2 can be simplified to equation 2-3, stating that the curl of the $\mathbf{H}$-field is equal to zero. Using this result it is possible to define a scalar magnetic potential V_m, which is presented in equation 2-4.

$$\nabla \times \mathbf{H} = \mathbf{J_f} + \frac{\partial \mathbf{D}}{\partial t} \tag{2-2}$$

$$\nabla \times \mathbf{H} = \mathbf{0} \tag{2-3}$$

$$\mathbf{H} \equiv -\nabla V_m \tag{2-4}$$

The second law of Maxwell, also known as Gauss law, states the magnetic field $\mathbf{B}$ has divergence equal to zero. Equation 2-5 shows this statement. The net magnetic flux through a closed surface must be equal to zero, meaning the number of field lines that enter and exit this surface are equal. The only way this is possible is using the concept of a North and South pole inside a magnet. The ring magnet inside the magnetic seal system contains a north and south pole oriented in radial direction. Field lines will travel from the north to the south pole of the ring magnet through the system.

$$\nabla \cdot \mathbf{B} = \mathbf{0} \tag{2-5}$$

Combining previous equations 2-1 till 2-5 a model of the magnetic field inside the ferrofluid seal can be generated. Equation 2-6 shows this model, which subsequently can be used in a Finite Element Model (FEM). Figure 2-2 presents the magnetic field lines of a permanent ring magnet surrounding a non magnetic shaft calculated using a FEM model based on equation 2-6.

$$-\nabla \cdot (\mu_0 \nabla V_m - \mu_0 \mathbf{M}_0) = 0 \tag{2-6}$$

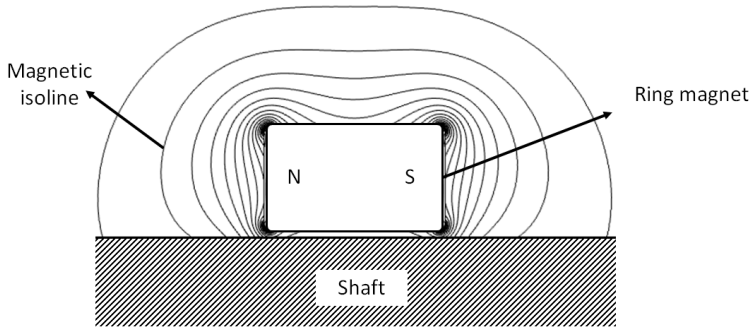

Figure 2-2: This figure presents the magnetic field lines generated by a permanent ring magnet surrounding a non magnetic shaft. The non magnetic shaft does not influence the magnetic field distribution of the ring magnet.

2-1-2 Magnetic Fluid Composition

As mentioned previously a magnetic fluid consists of a carrier liquid and suspended particles. The carrier of a magnetic fluid is usually an oil and the material used for the particles often is Magnetite (Fe_3O_4), Hematite (Fe_2O_3) or another compound containing iron. The reason a magnetic fluid is created by a colloid of magnetic particles and not by simply melting a magnetic material is because there is no known material that has a melting point lower

than it's Curie temperature [27]. As stated before there are two groups of magnetic fluids, ferrofluids and magnetorheological fluids, defined based on their behaviour and thus mainly its particle size. Equations 2-7 till 2-10 give an overview of the different energies present inside a magnetic fluid. These energies are useful in predicting stability of the magnetic fluid.

$$E_{thermal} = k_B T \tag{2-7}$$

$$E_{magnetic} = \mu_0 M_p H V_p \tag{2-8}$$

$$E_{gravitational} = \Delta\rho V_p g L \tag{2-9}$$

$$E_{dipole-dipole} = (1/12)\mu_0 M_p^2 V_p \tag{2-10}$$

where k_B is the Boltzmann constant [J/K], T temperature [K], μ_0 permeability of vacuum [H/m], M_p magnetisation of particles [A/m], H applied magnetic field [A/m], ρ_p density of the particle material [kg/m^3], V_p volume of the particle [m^3] ($V_p = \pi/6 \cdot d_p^3$), g gravitational constant [m/s^2] and L elevation in gravitational field [m]. Comparing these energies with each other stability of the magnetic fluid can be checked, which is presented in equations 2-11 till 2-13.

$$\frac{E_{thermal}}{E_{magnetic}} = \frac{k_B T}{\mu_0 M H V} \geq 1 \quad \rightarrow \quad d \leq \left(\frac{6}{\pi}\frac{k_B T}{\mu_0 M H}\right)^{1/3} \tag{2-11}$$

$$\frac{E_{thermal}}{E_{dipole-dipole}} = \frac{12 k_B T}{\mu_0 M^2 V} \quad \rightarrow \quad d \leq \left(\frac{72}{\pi}\frac{k_B T}{\mu_0 M^2}\right)^{1/3} \tag{2-12}$$

$$\frac{E_{gravitational}}{E_{magnetic}} = \frac{\Delta\rho V g L}{\mu_0 M H V} \tag{2-13}$$

Equation 2-11 gives the stability of magnetic fluid in a magnetic field gradient. Particles of the magnetic fluid are attracted to higher-intensity regions of the magnetic field of the seal system. When $E_{thermal}$ is larger than $E_{magnetic}$, agglomeration due to these differences in magnetic field intensity in the magnetic fluid seal can be prevented. The stability condition shown in equation 2-12 gives particle diameter d_p in order to prevent magnetic agglomeration inside the seal. When the particles of the magnetic fluid become too large, they can cluster due to dipole-dipole pair energy. Inserting typical values in equation 2-12 results in a particle diameter of $d_p \approx 10$ nm [9], which fits the magnetic fluid category of the ferrofluids. Finally equation 2-13 checks for settling due to gravity. Filling in typical values in this equation it can be concluded gravitational effects are less of a threat to segregation than magnetic effects.

Ferrofluids can further be classified when they are coated. Ferrofluids that use a surfactant molecule as coating are classified as surfacted ferrofluids (SFF), ferrofluids that use an electric shell are classified as ionic ferrofluids (IFF) [9]. Figure 2-3 presents ferromagnetic particles present inside a carrier liquid. It can be seen a surfactant is present in order to prevent agglomeration.

2-1-3 Magnetisation of Ferrofluid

The higher the magnetisation of the ferrofluid used in the ferrofluid rotary seal, the higher the capacity of the seal system becomes. Langevin's equation can be used to calculate the magnetisation curve of a ferrofluid [28, 29]. The magnetisation curve of the ferrofluid is required when the saturation magnetisation of the ferrofluid is not reached by the magnetic

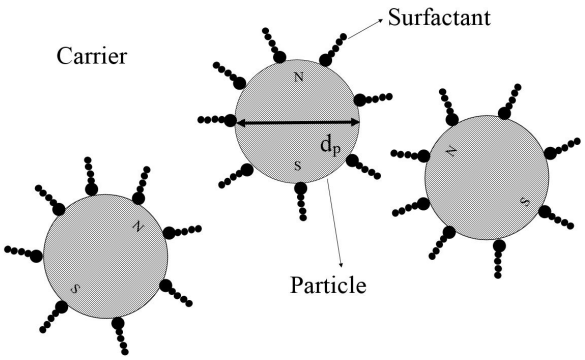

Figure 2-3: This figure presents the magnetic particles having diameter d_p which are present inside the carrier liquid of a ferrofluid. The particles are coated with a surfactant molecule in order to prevent agglomeration.

field strength present inside the ferrofluid rotary seal. Equation 2-14 presents the Langevin equation.

$$L(\alpha) \equiv \coth \alpha - \frac{1}{\alpha} = \frac{M}{\phi M_d} \quad \text{with,} \quad \alpha = \frac{\pi}{6} \frac{\mu_0 M_d H d^3}{k_B T} \tag{2-14}$$

where $L(\alpha)$ is the Langevin equation, M is the magnetisation of the ferrofluid [A/m], M_d is the domain magnetisation of the particles [A/m] and ϕ the volume fraction between the carrier liquid and the particles. The parameter α consists of the permeability of free space μ_0 [H/m], the applied magnetic field H [A/m], d_p the particle diameter [m], k_B the Boltzmann's constant [J/K] and T the absolute temperature [K]. For small values of the external magnetic field H, and thus α, the Langevin equation can be approximated by $L(\alpha) = \alpha/3$. Figure 2-4 presents the magnetisation curve of a ferrofluid taken from [30]. It can be seen that the ferrofluid magnetically saturates when the applied magnetic field becomes high enough.

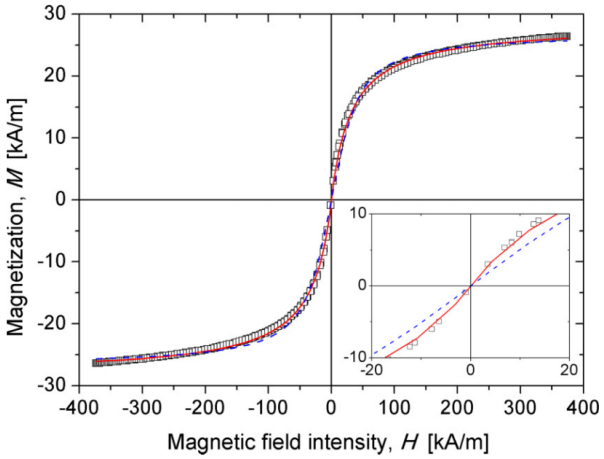

Figure 2-4: This figure presents the magnetisation curve of a ferrofluid. The blue dashed line corresponds to the Langevin equation, the points to experimental data. Figure taken from [30].

The magnetic susceptibility χ of ferrofluid is a measure of how much it will become magnetised

in presence of a magnetic field ($\mathbf{M} = \chi\mathbf{H}$). The initial magnetic susceptibility χ_i of ferrofluid can be calculated by equation 2-15.

$$\chi_i = \frac{\pi}{18}\phi\mu_0\frac{M_d^2 d_p^3}{K_B T} \tag{2-15}$$

2-2 Equation of Motion Ferrofluid

This section will discuss the behaviour of the ferrofluid in terms of its motion as a function of time. The motion of viscous fluids can be described using the Navier-Stokes equations. These equations can be seen as Newton's second law of motion applied to fluids. Unlike ordinary fluids ferrofluids become magnetised in presence of a magnetic field. Therefore an extra body force has to be defined in order to account for this magnetisation. Equation 2-16 gives the Navier-Stokes equations with added magnetic body forces for ferrofluids. $\rho\frac{\mathrm{D}\mathbf{v}}{\mathrm{D}t}$ is defined as the density of the ferrofluid times the material derivative of the ferrofluid and can be interpreted as mass times acceleration.

$$\rho\frac{\mathrm{D}\mathbf{v}}{\mathrm{D}t} = \mathbf{f}_p + \mathbf{f}_v + \mathbf{f}_g + \mathbf{f}_m \tag{2-16}$$

Where ρ is the density of the ferrofluid, $\mathbf{f}_p$ is the pressure gradient of the ferrofluid, $\mathbf{f}_v$ the viscous force per unit volume, $\mathbf{f}_g$ the gravitational force per unit volume and $\mathbf{f}_m$ the magnetic force per unit volume. Using equations 2-17 till 2-20 these body forces can be calculated. $\mathbf{f}_p$ is calculated by taking the gradient of the thermodynamic pressure inside the ferrofluid. $\mathbf{f}_g$ can be calculated by using the gravitational constant. The magnetic body force $\mathbf{f}_m$ and viscous body force $\mathbf{f}_v$ can be obtained respectively by taking the divergence of the magnetic stress tensor $\mathbf{T}_m$ and viscous stress tensor $\mathbf{T}_v$.

$$\mathbf{f}_p = -\nabla p_{ff}(\rho, T) \tag{2-17}$$

$$\mathbf{f}_g = \rho\mathbf{g} \tag{2-18}$$

$$\mathbf{f}_m = \nabla \cdot \mathbf{T}_m \tag{2-19}$$

$$\mathbf{f}_v = \nabla \cdot \mathbf{T}_v \tag{2-20}$$

The magnetic stress tensor $\mathbf{T}_m$ for a compressible non-linear ferrofluid as defined by Cowley and Rosensweig [31] can be seen in equation 2-21.

$$\mathbf{T}_m = -\left(\int_0^H \mu_0\left[\frac{\partial(\upsilon M)}{\partial\upsilon}\right]_{H,T} dH + \frac{1}{2}\mu_0 H^2\right)\mathbf{I} + \mathbf{BH} \tag{2-21}$$

Taking the divergence of the magnetic stress tensor by substituting equation 2-21 into equation 2-19 and rewriting using equation 2-1 results into the following equation for magnetic body force $\mathbf{f}_m$:

$$\mathbf{f}_m = -\nabla \left(\mu_0 \int_0^H \rho^2 \left[\frac{\partial (M/\rho)}{\partial \rho} \right]_{H,T} dH \right) + \mu_0 M \nabla H \tag{2-22}$$

The term $\mu_0 M \nabla H$ on the right side of equation 2-22 is considered to be the Kelvin body force [32]. By rewriting equation 2-22 Rosensweig has derived an alternative form of the magnetic body force $\mathbf{f}_m$ [27], which can be seen in equation 2-23.

$$\mathbf{f}_m = -\nabla \left(\underbrace{\mu_0 \int_0^H \upsilon \left[\frac{\partial M}{\partial \upsilon} \right]_{H,T} dH}_{p_s} + \underbrace{\mu_0 \int_0^H M dH}_{p_m} \right) + \mu_0 M \nabla H \tag{2-23}$$

where p_s is defined as the magnetostrictive pressure and p_m as the fluid magnetic pressure. Magnetostriction is a property of ferrofluid that causes it to change its shape due to its magnetisation by the magnetic field the ring magnet generates. The fluid magnetic pressure is same as the pressure generated by the kinetic energy of the molecules, only now it is carried by the magnetic field. The magnetic body force $\mathbf{f}_m$ can now be written as the gradient of the sum of the magnetic fluid and magnetostricitve pressure with an additional body force term shown in equation 2-24.

$$\mathbf{f}_m = -\nabla (p_s + p_m) + \mu_0 M \nabla H \tag{2-24}$$

The viscous stress tensor $\mathbf{T}_v$ models the stress inside the ferrofluid due to the strain rate of the fluid. For isotropic Newtonian fluids the viscous stress tensor can be defined using the following equation:

$$\mathbf{T}_v = \eta (\nabla \mathbf{v} + (\nabla \mathbf{v})^T) - \left(\frac{2}{3} \eta - \kappa \right) (\nabla \cdot \mathbf{v}) \mathbf{I} \tag{2-25}$$

where η is defined as the ratio of the shearing stress to the velocity gradient and κ is the bulk viscosity coefficient. The bulk viscosity is the internal friction that resists shearless compression or expansion of fluid. Considering the ferrofluid as an incompressible fluid, the divergence of the velocity $\nabla \cdot \mathbf{v}$ will be equal to zero. Using this the viscous stress tensor of an incompressible Newtonian fluid shown in equation 2-26 can be derived. Subsequently the viscous body force can be calculated by substituting equation 2-26 into equation 2-20, which results into equation 2-27.

$$\mathbf{T}_v = \eta (\nabla \mathbf{v} + (\nabla \mathbf{v})^T) \tag{2-26}$$

$$\mathbf{f}_v = \eta \nabla^2 \mathbf{v} \tag{2-27}$$

Now all body forces of the ferrofluid are defined the equations of motion can be formulated. The equation of motion for a Newtonian incompressible ferrofluid is presented in equation 2-28. Pressure terms p_{ff}, p_s and p_m are written together. Using this equation of motion, design properties such as sealing capacity can be calculated for a ferrofluid rotary seal.

$$\rho \frac{\mathrm{D}\mathbf{v}}{\mathrm{D}t} = -\nabla(p_{ff} + p_s + p_m) + \eta\nabla^2\mathbf{v} + \rho\mathbf{g} + \mu_0 M \nabla H \tag{2-28}$$

where $\rho\frac{\mathrm{D}\mathbf{v}}{\mathrm{D}t}$ is the density of the ferrofluid times the material derivative, p_{ff} the thermodynamic pressure of ferrofluid, p_s pressure due to magnetostrictive effects, p_m the magnetic fluid pressure, $\eta\nabla^2\mathbf{v}$ viscosity effects, $\rho\mathbf{g}$ gravitational effect and $\mu_0 M\nabla H$ the magnetic body force.

2-3 Static Sealing Capacity

An important design property of a ferrofluid rotary seal is the maximum pressure it can withstand before it fails, the so-called sealing capacity. This section will elaborate the calculation of the sealing capacity of a ferrofluid rotary seal sealing a liquid. Using either Bernoulli's principle or Navier-Stokes the sealing capacity can be predicted.

2-3-1 Boundary Condition Seal

First, a boundary condition has to be formulated in order to relate pressure p_l of the liquid that is sealed to the pressure build up inside of the ferrofluid seal. Figure 2-5 presents the interface between the liquid contained and the ferrofluid of the seal. The dashed box indicates the boundary condition between the two liquids.

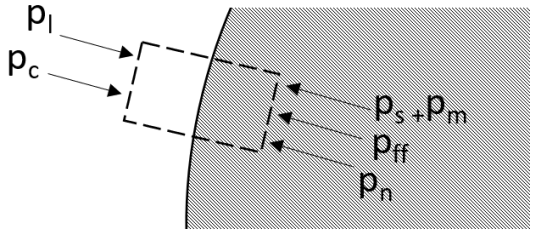

Figure 2-5: This figure presents the interface between a non magnetic liquid that is contained and the ferrofluid of the seal. The dashed box shows the boundary condition between the liquids.

The capillary pressure difference p_c between the ferrofluid and the liquid sealed can be calculated using the Young-Laplace equation presented in equation 2-29.

$$p_c = 2\gamma\xi \tag{2-29}$$

where γ is the surface tension [N/m] and ξ the mean curvature [m^{-1}] ($\xi = \nabla \cdot \mathbf{n}/\mathbf{2}$). The vector $\mathbf{n}$ is defined as the normal vector of the contact surface between the two liquids. The direction of the capillary pressure can be determined by the wettability of the system. For a water-oil interface the capillary pressure is equal to $p_c = p_{oil} - p_{water}$. Magnetic surface pressure p_n can be calculated using equation 2-30 [32]. The magnetic normal traction M_n is equal to $\mathbf{n} \cdot \mathbf{M}$. Equation 2-31 presents the boundary condition between ferrofluid and the sealed liquid.

$$p_n = \mu_0 M_n^2/2 \tag{2-30}$$

$$p_{ff} + p_s + p_m + p_n = p_l + p_c \tag{2-31}$$

2-3-2 Bernoulli's Principle

Rosensweig has derived an augmented Bernoulli equation for ferrofluids [33]. It is assumed viscous effects are absent and the ferrofluid is in static equilibrium and steady flow situation. Equation 2-32 presents the steady state Bernoulli equation for ferrofluids.

$$p_{ff} + p_s + p_m + \frac{1}{2}\rho v^2 + \rho g h - \mu_0 \bar{M} H = \text{const} \tag{2-32}$$

where p_{ff} is the thermodynamic pressure, p_s pressure due to magnetostriction, p_m the fluid magnetic pressure, $\frac{1}{2}\rho v^2$ the velocity potential of the ferrofluid, $\rho g h$ the gravitational potential and $\mu_0 \bar{M} H$ the magnetic potential with $\bar{M}$ defined as the field-averaged magnetisation $\bar{M} = 1/H \int_0^H M dH$. Figure 2-6 shows a basic ferrofluid seal which has two interfaces 1 and 2. Interface 1 is defined as the interface between the liquid sealed and the ferrofluid of the seal and interface 2 as the interface between the ferrofluid and air at atmospheric pressure. The augmented Bernoulli equation can be used to calculate the sealing capacity of the ferrofluid seal. When gravitational effects are neglected and a static non rotating shaft situation is considered, equation 2-32 can be simplified to:

$$p_{ff} + p_s + p_m - \mu_0 \bar{M} H = \text{const} \tag{2-33}$$

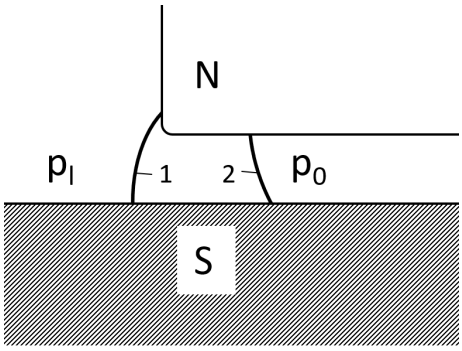

Figure 2-6: This figures presents a cross section of a ferrofluid seal between a shaft and ring magnet having interfaces 1 and 2.

It will be assumed the shape of the ferrofluid will align exactly alongside the H-field generated by the ring magnet [34] and that the magnetisation of the ferrofluid is collinear with this field. This means magnetic surface pressure p_n is equal to zero. Further capillary pressure p_c is neglected, considering that magnetic pressures have much greater impact [35]. Now the boundary conditions at interface 1 and 2 of the seal show in figure 2-6 can be defined. Equations 2-34 and 2-35 present these boundary conditions.

$$p_l = p_{ff,1} + p_{m,1} + p_{s,1} \tag{2-34}$$

$$p_0 = p_{ff,2} + p_{m,2} + p_{s,2} \tag{2-35}$$

The boundary conditions of both interfaces are substituted into equation 2-33, resulting into equation 2-36. Using the boundary conditions defined in equations 2-34 and 2-35 the pressure

build up of the seal $\Delta p = p_l - p_0$ can be calculated using equation 2-37. According to literature predictions of burst pressure using equation 2-37 are in agreement with experimental results [36].

$$p_{ff,1} + p_{s,1} + p_{m,1} - \mu_0 M_s H_1 = p_{ff,2} + p_{s,2} + p_{m,2} - \mu_0 M_s H_2 \tag{2-36}$$

$$\Delta p = p_l - p_0 = \mu_0 M_s (H_1 - H_2) \tag{2-37}$$

When pressure difference Δp over the seal becomes larger than predicted by equation 2-37, the seal will burst. Figure 2-7 shows the static burst mechanism of the ferrofluid seal. The seal will fail at its weakest spot. Analysing equation 2-37 leads to the conclusion this will be at the place where difference in magnetic field strength $H_2 - H_1$ is lowest. When seal gap h increases, the difference between magnetic field strength H_1 and H_2 decreases. Li Decai et al have done research to a large gap magnetic fluid static seal [37]. They concluded that the sealing capacity of a ferrofluid seal reduces with the increasing of the seal gap dimension.

Another way of calculating the seal capacity is proposed by Ravaud et al. [38]. By comparing the potential energy of the ferrofluid seal with and without perforation the pressure work can be obtained. By using the surface area of the gap and the thickness of the perforation the pressure capacity of the seal is obtained.

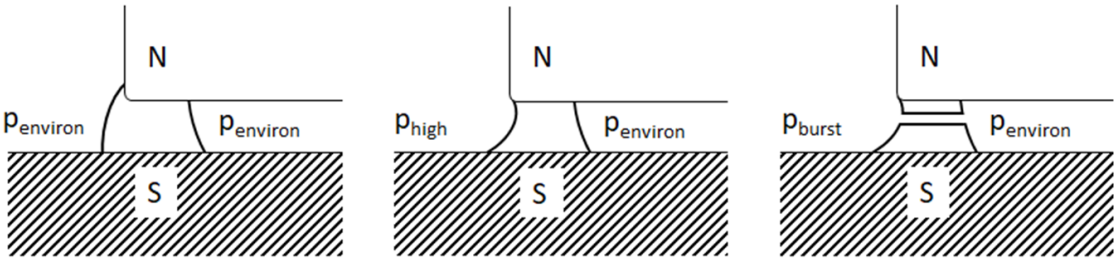

Figure 2-7: This figure presents the static burst mechanism of a ferrofluid seal. The shape of the ferrofluid seal changes when the sealing pressure rises. When the pressure of the sealed medium becomes larger than the sealing capacity of the seal, the seal bursts and the sealed medium will leak through the seal gap.

When multiple similar stages of ferrofluid seals are designed, the seal capacity of the system can be increased [39, 40]. Equation 2-38 can be used to calculate the burst pressure of the total system.

$$\Delta p = N \Delta p_i = N \mu_0 M_s (H_{max} - H_{min}) \tag{2-38}$$

where N is number of stages, Δp_i the seal capacity of each stage, M_s the saturation magnetisation, H_{max} the maximum magnetic field strength and H_{min} the minimum field strength of a stage.

2-3-3 Navier-Stokes

Section 2-2 presented the equations of motion for incompressible Newtonian ferrofluids. Assuming a static shaft condition the equations of motion can be simplified to equation 2-39.

$$-\nabla(p_{ff}+p_s+p_m)+\rho\mathbf{g}+\mu_0 M\nabla H=0 \tag{2-39}$$

If also gravitational effects are neglected, equation 2-39 can further be simplified and rewritten:

$$\nabla(p_{ff}+p_s+p_m)=\mu_0 M\nabla H \tag{2-40}$$

Equation 2-40 learns that the iso-lines of the pressure distribution have the same shape as the iso-lines of the magnetic field distribution. The maximum pressure difference between the liquid sealed p_l and the environment p_0 then can be calculated by integrating along the length of the seal in radial direction, which is shown in equation 2-41.

$$\int_c \nabla(p_{ff}+p_s+p_m)\cdot dr=\mu_o M_s\int_c \nabla H\cdot dr=\mu_o M_s(H_1-H_2) \tag{2-41}$$

Previously derived equations used for the calculation of the sealing capacity of a ferrofluid seal do not account for instability of the ferrofluid in the magnetic field gradient of the seal system, which has been elaborated in section 2-1-2. When the shaft in the ferrofluid rotary seal system has been static for a certain amount of time, critical pressures can become higher than predicted. The magnetic field gradient inside of the system can cause distribution of particles. The ferrofluid becomes non-uniform and particle concentration becomes higher in areas with higher magnetic field intensity. Polevikov and Tobiska have derived a mathematical model for studying the stability of a magnetic fluid seal under the action of external pressure drop [41]. It has been demonstrated that there is a non neglectable influence on the burst pressure of the system. When the shaft rotates, the ferrofluid will be stirred and becomes uniform again. Measured burst pressures will become close to predicted pressures again.

Chapter 3

Dynamic Operation in Aqueous Environments

Literature learns that dynamic operation of a ferrofluid rotary seal in aqueous environments is not obvious. This chapter elaborates the dynamic failure of a ferrofluid rotary seal when it seals a liquid and discusses important design aspects that have to be taken into consideration when designing such sealing system.

3-1 Dynamic Seal Failure

In chapter 2 the static sealing capacity of a ferrofluid seal has been elaborated. However, when dynamic shaft conditions are considered it becomes more complicated to predict the behaviour and performance of a ferrofluid rotary seal. Dynamic seal failure still can not be predicted and is not fully understood. This section discusses mechanisms which may attribute to the premature failure of a ferrofluid rotary seal that dynamically seals a liquid.

3-1-1 Kelvin-Helmholtz Instability

The Kelvin-Helmholtz instability is a hydrodynamic instability in which two inviscid fluids are in relative and irrotational motion. The velocity and density profiles are discontinuous at the interface between the two fluids. This phenomenon also plays an important role in the design of a ferrofluid seal for liquids. Kurfess and Muller considered the Kelvin-Helmholtz instability as main cause of dynamic seal failure [3]. Figure 3-1 shows the interface of the sealed liquid and the ferrofluid of the seal. As can be seen this interface is not exactly flat, but contains waves travelling along this interface. In general these waves are affected by the surface tension and gravity.

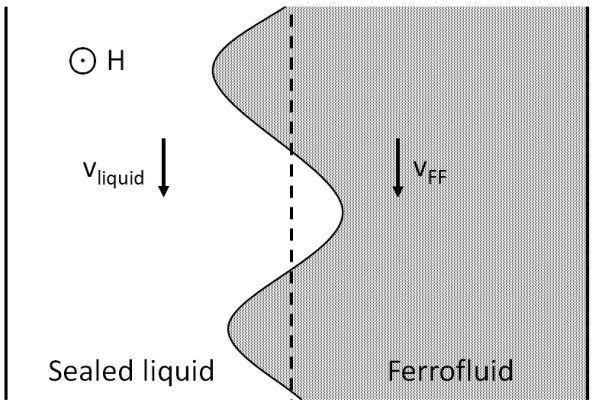

Figure 3-1: This figure presents the interface between the liquid that is contained and the ferrofluid of the seal. Disturbance waves propagate along the interface in the direction of the flow.

The spatial frequency of these disturbance waves can be defined using a wave number k. The dependence of the frequency on the wave number can be described by a dispersion relationship. This dispersion relationship can be seen as an eigenrelation and stability of the interface can be calculated by calculating the eigenvalues of this dispersion relationship. These eigenvalues can be used to determine the maximum difference in velocity of the liquid that is sealed and the ferrofluid before the interface becomes unstable and the seal fails. Rosensweig has developed a relationship for the stability of the interface between ferrofluid and another liquid [27]. Equation 3-1 shows the condition for this instability and can be used to define the margins of stability of the interface between ferrofluid and another liquid. In literature equation 3-1 often is included and used to explain dynamic failure of the rotary ferrofluid seal that seals a liquid [17, 42, 3].

$$(v_{ff} - v_l)^2 > \frac{\rho_{ff} + \rho_l}{\rho_{ff}\rho_l}\left(2[g(\rho_{ff} - \rho_l)\sigma_{l-ff}]^{1/2} + \frac{(\mu_l - \mu_{ff})^2 H^2}{\mu_l + \mu_{ff}}\right) \tag{3-1}$$

where v_{ff} and v_l are the velocity of respectively the ferrofluid and the sealed (non magnetic) liquid [m/s], ρ_{ff} and ρ_l the density [kg/m^3], μ_{ff} and μ_l the magnetic permeability [N·A^{-2}], H the applied magnetic field strength collinear with the wave propagation [A/m], g the gravitational acceleration [m/s^2] and σ_{l-ff} the interfacial surface tension [N/m].

Using equation 3-1 the critical velocity difference $v_{ff} - v_l$ between a layer of ferrofluid and another non magnetic liquid can be found. The stability criterion of equation 3-1 assumes the H-field is collinear with the flow of the two liquids. Analysing the magnetic field present inside ferrofluid rotary seal and comparing this with the drawing of figure 3-1 it can be concluded the H-field inside of a rotary ferrofluid seal is not collinear with the shear flow between the two fluids. This means the right term of equation 3-1, which incorporates the stabilising effect of the magnetic field on the interface, is not present in the rotary ferrofluid sealing system. The fluid interface is not stiffened by the magnetic field for wave propagation along the interface. The term containing H in equation 3-1 is thus equal to zero.

However, wave propagation normal to the liquid-liquid interface also could occur. The magnetic field normal to the interface is not uniform and contains a gradient. A magnetic field

having a gradient is capable of stabilising the interface between ferrofluid and another fluid for disturbance waves having any direction [33]. Due to this non uniformity of the magnetic field, this gradient field stabilisation theory is complex.

The Kelvin-Helmholtz instability presented in equation 3-1 learns that a relative velocity between the liquid that is sealed and ferrofluid of the sealing system can introduce instabilities. Therefore it is important to understand how a relative velocity between the liquid sealed and the ferrofluid of the seal arises. Figure 3-2 shows a potential velocity difference between the liquids in a ferrofluid rotary seal. When there is a difference in seal gap height between the ferrofluid and sealed liquid, velocity of the ferrofluid and the sealed liquid can be related. This can be done by assuming a no-slip condition and linear velocity profile inside the fluids. The velocity difference then can be calculated by the relation presented in equation 3-2. If a ferrofluid rotary seal is considered with large difference seal gap height h and h_0, velocity difference for the Kelvin-Helmholtz instability can be approximated by the shaft surface speed v_s.

$$\Delta v = v_{ff} - v_l = \frac{h_0}{h_0 + h} v_s \qquad v_s = \frac{\pi n}{30} r_s \tag{3-2}$$

where v_{ff} is velocity of the ferrofluid [m/s], v_l the velocity of the liquid that is sealed [m/s], v_s surface speed of the shaft [m/s], h height of the seal gap between the ring magnet and the shaft [m], h_0 the difference in gap height between the liquid sealed and ferrofluid [m], n the shaft speed [rpm] and r_s radius of the shaft [m].

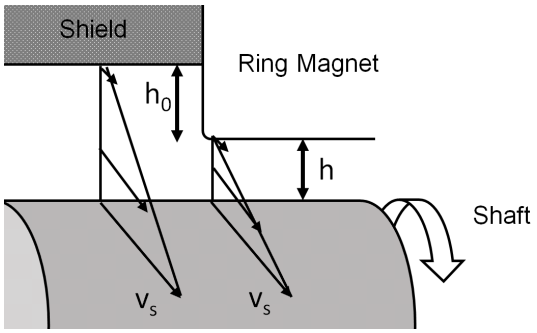

Figure 3-2: This figure presents the linear velocity profiles of the liquid that is sealed and the ferrofluid of the seal. A difference in seal gap height (h_0) introduces a relative velocity between the liquids when linear velocity profiles and a no-slip condition are assumed.

3-1-2 Shear Force at the Interface

The Kelvin-Helmholtz instability elaborated in previous section does not explain gradual performance drop resulting in premature failure when a ferrofluid rotary seal is operated at low velocities [17]. Jarmo et al. suggested possible cause of this performance drop is gradual removal of the ferrofluid [23]. An important parameter that has to be taken into consideration when designing a ferrofluid rotary seal is the seal gap of the system. The seal gap is the gap between the rotating shaft and the housing of the system. Experimental results of Wang et al. indicate that service life of the seal decreases when the seal gap becomes larger [43]. A

larger seal gap results in larger shear forces at the interface between the sealed liquid and the ferrofluid of the seal.

The ferrofluid flow inside the seal can be regarded as an one dimensional laminar flow in tangential direction due to the small seal gap and high viscosity of the fluid. If it is assumed the ferrofluid has a constant density, is a incompressible Newtonian fluid and gravitational effects can be neglected, Newton's law for internal friction for fluids can be used to obtain the shear force between the fluids. This relation is presented in equation 3-3.

$$F_{shear} = \mu \frac{\partial v}{\partial x} A_{contact} = \mu \frac{\Delta v}{b} A_{contact} \tag{3-3}$$

where μ is the dynamic viscosity of the ferrofluid [Pa·s], Δv the velocity difference between the two liquids [m/s] and b the transitional layer [m] where the velocity gradient exists between the ferrofluid and the sealed liquid. Linear velocity distribution over a distance b between the ferrofluid and sealed liquid is assumed. Wang et al. have derived a relation for calculating the shear force on the ferrofluid seal, presented in equation 3-4 [43]. It is assumed seal gap h is infinitely smaller than shaft radius r_s. Elaborating shear force at the contact area $F_{shear} = \iint_A \tau dA$, equation 3-4 is derived.

$$F_{shear} = \frac{\pi r_s^2 \mu \omega h}{b} = \frac{D^2 \mu N h}{8b} \tag{3-4}$$

where F_{shear} is the shear force at the contact area [N], r_s radius of the rotating shaft [m], μ dynamic viscosity of the ferrofluid [Pa·s], ω angular velocity of the shaft [Rad/s], h gap height [m]and b the transitional layer width [m].

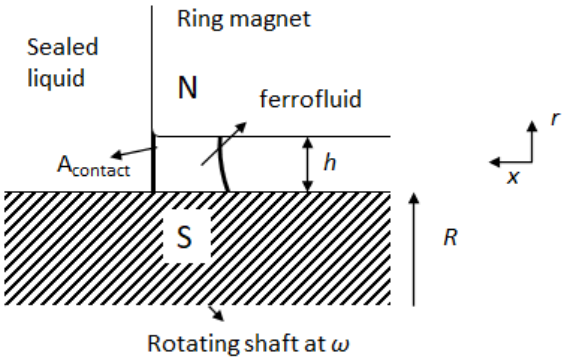

Figure 3-3: This figure presents the cross section of a ferrofluid seal and indicates its contact area with the liquid sealed.

Equation 3-4 may be useful for identifying and predicting influence of certain parameters on the performance of the ferrofluid rotary seal that seals a liquid. According to equation 3-4 the shear force is proportional to the cross section area of the rotating shaft, the viscosity of the ferrofluid, angular velocity of the shaft and finally the height of the seal gap. However, Wang et al. have discovered during their experiments seal life time is not proportional to seal gap height. Instead, seal life also appears to be dependent on the sealing pressure. Seal life was not proportional with shaft speed.

3-1-3 Deterioration of Ferrofluid

Another phenomenon that could attribute to the dynamic seal failure of ferrofluid rotary seal that seals a liquid is the deterioration of the ferrofluid inside the sealing system. When ferrofluid contacts a liquid, for example water, the magnetic properties of the ferrofluid tend to decrease. Decrease of the magnetic property of the ferrofluid results into a decrease of sealing pressure and therefore shortens seal service life. Mitamura et al. have investigated the magnetic properties of ferrofluids after it has been in contact with water [22]. The magnetic properties of ferrofluid has been tested for three different groups. For the first group the ferrofluid is poured in a beaker with distilled water and magnetic properties were tested after 5 and 10 days. In the second group the ferrofluid in water is stirred for 5 days. In the last group the liquids were stirred for 10 days. The saturated magnetisation of the ferrofluid for all groups in distilled water decreased. The measurements of the magnetic properties, the thermogravimetric analysis and the Fourier transform infrared spectroscopic analysis of the ferrofluid stirred in water suggest deterioration of ferrofluid in water.

3-1-4 Inertial, Magnetic and Viscous Forces

At certain high shaft speed the ferrofluid rotary seal fails, even when it is not pressurised. It is very useful to understand how the various ferrofluid properties and seal design principles affect the high speed failure of a ferrofluid seal system. At high shaft speeds the centrifugal force will increase with respect to the magnetic force. Using the centrifugal force for a point mass shown in equation 3-5 the centrifugal force of ferrofluid can be derived. Equation 3-6 presents the formula for calculating the centrifugal force acting on the ferrofluid. It can be seen the centrifugal force in ferrofluid scales quadratic with shaft speed. Equation 3-7 shows magnetic force acting on the ferrofluid. Magnetic force is independent of shaft speed, so this may suggest centrifugal forces become larger than magnetic forces at certain shaft speeds and thus causing maximum speed seal failure. However, as can be seen in figure 3-4 centrifugal forces act in radial direction, whereas the magnetic forces acts in axial direction. The relationship between those forces is not obvious.

$$F_{c,point} = m\omega^2 r \tag{3-5}$$

$$F_c = 2\pi^2 \rho D N^2 \tag{3-6}$$

$$F_m = \frac{MH}{h} \tag{3-7}$$

where $F_{c,point}$ is centrifugal force of a point mass, m mass, ω rotational speed and r radius of the shaft. Centrifugal force F_c of ferrofluid in the seal can be calculated using density of the ferrofluid ρ, shaft diameter D and shaft speed N. Magnetic force on the ferrofluid F_m can be calculated using magnetisation M, minimum magnetic field intensity H and gap height h.

Bonvouloir has done research to high speed seal failure [44]. In his research the ratio between centrifugal and magnetic forces F_r, presented in equation 3-8, is investigated as possible predictor of high speed seal failure.

$$F_r = \frac{F_c}{F_m} = \frac{2\pi^2 \rho D N^2 h}{MH} \tag{3-8}$$

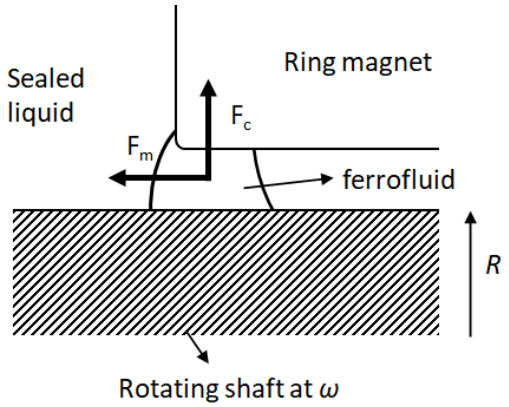

Figure 3-4: This figure presents the centrifugal and magnetic force acting on the ferrofluid of the ferrofluid rotary seal.

It is concluded that the ratio between those forces could not be related to the maximum failure speed of a rotary ferrofluid sealing system. Also it is concluded magnetic forces have weak influence on maximum failure speed of the system. Instead of the force ratio shown in equation 3-8, viscosity appears to be a better predictor of high speed failure. The Reynolds number shown in equation 3-9 relates inertial forces to viscous forces of the ferrofluid. It was observed that failure speed is roughly proportional to fluid viscosity and inversely proportional to shaft diameter, maximum radial gap, and fluid density [44]. This suggests an empirical relation in the form of Reynolds number can be a better predictor.

$$\mathrm{Re} \equiv \frac{v\rho L_{char}}{\mu} \quad \rightarrow \quad \mathrm{Re}_{seal} = \frac{\pi D N \rho h_{max}}{\mu} \tag{3-9}$$

where v the velocity of the fluid, L_{char} characteristic linear dimension, μ viscosity of the ferrofluid, D shaft diameter, ρ density of ferrofluid and N shaft speed.

3-1-5 Ferrofluid Taylor-Couette Flow

The flow of the ferrofluid between the ring magnet and shaft can be considered to be the so-called Taylor-Couette flow [45]. The Taylor-Couette flow consists of a viscous fluid confined in the gap between two rotating cylinders. The Taylor number is a dimensionless number that is used to characterise the importance of inertial forces due to rotation of the ferrofluid about an axis relative to viscous forces. When the Taylor number of the flow exceeds a critical value Taylor vortices may arise. Using equation 3-10 the Taylor number of a ferrofluid flow inside a rotary seal can be calculated. Magnetic effects are neglected.

$$\mathrm{Ta} = \frac{2\pi^2 D N^2 h_{max}^3 \rho^2}{\mu^2} \tag{3-10}$$

where D is shaft diameter, N shaft speed, h_{max} maximum seal gap, ρ density of the ferrofluid and μ viscosity of the ferrofluid.

Stiles et al. have investigated instability of the Taylor-Couette flow of a radially magnetised ferrofluid [46]. They have observed influences of centrifugal diffusion and magnetodiffusion slowly create a radial gradient in the distribution of the colloidal particles. Also they have observed both the critical Taylor number and wave number increase as the magnetic field strength increases. In a different research Stiles et al. concluded that ferrofluid magnetised by a strong radial magnetic field has rapid decrease in stability of Taylor-Couette flow for small radial temperature gradients [47]. Niklas has done research to Taylor vortex formation in ferrofluid Taylor-Couette flow under influence of axial, radial and azimuthal magnetic fields [48]. All three magnetic fields have a stabilizing effect on the primary circular Coutette flow. The critical wave number is enlarged by applying a radial magnetic field. Changing the magnetic field strength the critical wave number can be controlled of the ferrofluid. The Ultrasonic Velocity Profile (UVP) method can be used to provide information on the structure of Taylor-Couette flow with small aspect ratio in ferrofluid [49, 50, 51].

3-2 Design Principles

In this section some important design aspects for ferrofluid rotary seals operating in aqueous environments are discussed.

3-2-1 Shielding

Section 3-1 elaborated possible phenomena contributing to dynamic seal failure when sealing liquids. It is concluded dynamic seal service life is increased when the relative velocity between the sealed liquid and the ferrofluid of the sealing system is minimised. In order to minimise this relative velocity a shield in front of the seal can be constructed. Figures 3-5 and 3-6 show two different shield constructions which can be incorporated in the system.

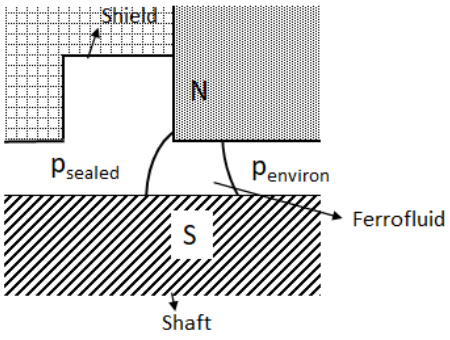

Figure 3-5: This figure presents a shielding structure creating a buffer zone for absorbing disturbances.

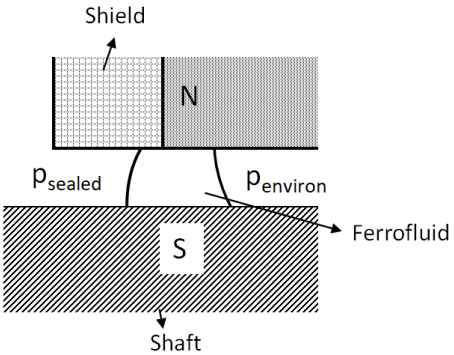

Figure 3-6: This figure presents a shielding structure for minimising relative velocity.

The construction shown in figure 3-5 uses a buffer of the sealed liquid to absorb disturbances in the sealed liquid [52]. However, relative velocity at the interface between the two liquids is not equal to zero. During experiment conducted by Mitamura et al. it is concluded that the

construction presented in figure 3-6 results in a longer seal service life than the construction presented in figure 3-5. CFD analyses of the flow in the shielding channel of the sealing system having the construction presented in figure 3-6 show the interface between the water and ferrofluid is stable [42].

Another way for improving the service life is by preventing contact between the liquid sealed and the ferrofluid of the system. This could be done by adding gas between the sealed liquid and ferrofluid, functioning as an isolation device. Wang et al. have done research to this concept and concluded it may be a possible solution to further increase life time of the seal system [53]. From their experiments it can be concluded critical pressure of the seal system using gas isolation is no longer dependent on shaft speed. However, as for the original seal system with no gas isolation seal service life was short.

3-2-2 Magnetic Field Generation and Guidance

For the design of a ferrofluid rotary seal a suitable permanent magnet has to be selected. Important properties of the magnet are maximum operational temperature, material grade and coating. The two main categories of permanent magnets are the rare-earth magnets and composite magnets. Rare-earth magnets Neodymium and Samarium Cobalt have better magnetic properties than composite magnets of Ferrite or AlNiCo. However, these magnets are more expensive and brittle. It is important that magnets located in aqueous environments are coated in order to prevent performance loss of the magnet due to corrosion. Common used coatings in such environments are epoxy, teflon or parylene. Due to their low permeability these plastics have little to no influence of the magnetic field distribution. Local temperatures in the sealing system must not rise near the Curie temperature of the magnet. This temperature is defined as the temperature at which a material loses its permanent magnetic properties.

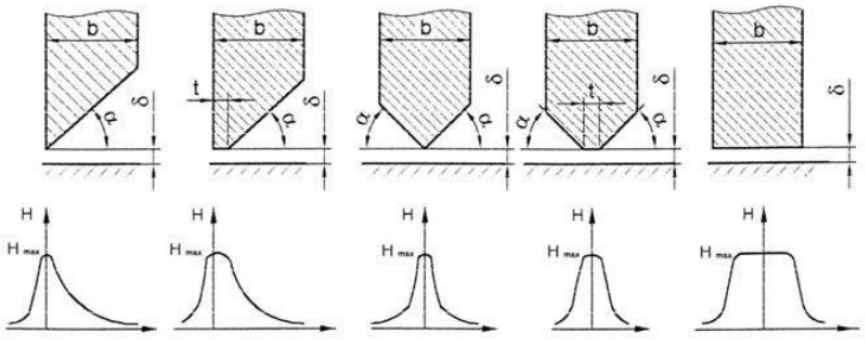

Figure 3-7: This figure presents different pole piece designs proposed by Ochonski [54]. Underneath the designs the magnetic field intensity in the seal gap is displayed.

The magnetic field generated by the ring magnet can be directed using polepieces. A pole piece is a structure made of material of high permeability and extends the pole of a magnet. Traditional material for pole pieces is soft iron. However, it is important the polepieces can not be affected by corrosion. The shape of the polepiece can be changed in order to obtain the desired magnetic field configuration. Ochonski has proposed different pole piece designs [54], presented in figure 3-7. It can be seen the magnetic field strength H in the seal gap can

be manipulated by changing the shape of the pole piece. Besides pole pieces, also magnetic properties of the shaft can be considered. Liu et al. have proposed a design using a bushing on the shaft [19] in order to guide the magnetic field. For stability of the interface between the ferrofluid and the sealed liquid the magnetic field distribution is important. Melcher stated that a flat interface between two stationary fluids of which one is a ferrofluid may be unstable when there is a normal magnetic field [55].

3-2-3 Shaft Properties and Torque

The shaft in the ferrofluid rotary sealing system transmits torque and rotation and is usually connected to other components of a drive train. An example is the drive train of a vessel, often consisting of a drive shaft connecting the transmission of the vessel directly to a propeller. As the propeller is pushing the vessel forward, the drive shaft is subjected to compression. When the vessel is moving backwards, the drive shaft is under tension. Due to the torque subjected on the shaft, the shaft is subjected to torsion and shear stress. The shaft has to be designed in such way these stresses can be withstand. A ferrofluid seal system also introduces torque on the shaft by fluid friction. Torque transmitted by fluid friction can be calculated using equation 3-11 [44]. The ferrofluid flow in the ferrofluid seal system is assumed to be laminar.

$$T_{ff} = \tau_{ff} A_{seal} \quad \rightarrow \quad T_{ff} = \frac{\pi^2 \mu N D^3 w}{2h} \tag{3-11}$$

where T_{ff} is torque generated by the ferrofluid seal [Nm], μ is viscosity of the ferrofluid [Pa·s], N shaft speed [rpm], D shaft diameter [m], w effective stage length [m] and h seal gap [m]. The torque of the motor that drives the shaft is proportional to the current supplied to the motor. The total motor current I_{total} with a ferrofluid seal at a certain speed can be measured. If the motor current without ferrofluid in the system I_{absent} is measured, torque T_{ff} of the ferrofluid seal can be calculated. Equation 3-12 presents the relation between the motor current and torque of a ferrofluid seal. The motor constant K_t and motor efficiency η need to be known. Effects of bearing friction, hysteresis and eddy currents are neglected.

$$T_{ff} = K_t \eta (I_{total} - I_{absent}) \tag{3-12}$$

Using equations 3-11 and 3-12 it is possible to identify parameters like the actual seal gap height h given that other variables are known. For example alignment of the shaft can be checked by doing so. Because of the aqueous environment the shaft is operating in corrosion of the shaft can occur. Corrosion is the gradual destruction of materials by chemical or electrochemical reaction with their environment. Besides mechanical and chemical properties mentioned before, magnetic properties of the shaft are also important when designing a ferrofluid sealing system. Magnetic properties of the shaft will influence the magnetic field distribution inside the system.

Stainless steels are often used for drive shafts in aqueous environments. Unlike carbon steels, stainless steels do not suffer from uniform corrosion. Stainless steels can be classified according to their crystalline structure into different groups. Most important groups are austenitic stainless steels, ferritic stainless steels, martensitic stainless steels and duplex stainless steel. Stainless steel is created by adding other elements like chromium and nickel to carbon steel.

Ferritic and martensitic stainless steels can be considered magnetic, austenitic stainless steels not [56]. Duplex stainless steels have a mixed microstructure of autenite and ferrite. This means magnetic properties are poor compared to ferritic stainless steels.

3-2-4 Environmental Impact

The spread of a wide range of contaminants in surface water and ground water has become a critical issue worldwide [57]. Depending on the application of the ferrofluid rotary seal for sealing liquids, environmental impact can also become an important design aspect for the ferrofluid seal. A potential new application of the ferrofluid rotary seal for sealing liquids is in the marine industry. In order to minimise or exclude harm to marine ecosystems leakage of ferrofluid into the environment should be minimised and the usage of environmental friendly ferrofluids could be preferred in the sealing device. As discussed before ferrofluids consist of a carrier liquid with suspended magnetic nanoparticles.

In addition to use in ferrofluids, magnetic nanoparticles have also been found to be very efficient in wastewater decontamination [58]. Especially iron oxide based nanoparticles such as magnetite have gained extensive attention due to their enhanced magnetic properties and lack of toxicity [59]. Additional iron oxide nanoparticles show many potential applications in biotechnology, for example drug delivery and tissue repair [60]. Nadejde et al. have successfully synthesised environmentally friendly ferrofluid based on magnetite nanoparticles [61]. Stability of the fluid is ensured by capping the magnetite nanoparticles with non-hazardous natural occurring molecules. Moreover, they conclude their method for synthesising the fluid is facile, rapid and cost effective.

Also research is done to the application of magnetic separation technology to remove oil from water after an oil spill [62, 63]. By adding magnetic nanoparticles to the oil it becomes a magnetic fluid. Subsequently magnets can be used to remove the fluid from the water. These new techniques stimulate the development of environmental friendly ferrofluids.

Chapter 4

Ferrofluid Seals in Literature

In literature several applications of ferrofluid seals can be found. The most important application of ferrofluid seals in industry is the sealing of rotating shafts in vacuum and gas systems. Research done to the sealing of liquids by ferrofluid seals can be found in a number of published papers. Two main applications that are investigated are the use of ferrofluid seals in rotary blood pumps and marine systems. Also research to the working principles of ferrofluid seals and the influence of the sealing conditions and design variables on its performance is done. This chapter elaborates most important designs of ferrofluid seals and experimental setups found in literature in order to create insight in the state of the art of the sealing technology.

4-1 Vacuum and Gas Systems

As stated before ferrofluid rotary seals have already proven themselves in vacuum and gas environments. However, most knowledge on the design of these sealing devices is kept confidential by companies exploiting the technology. The most commonly known ferrofluid sealing devices are ferrofluid rotary vacuum seals in machinery operating in a vacuum chamber [13]. Also other applications for ferrofluid seals in vacuum and gas environment can be found in literature. Raj et al. have presented ferrofluid sealing used in a belt edge seal and a centrifugal seal [15]. The belt edge seal is a seal between an endless moving belt with both top and bottom sealed by ferrofluid, shown in figure 4-1. A centrifugal seal uses centrifugal forces in order to keep the fluid positioned. By adding ferrofluid and a magnetic field this seal works also at low speeds when centrifugal forces are low. Bonvouloir has built a ferrofluid rotary seal test setup for testing sealing capacity at high speeds [44]. The test setup can be seen in figure 4-2. Using a hand pump the ferrofluid seal is subjected to pressurised air. An empirical relation for high speed failure has been derived. Applicability of this relation however appears to be very limited.

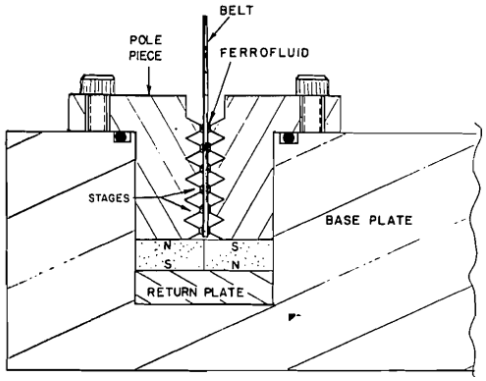

Figure 4-1: This figure presents a ferrofluid sealing device used in order to seal the top and bottom of an endless belt [15].

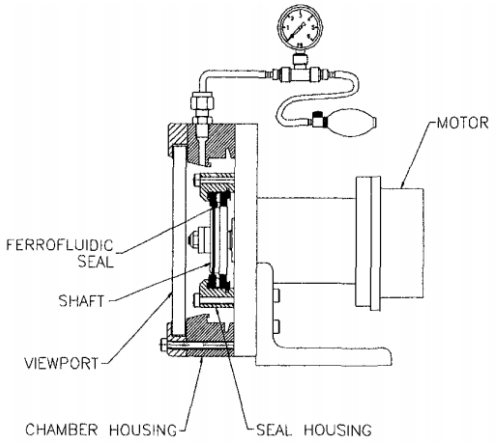

Figure 4-2: This figure presents the ferrofluid rotary seal test setup by Bonvouloir in order to test high speed seal failure [44]. A hand pump has been used to pressurise the ferrofluid seal.

Anton et al. have reviewed some applications of ferrofluid sealing devices for vacuum [14]. Two ferrofluid seals incorporated in an aluminium equipment for headlights manufacturing ensure the vacuum tight rotation of a support with headlights. After 18 months of continuous operation both seals maintained their initial performances. Low vapor pressure diester based magnetic fluids were used. In vacuum or gas systems having special safety requirements a ferrofluid seal often is used in combination with a mechanical seal. The ferrofluid seal then is used as a secondary seal in order to minimise leakage. Ferrofluid seals are playing an important role in preserving the environment [16]. It is very difficult to hermetically seal for example a rotating pump shaft in chemical plants and refineries which emit volatile compounds and hazardous gasses that pollute the atmosphere. By implementing a ferrofluid seal it is possible to reduce emissions from 50 ppm to virtually 0 ppm. Today several ferrofluid sealing devices are successfully operating under demanding circumstances in vacuum and gas systems.

4-2 Marine Systems

Literature learns that the application of ferrofluid sealing technology in the marine industry seems very interesting. Nowadays elastomer lipseals are used for the sealing of rotary shafts against (sea)water [1]. Due to mechanical contact of the lipseals with the rotating shaft wear occurs, limiting its service life to a couple of years and causing leakage. Lipseals used in the sterntubes of propeller shafts in ships are reported to leak oil into the sea, polluting the marine environment [2]. The replacement of the lipseal is an expensive procedure because it results in downtime of the system.

Matuszewski has done research to ferrofluid rotary seals for sealing against water in marine applications. In his first paper he shows that a ferrofluid seal a 50 mm diameter shaft at 3000 rpm rotational speed can effectively work in water for a short amount of time [26, 18]. The longest test run performed on the setup was 201 hours. The shaft diameter of the propeller

of small boats and fish cutters is equal to 50 mm. In order to check if ferrofluid seals also could propeller shafts of medium sized ships, shaft diameter as to be increased to 200 mm. According to Matuszewski ferrofluid seals are very promising for ship propeller shafts due to their low resistance of motion [25]. In a new one stage test setup Matuszewski shows service life greatly depends on motion speed of the seal [18, 64]. This test setup is shown in figure 4-3. By using a pressure chamber containing water the sealing environment has been simulated. Matuszewski also has built a two stage ferrofluid sealing setup [65]. It was concluded that multi-stage ferrofluid seals can be efficiently used in water for rotating shaft seal for a limited range of motion velocity and cycles quantities (service life). Figure 4-4 shows a drawing of a patent filed by Tamama et al. in 1984 for the use of a ferrofluid seal in the driving propeller system of a ship [66]. Number 14 in the figure indicates the location of a ferrofluid sealing device which prevents water from entering the ship.

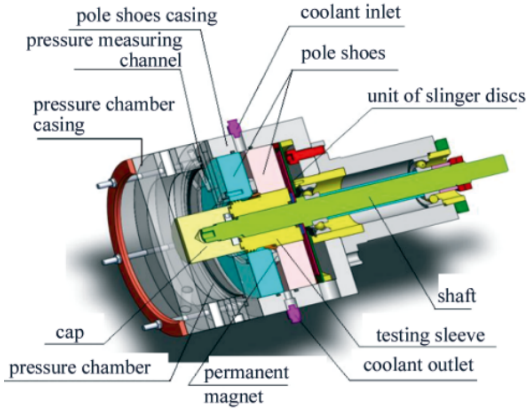

Figure 4-3: This figure presents the one stage ferrofluid seal test setup by Matuszweski [64].

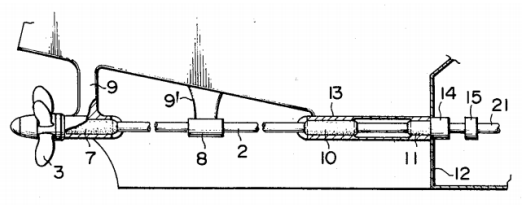

Figure 4-4: This figure presents an overview of the propeller system of a ship which implements a rotary ferrofluid seal (14). This patent has been filed by Tamama et al. in 1984 [66].

4-3 Rotary Blood Pump

Left ventricular assist device (LVAD) therapy has become an established treatment for patients with advanced heart failure. A rotary pump using a direct drive system that connects an impeller to the motor requires a shaft seal. This shaft seal has to create a boundary between the blood chamber and the motor. Mitamura and others have done research to the implementation of ferrofluid seals in rotary blood pumps [20]. Traditional mechanical seals in rotary blood pumps have drawbacks such as wear and power consumption. The first ferrofluid sealing device designed by Mitamura consists of a ring magnet with two pole pieces and a 3 mm rotating shaft [20]. A shield containing buffer blood was designed to stabilise the flow of the blood and to prevent mixing between ferrofluid and blood. This design remained intact for 51 days at 8000 rpm and 594 days under static conditions in water at 0.25 bar. Two years later, another paper has been published by Mitamura in corporation with Sekine on a similar design of the sealing device [52]. This design has been tested for the use in an axial flow pump. The results of a long-term durability test showed that the durability of the seal was more than 6 months. In 2010 Mitamura has published an article on a new ferrofluid seal design [5], presented in figure 4-5. This seal design has performed for over 275 days.

Most important change was the design of the shield structure. As can be seen in figure 4-5 the shield structure consists of a ring having same dimensions as the pole piece, instead of a structure creating a buffer. This ferrofluid sealing device is incorporated into the design of an axial rotary blood pump, which can be seen in figure 4-6. An impeller of 27 mm is attached to the rotating shaft. Distilled water was pumped at about 4 L/min. Also a variation on this design containing no shield has been tested in the pump system. Service life of this sealing device was only 6 and 11 days in experiments. It can be concluded the design of the shield structure is crucial for the service life of a ferrofluid sealing device in an axial rotary blood pump. This seal structure may also be useful in industrial applications.

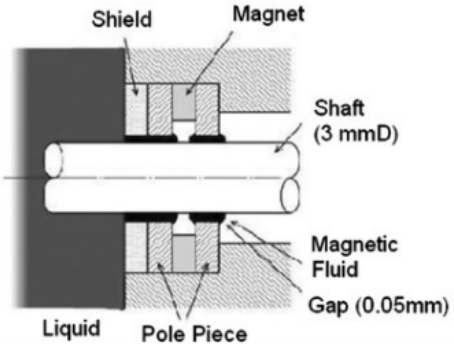

Figure 4-5: Design of a ferrofluid seal for a rotary blood pump by Mitamura et al. which performed for 275 days at sub-critical sealing conditions [5, 67, 42].

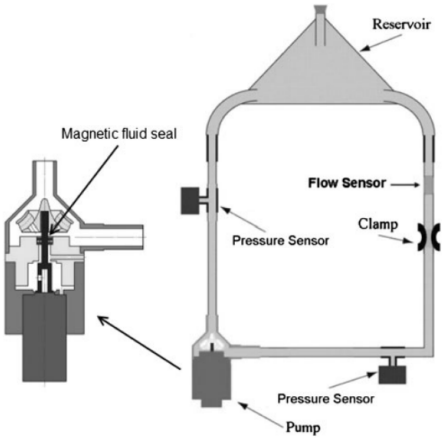

Figure 4-6: Overview of the rotary blood pump with a ferrofluid rotary seal designed by Mitamura [67].

4-4 Experimental Setups for Sealing Liquids

In literature some papers describing experimental setups for ferrofluid rotary seals operating in liquids have been published. Main goal of these experimental test setups is to identify parameters influencing the service life and sealing capacity of a ferrofluid rotary seal that seals liquids. One of the first papers published about an experimental setup for a ferrofluid rotary sealing device sealing liquid has been published by Kurfess and Müller [3]. They have built three rigs for testing ferrofluid sealing devices. Figure 4-7 shows one of the test setups containing a hollow glass shaft. A mirror and microscope allow to observe the liquid-liquid interface at the running shaft between the sealed liquid and the ferrofluid. The shafts of the setups have diameters 60 mm, 89 mm and 80 mm. Different hydrodynamic seal concepts have been placed in front of the ferrofluid and have been tested at speeds up to 3000 rpm. Above this speed the ferrofluid seals failed within less than one hour due to turbulence of the hydrodynamic seal at the interface of the liquid and ferrofluid. The longest test run was 6 weeks at a speed ranging from 500 to 3000 rpm. A radial run out of the rotating shaft up to 80% did not noticeably influence seal life of the ferrofluid seals. It was also concluded shielding can extend life time of a ferrofluid sealing device tremendously.

Szczech and Horak have conducted experiments focused on the dynamic tightness loss of ferrofluid seals on an one stage ferrofluid seal test setup without shield [17]. The nominal

seal diameter is 50 mm and the gap height 0.1 mm. Four different ferrofluids have been used in order to create a ferrofluid seal having a volume of 50 µl. Static and dynamic burst pressure experiments are performed. It is concluded a hydrophobic carrier liquid is preferred for the ferrofluid, resulting in the highest dynamic sealing capacity. Also the results showed ferrofluids with the lowest density and saturation magnetisation have the worst suitability for usage in water environment. The rate of water pressure decrease in the pressure chamber can be taken as the tightness loss of the ferrofluid seal. The authors considered that the increase in the viscosity difference between water and ferrofluid decreases the dynamic sealing capacity of the seal. This corresponds with the Kelvin-Helmholtz instability relation which is derived by Rosensweig. A mathematical model is proposed for the calculation of the sealing capacity of the seal as function of the shaft speed and properties of the ferrofluid used.

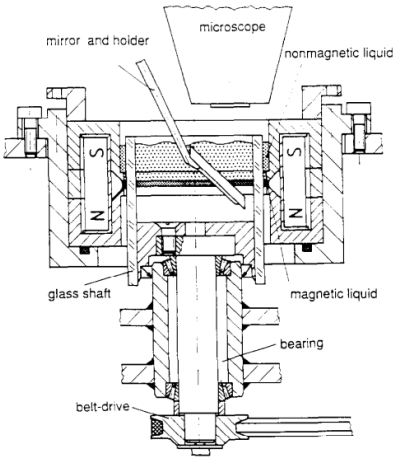

Figure 4-7: Ferrofluid seal test rig built by Kurfess and Müller which has a hollow glass shaft. A mirror and microscope are used to observe the liquid-ferrofluid interface around the running shaft [3].

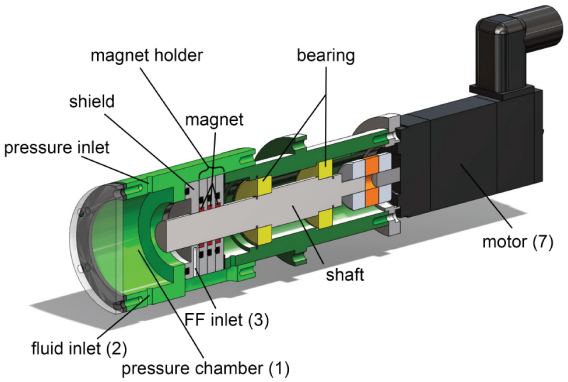

Figure 4-8: Demonstrator model built by Potma [4]. A manually operated syringe connected to the supply hole is used to add ferrofluid in bursts.

Liu et al. have designed a ferrofluid rotary seal test setup with an intention to establish a stable interface between the liquid sealed and the ferrofluid [19]. By introducing a bushing on the shaft and adding a shield they try to minimise magnetic leakage and relative velocities in order to improve the stability of the interface. The shaft of the device has a diameter of 20 mm and 5 ml of KLS-40 ferrofluid is injected in the sealing gap. The shaft was rotating at a speed of 1200 rpm and the sealing pressure was 3 kPa. The setup has sealed oil at these conditions for 10 weeks.

Potma has built an experimental test setup of a ferrofluid seal for liquids consisting of a shield and three magnets surrounding a 20 mm diameter shaft [4]. The test setup can be seen in figure 4-8. The theoretical static critical pressure of the system (37.47 kPa) was found to match the results of the experiments. An ferrofluid inlet connected to a syinge has been added in front of the first seal in order to supply ferrofluid to the seal. At a shaft speed of 6000 rpm and water pressurised at 22.5 kPa the seal failed after 51 minutes. In another experiment ferrofluid was added to the seal in bursts of 0.1 ml every couple of minutes while sealing sealing water at a pressure of 20 kPa. During the experiment the shaft speed also was

increased every couple of minutes from 0 rpm till 3000 rpm. It is concluded in the research that the burst addition of the ferrofluid at 3000 rpm resulted in a premature failure of the seal (12 minutes service life). For short periods of time the seal was capable to seal sub-critical pressurised water at a speed range between 0 and 6000 rpm.

4-5 Patents

Since the 1970's different design configurations for ferrofluid seals have been patented. This section discusses some of the patents that have been filed. Patents of ferrofluid rotary seals are classified as sealings between relatively-moving surfaces by means of a fluid kept in sealing position by magnetic force. Most of these patents are already expired. Figure 4-9 presents a drawing taken from a patent on a magnetic fluid seal filed by Ezekiel in 1981 [68]. In this patent a magnetic fluid seal comprises a single axially magnetised permanent magnet in the shape of a flat ring having magnetic liquid captured on the inside or outside diameters is described. Moskowitz and others have filed a patent that describes a design configuration consisting of a dynamic lip seal using a ferrofluid seal as sealant and lubricant [69]. An overview of the design can be seen in the drawings of figure 4-10. The ferrofluid forms a film between the shaft and the elastomer material seal element. By cooling and lubricating the contact interface the ferrofluid film extends the service life of the elastomer material. The seal assembly has permanent magnetic elements which create a magnetic field.

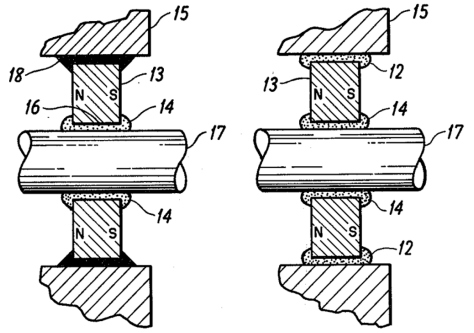

Figure 4-9: Drawing of a basic rotary ferrofluid seal design found in a patent filed by Ezekiel [68].

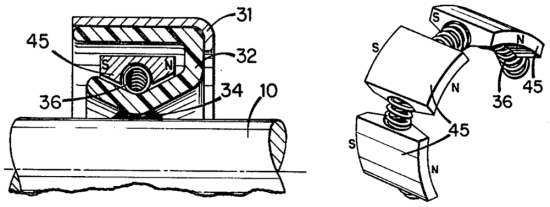

Figure 4-10: Hybrid design of a dynamic lip seal using a ferrofluid seal as sealant and lubricant [69].

Raj and Casciari have filed a patent for a single pole piece ferrofluid rotary seal, presented in figure 4-11. By using a pole piece the magnetic flux path is directed and the ferrofluid can be positioned. Figure 4-12 shows a design of a ferrofluid seal for a shaft having several sealing gaps concentrically arrayed around the shaft [70]. By doing so the pressure difference that the device has to withstand is divided on multiple ferrofluid seals, thereby increasing the sealing capacity of the device.

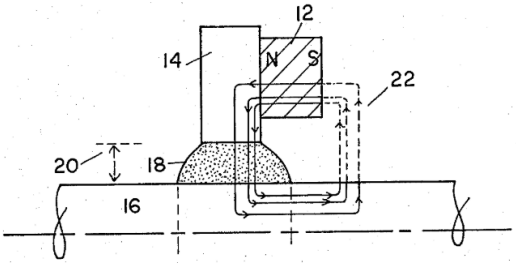

Figure 4-11: Drawing of a single pole piece ferrofluid rotary seal in a patent filed by Raj and Casciari [71].

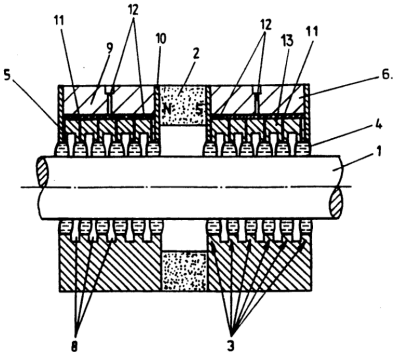

Figure 4-12: Ferrofluid seal for a shaft comprising several sealing gaps concentrically arrayed around a shaft [70].

Figure 4-13 shows the drawing of a patent which describes a ferrofluid seal that is used to seal a shaft that is engaged in linear motion [72]. Typically environments in which the system could operate is vacuum. The design of a bearing assembly with an integrated ferrofluid seal can be seen in figure 4-14 [73]. This design can be used to support the spindle disk driveshaft that drives a computer magnetic disk. An integrated ferrofluid seal located at number 40 in figure 4-14 protects the computer disk and memory head against contamination from the outside environment.

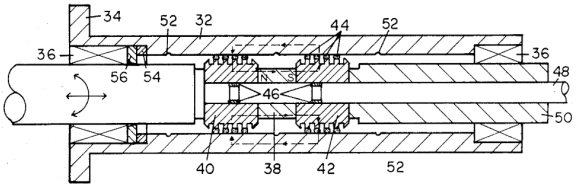

Figure 4-13: Ferrofluid seal to provide a hermetic seal about a shaft engaged in linear motion [72].

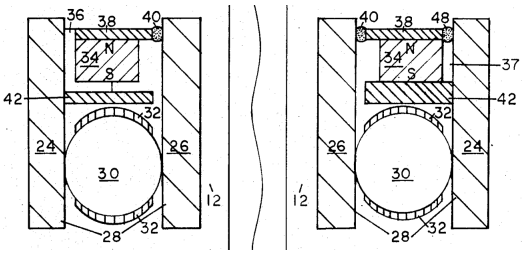

Figure 4-14: Design of a bearing assembly with integrated ferrofluid seal [73]. The ferrofluid seal is located at number 40.

Chapter 5

Paper: Ferrofluid Rotary Seal with Replenishment System for Sealing Liquids

Ferrofluid Rotary Seal with Replenishment System for Sealing Liquids

K. van der Wal, R. A. J. van Ostayen, and S. G. E. Lampaert
Department of Precision and Microsystems Engineering, Delft University of Technology, The Netherlands

Ferrofluid rotary seals are mechanical contact-free magnetic liquid seals and are characterised by their simple structure, low friction and ability to hermetically seal. Although ferrofluid rotary seals for sealing vacuum and gases are part of a well established industry, the sealing of liquids has not been implemented yet. Literature learns that degradation of the ferrofluid seal over time when it dynamically contacts a liquid results into premature seal failure. This paper presents a new type of ferrofluid rotary seal which implements a ferrofluid replenishment system that renews its ferrofluid seals while sealing capacity is maintained. By replacing the degraded ferrofluid seals at a sufficient rate service life of the ferrofluid rotary seal that seals liquids can theoretically be extended towards infinity. An analytical model and FEM analysis are used to design the ferrofluid sealing device and to predicts its sealing capacity. An experimental test setup has been built on which the sealing capacity and service life of the device has been tested for different sealing conditions. It is demonstrated that the ferrofluid replenishment system successfully extends and controls the service life of the ferrofluid rotary seal that dynamically seals pressurised water.

Keywords: magnetic liquid seal, lip seal, water, ferrofluid transport, magnetics

1 Introduction

In the 1960's the world's first patented magnetic fluid was created by adding magnetic properties to rocket fuel, enabling control of the fluid in outer space using magnets [1]. Funded by space agency NASA Ronald E. Rosensweig led the development of a wide variety of magnetic fluids and the research to the fluid mechanics of magnetic liquids [2, 3]. Ferrofluid is a magnetic fluid that consists of ferromagnetic nanoparticles suspended in a carrier liquid [4]. The three main application areas of ferrofluids are sealing, damping and heat transfer [5]. In most of these applications ferrofluid is positioned magnetically and secondary properties of the fluid are then exploited. An example of application are ferrofluid planar bearings, where absence of both stick slip and mechanical contact result in respectively a high precision and high durability [6, 7].

Since the 1930's radial lip seals are industries standard to retain lubricant and exclude contamination in rotating shaft and bearing applications [8]. This contact-based rotary seal is inherently subjected to wear, which limits its service life and causes leaks. Ferrofluid rotary seals are contact-free magnetic liquid seals and are characterised by their simple structure, low friction and ability to hermetically seal. Ferrofluid rotary seals operating in vacuum and gas environments already have proven themselves in industry [9, 10, 11]. Ferrofluid sealing is also considered to be very important in preserving the environment, since ferrofluid is able to create hermetic sealing for hazardous gases [12].

However, literature learns that ferrofluid rotary seals fail prematurely when they are used for sealing liquids [13, 14, 15, 16, 17]. The driving mechanisms causing this premature failure are not fully understood and prevent current implementation for sealing liquids. Many authors attribute this limited service life to the arise of interfacial instabilities between the liquid that is sealed and the ferrofluid of the seal [18, 13]. When the liquid-ferrofluid interface becomes unstable, ferrofluid emulsifies with the liquid sealed which results in failure of the seal. Mitamura et al. have shown that a shielding structure in front of the ferrofluid rotary seal can be used to stabilise the interface between the two fluids [19, 20, 21]. Despite shielding prevents instant seal failure caused by interfacial instability, the service life of the seal is still limited and unpredictable.

It is reported in literature that the magnetic properties of ferrofluid in contact with water decrease [22]. Also it is suggested that the existence of shearing forces at the interface of the ferrofluid seal and liquid contained limits its service life [23]. Shear forces between the liquid sealed and ferrofluid could cause gradual removal of ferrofluid [24]. All these effect could attribute to the degradation of the ferrofluid seal when it dynamically seals a liquid. Degradation decreases the sealing capacity of the seal over time and causes seal failure when its sealing capacity becomes lower than its required operational sealing pressure. When service life can be improved ferrofluid sealing technology seems very promising for marine applications [25, 26].

This paper presents a new type of ferrofluid rotary seal which implements a ferrofluid replenishment system that renews its ferrofluid seals while sealing capacity is maintained. By replacing the degraded ferrofluid seals at a sufficient rate service life of the

ferrofluid rotary seal that seals liquids can theoretically be extended towards infinity. First an analytical model and FEM analysis of the ferrofluid sealing device is presented. Next stability of ferrofluid in the seal, shielding and ferrofluid replenishment is discussed. The acquired knowledge is used to design an experimental test setup for a series of experiments in order to identify both static and dynamic sealing capacity of the system. Finally these results are used to perform an series of experiments in order to validate the ferrofluid replenishment system improves the service life of the ferrofluid rotary seal that dynamically seals pressurised water.

2 Methods

In order to design a ferrofluid rotary seal that seals liquids first an analytical model that describes its sealing capacity is derived. Subsequently the required magnetic field intensities for this analytical model are calculated by FEM analysis performed using COMSOL Multiphysics©. Next, the influence of the magnetic field gradient stability of ferrofluid on its sealing capacity is discussed. In order to prevent dynamic seal failure shielding of the seal is discussed and the new concept of ferrofluid replenishment is introduced. Finally, the experimental test setup and experimental procedures are elaborated.

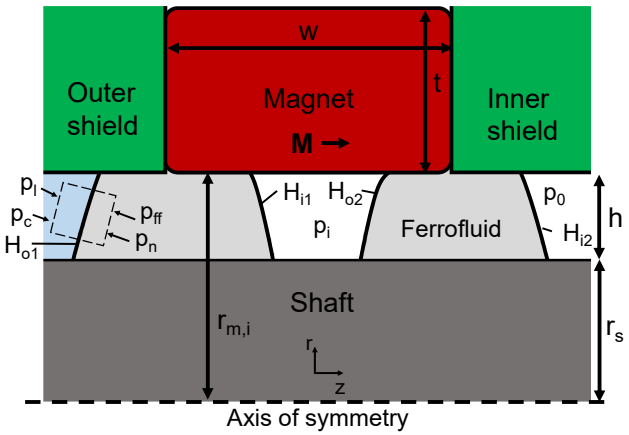

Figure 1: This figure presents a cross-sectional overview of the ferrofluid rotary sealing system that consists of an axially magnetised ring magnet surrounding a ferromagnetic shaft. Ferrofluid magnetically positioned in the seal gap prevents liquid to leak through the seal gap. The inner and outer shield are made of non ferromagnetic material.

2.1 Analytical model

A cross-sectional overview of a basic ferrofluid rotary sealing system is presented in figure 1. The system consists of an axially magnetised ring magnet that is placed around a ferromagnetic shaft and supported by a non magnetic structure (green). Two ferrofluid seals that are located in the seal gap maintain the pressure difference between the liquid that is sealed and the atmosphere $(p_l - p_0)$. In order to calculate the static sealing capacity of the two ferrofluid seals in the sealing system an analytical model will be derived. The behaviour of the ferrofluid in terms of its motion as a function of time can be described using the Navier-Stokes equations for Newtonian incompressible magnetic fluids [27], presented in relation 1.

$$\rho_{ff}\frac{\mathrm{D}\mathbf{v}}{\mathrm{D}t} = \underbrace{-\nabla p_{ff}}_{\text{Pressure}} + \underbrace{\eta\nabla^2\mathbf{v}}_{\text{Viscous}} + \underbrace{\rho_{ff}\mathbf{g}}_{\text{Gravity}} + \underbrace{\mu_0 M\nabla H}_{\text{Magnetic}} \qquad (1)$$
$$\nabla\cdot\mathbf{v} = 0$$

The left side term is the density of the ferrofluid ρ_{ff} times the rate of change following the mass motion $\mathbf{v}$, also known as the material derivative. The right side of equation 1 is the sum of the pressure, viscous, gravity and magnetic body forces normalised to a unit volume. Only non-rotating static shaft conditions are considered, which means that inertial and viscous effects on the pressure distribution can be neglected. Gravitational effects will also be neglected in this analysis since they are small. The relation presented in equation 1 can now be reduced to the relation shown in equation 2 and now only contains the pressure and magnetic terms.

$$\nabla p_{ff} = \mu_0 M\nabla H \qquad (2)$$

where p_{ff} is the pressure inside of the ferrofluid, μ_o the permeability of vacuum, M magnetisation of the ferrofluid and H the magnetic field intensity. In order to calculate the sealing capacity of both ferrofluid seals combined $(p_l - p_0)$, the boundary conditions at the interfaces of the seals have to be investigated. In figure 1 the dashed box indicates the boundary condition at the interface between the liquid that is sealed and the ferrofluid of the first seal. Equation 3 presents this boundary condition.

$$p_l + p_c = p_{ff} + p_n \qquad (3)$$

Besides bulk pressures p_l and p_{ff} also interfacial pressures p_n and p_c are present at the liquid-ferrofluid interface. Pressure p_c is the capillary pressure between the liquid that is contained and the ferrofluid and pressure p_n is the normal magnetic pressure.

Capillary pressures will be neglected in the analytical model of the sealing capacity, considering its impact is low compared to the magnetic pressures generated inside of the ferrofluid [28]. The magnetic normal pressure p_n is equal to $\mu_0 M_n^2/2$, where M_n is the normal magnetisation force vector at the interface of the ferrofluid seal. The normal magnetic pressure p_n for the ferrofluid seals can also be neglected since the magnetic field is uniform and tangential to the interfaces of the ferrofluid seals [27].

Due to previous assumptions the pressure build up in the first seal can be calculated by using only equation 2. The magnetisation M of the ferrofluid is a function of the magnetic field intensity. Since magnetic field intensity in the sealing gap is high compared to the saturation magnetisation of ferrofluid, it is safe to assume the ferrofluid will be fully magnetically saturated ($M = M_s$). The maximum pressure difference between p_l and p_i then can be calculated by integrating in axial direction along the length of the seal, which is presented in equation 4.

$$\begin{aligned} p_l - p_i &= \int_c \nabla p_{ff} \cdot \mathrm{d}\mathbf{z} = \mu_0 M_s \int_c \nabla H \cdot \mathrm{d}\mathbf{z} \\ &= \mu_0 M_s (H_{o1} - H_{i1}) \end{aligned} \tag{4}$$

Equation 4 learns the pressure build up of the first seal depends on the magnetic field intensity H_{o1} at the liquid-ferrofluid interface and the magnetic field strength H_{i1} at the ferrofluid interface on the inside of the seal. The sealing capacity of the second seal can be calculated in a similar way, only now the magnetic field strength H_{o2} at the interface on the inside of the seal and the magnetic field strength H_{i2} at the ferrofluid-air interface have to be used. Relation 5 presents the calculation of the total pressure build up $p_l - p_0$ of both seals combined.

$$p_l - p_0 = \mu_0 M_s \left((H_{o1} - H_{i1}) + (H_{o2} - H_{i2}) \right) \tag{5}$$

When pressure difference $p_l - p_0$ on the two ferrofluid seals becomes larger than the sealing capacity of the two seals that is predicted by relation 5, the seals will burst and the liquid that is sealed will leak through the seal gap.

2.2 FEM Analysis

Equation 5 presented in section 2.1 learns that the magnetic field intensities ($H_{o1}, H_{i1}, H_{o2}, H_{i2}$) at the interfaces of the two ferrofluid seals are required in order to calculate its static sealing capacity. These magnetic field intensities are calculated using the numerical analysis package COMSOL 5.3 Multiphysics.

The magnetic properties of the shaft material have a lot of impact on the distribution of the magnetic field intensity in the seal system. Shafts that operate in aqueous environments and transmit torque often are made of stainless steel. There are four main families of stainless steels which are primarily classified by their crystalline structure. These are ferritic, austenitic, martensitic and duplex stainless steels. Of these four ferritic stainless steels have the best magnetic properties. Therefore the material of the shaft is selected to be ferritic stainless steel (AINSI 430F) and is modelled using the BH curve from the COMSOL material library (stainless steel 430F annealed). The ring magnet is modelled by a remanence magnetisation $\mathbf{B}_r$ and is magnetised in axial direction. Fillets of radius r_{fil} of the used ring magnet are constructed in all corners. Seal gap h of the seal system is 100 µm. Table 1 presents an overview of the parameters of the ferrofluid sealing device that is used in the FEM analysis.

Table 1: This table presents parameters of the sealing system which are used in the FEM.

Design Parameters			
r_{fil}	0.3 mm	$\mathbf{B}_r$	1.28 T
r_s	3.9 mm	w	6 mm
$r_{m,i}$	4 mm	h	100 µm
t	3.5 mm	M_s	35 kA/m

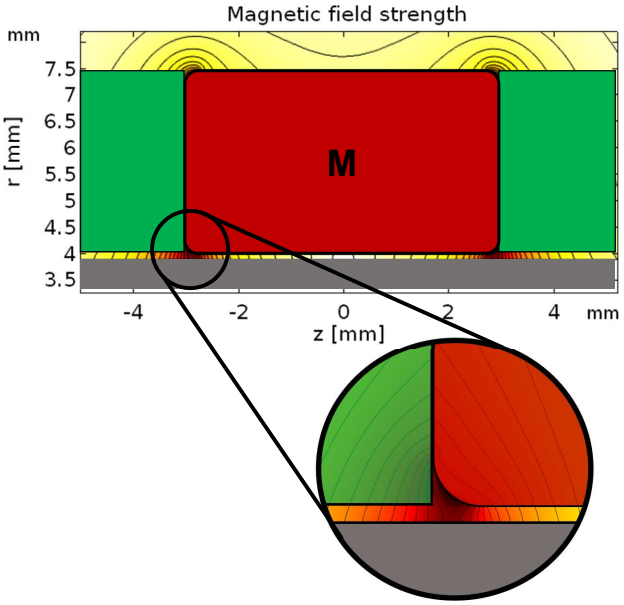

Figure 2: This figure presents the magnetic field intensity of the seal having a ferritic stainless steel (AINSI 430F) shaft. The isolines of the magnetic field intensity are also the isolines of the pressure distribution in the ferrofluid. When the seal is not pressurised the ferrofluid shapes according to these isolines.

Figure 2 presents a two dimensional plot of the magnetic field intensity in the system. Due to symmetry only half of the system has to be modelled. The colour grade represents the strength of the magnetic field, where red is highest magnetic field intensity and white the lowest. Black lines in the seal gap represent the magnetic isolines. Equation 2 learns these isolines are equal to the isolines of the pressure distribution in the system. When the seal is not pressurised the ferrofluid will shape according to these isolines. Analysing the course of these lines also results in the conclusion that two independent ferrofluid seals can be formed by the magnetic field distribution in the seal.

The magnetic field distribution of the seal system is evaluated along two horizontal lines in the sealing

gap, one at the top of the gap (h) and one at bottom. Figure 3 presents a lineplot of these magnetic field intensities. Previous section showed the sealing capacity of the ferrofluid seals depends on the magnetic field difference $H_{o1} - H_{i1}$ and $H_{o2} - H_{i2}$. Since the seal will start to fail at its weakest spot, the magnetic field intensities that predict the lowest sealing capacity have to be used.

In order to reach full performance potential of the seal system the magnetic field difference ΔH on each ferrofluid seal has to be as high as possible. The inner shield, also shown in figure 1, makes sure the ferrofluid of the second seal is directed to a region of low magnetic field intensity (H_{i2}). The magnetic field intensity plot of figure 3 learns that the inner shield has to have a width of around 6 mm in order to create a high magnetic field difference on the second seal and therefore a high sealing capacity.

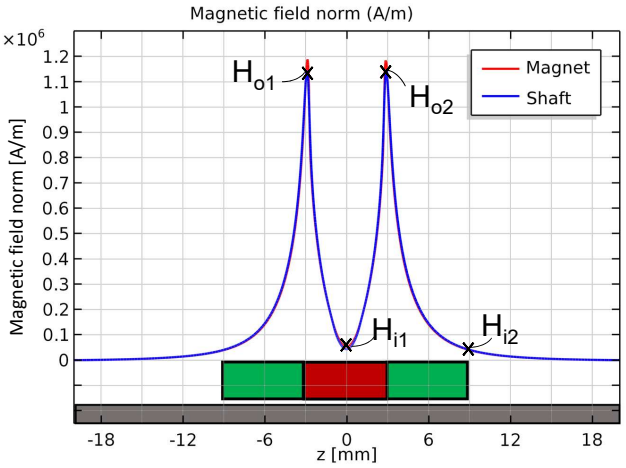

Figure 3: This figure presents the magnetic field intensity evaluated at two horizontal lines along t axial direction at the top and bottom surfaces of seal gap h. The material of the shaft is ferritic stainless steel (AINSI 430F).

The ferrofluid (Ferrotec EFH1) that will be used in the sealing system consists of a light hydrocarbon carrier liquid with magnetite (Fe_3O_4) suspended particles. The saturation magnetisation of the ferrofluid M_s equals 35 kA/m. Table 2 gives an overview of the magnetic field intensities at the two interfaces of both seals which have been found in the FEM analysis. The sealing capacity of both seals now can be calculated using equation 2 The total predicted sealing capacity of the two ferrofluid seals combined equals 96.2 kPa.

Table 2: This table presents magnetic field intensities at the seal interfaces and predicted sealing capacity of both seals.

	$H_o \cdot 10^5$ [A/m]	$H_i \cdot 10^5$ [A/m]	Δp [kPa]
Seal 1	11.4	0.541	47.8
Seal 2	11.4	0.410	48.4

2.3 Magnetic field gradient stability of ferrofluid

Since the ferrofluid in the sealing system is a colloidal dispersion of magnetic particles in a liquid carrier, stability of that colloid is an important property of the seal. In static sealing conditions the magnetic field gradient in the seal generated by the ring magnet, shown in figure 2, can cause migration of the magnetic particles. Particles travel through the fluid to a higher intensity region of the magnetic field [29]. This phenomenon results in a non homogeneous ferrofluid that has a higher effective magnetisation. The sealing capacity that is measured will be higher than predicted using relation 5. By rotating the shaft at sufficient speed the ferrofluid in the seal could become homogeneous again.

The stability of the magnetic particles in the magnetic field gradient can be analysed by comparing their thermal energy E_{Therm} and magnetic energy E_{Mag}. Thermal motion counteracts the magnetic field force and provides statistical motion that results in a distribution of the particles in the magnetic fluid. In equation 6 the ratio between both energies is presented.

$$\frac{E_{Therm}}{E_{Mag}} = \frac{k_B T}{\mu_0 M_p H V_p} \tag{6}$$

The thermal energy per particle can be calculated by the product of the Boltzmann's constant k and absolute temperature T. The magnetic energy represents the work in transferring the particle to the higher magnetic intensity region in the fluid. The magnetic energy per particle E_{Mag} can be calculated by the product of magnetic permeability of vacuum μ_0, magnetisation of the particle M_p, magnetic field intensity H and particle volume V_p. It can be concluded that particle size is an important property of the ferrofluid that influences its stability in the seal.

2.4 Shielding

A relative velocity between the liquid that is sealed and ferrofluid of the seal can cause interfacial instability which results into seal failure [13, 30]. By introducing a shield into the design of a ferrofluid seal sealing liquids the liquid-ferrofluid interface can be stabilised and instant seal failure due to interfacial instability prevented [21, 19]. The simple outer shield structure presented in figure 1 is found to be most effective [19]. Experiments and CFD analyses of flow in a ferrofluid seal showed the shield stabilises the interface between water and the ferrofluid. Figure 4 visualises the velocity profiles of the liquid sealed and the ferrofluid of the seal when a no slip condition is assumed. Also it is assumed flows in and in front of the seal gap are laminar and that the velocity profiles are linear.

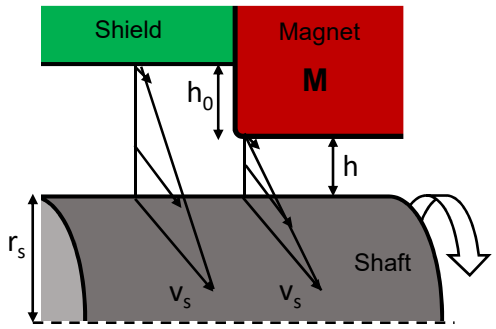

Figure 4: This figure presents the velocity profiles of the liquid that is sealed and the ferrofluid of the seal. Due to a height difference h_0 between the magnet and shield of the system a relative velocity between the fluids is created.

Equation 7 presents a relation for calculating the relative velocity between the liquid that is sealed and ferrofluid of the system.

$$v_{ff} - v_l = v_s \cdot \frac{h_0}{h_0 + h} \tag{7}$$

where v_{ff} and v_l are the velocities of ferrofluid and liquid that is sealed, v_s the surface speed of the shaft and h_0 the difference in gap height between the shield and seal gap h. If a seal system design is considered with large difference in h and h_0, velocity difference can be approximated by surface speed v_s. It can be seen that height difference h_0 is an important design parameter for minimising relative velocity between the liquids and preventing premature seal failure.

The Kelvin-Helmholtz instability for magnetic liquids derived by Rosensweig is often used to describe the stability of the liquid-ferrofluid interface [27, 18, 13]. The Kelvin-Helmholtz is a hydrodynamic instability in which two inviscid fluids are in relative and irrotational motion. The velocity and density profiles are discontinuous at the interface between the two fluids. Besides preventing instability of the interface between the liquid sealed and ferrofluid, shielding also decreases shearing forces on the ferrofluid. Shearing force on the ferrofluid is dependent on viscosity, relative velocity of the fluids and the contact area between the liquids. When shaft diameter and seal gap of the system increases, shear forces affecting the performance of the seal could also increase.

2.5 Ferrofluid replenishment system

Although shielding of a ferrofluid rotary seal that seals liquids prevents instant dynamic seal failure due to interfacial instability, service life of the seal is still limited. Degradation of the ferrofluid seal decreases the sealing capacity over time and causes failure of the seal when its sealing capacity becomes lower than the required operational sealing pressure.

In order to solve this problem, the work introduces and implements a ferrofluid replenishment system into the design of a ferrofluid rotary seal (also partially presented in [31, 32]). The system replenishes the ferrofluid of the seals by facilitating axially transport of ferrofluid from one seal to another.

Figure 5 presents an overview of the process of ferrofluid transport through the two seals of the ferrofluid rotary sealing system that also was elaborated in sections 2.1 and 2.2. First an amount of new ferrofluid is radially injected through a supply channel in front of the first seal (step 1). By doing so the same amount of original ferrofluid at the lowest pressure region of the first seal (interface of H_{i1}) will jump from the first seal to the second seal. This can be seen in steps 2 and 3 presented in figure 5. When the second seal is supplied with ferrofluid from the first seal, ferrofluid at the lowest pressure region of the second seal (interface of H_{i2}) will be pushed to the right through the sealing channel (step 4). This ferrofluid will eventually be pushed to the end of the sealing channel where it can be collected, potentially for recycling.

The sealing capacity of the ferrofluid seals is restored when the degraded ferrofluid is replaced by new ferrofluid. If the ferrofluid in the seal constantly is being replaced at sufficient rate, the service life of the ferrofluid rotary seal theoretically could be extended towards infinity.

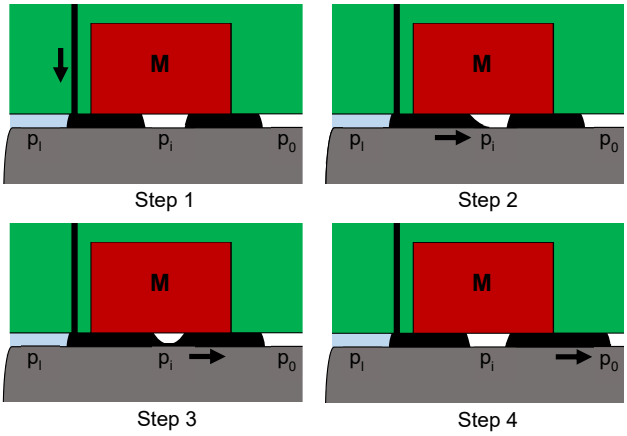

Figure 5: This figure presents the concept of axial ferrofluid transport through the seal. During step 1 new ferrofluid is radially added in front of the first seal. In steps 2 and 3 ferrofluid flows from the first seal to the second seal. In step 4 ferrofluid of the second seal is pushed to the ferrofluid outlet at the right.

In order to prevent the ferrofluid from flowing towards the liquid that is sealed instead of through the seals, it is required that the liquid pressure p_l is sufficiently high in order to let the ferrofluid jump from the first to the second seal. In figure 3 the magnetic field intensity H_{i1} between the two seals can be seen. This magnetic field intensity can be used to calculate a pressure p_{min}, in order to define the operational range of the sealing system having axial ferrofluid trans-

port. The sealing capacity of the seal system can be increased when multiple seals are placed after each other [33]. Equation 8 presents a general relation for the upper- and lower-bound of liquid pressure p_l for the ferrofluid rotary sealing system when ferrofluid is axially transported through its seals.

$$p_0 + p_{min} < p_l < p_0 + N\Delta p_j \tag{8}$$

where p_0 is the atmospheric pressure, p_{min} minimum pressure, N the number of seals and Δp_j the seal capacity of each seal. It can be seen that if the number of seals increases, the operational range of sealing pressure p_l also increases. It is important to note that the sealing capacity decreases when the shaft speed increases. This also means that the operational range of the sealing system having ferrofluid transport is different for static and dynamic sealing conditions. The refreshment rate of the seal system has to be sufficiently high in order to compensate for the degradation rate of the seal and thus to prevent seal failure. If the volume of the seal is known the replacement rate of the ferrofluid seal can be calculated using the relation presented in equation 9.

$$R = \frac{\pi \cdot \left((r_s + h)^2 - r_s^2\right) \cdot w_{seal}}{Q_{ff}} \tag{9}$$

where R is the rate at which the seal is being replaced, r_s the shaft radius, h the seal gap height, w_{seal} the total seal width and Q_{ff} the ferrofluid supply rate. Equation 9 assumes that new and original ferrofluid in the sealing system do not mix and that ferrofluid only flows from the high pressure region to the low pressure region.

2.6 Experimental test setup

The theory presented before is used to design and manufacture a ferrofluid rotary seal module and test setup in order to validate if the ferrofluid replenishment system improves and controls the service life of a ferrofluid rotary seal that seals. An axial magnetised ring magnet (HKCM R15x08x06ZnPc-42SH) having a remanent magnetisation B_r of 1.28 T, also discussed in section 2.2, generates the magnetic field distribution inside of the ferrofluid sealing module. Corrosion of the magnet is prevented by its coating of parylene and zinc. The shaft ($\varnothing = 8$ mm) is made of ferritic stainless steel (AINSI 430F), creating the magnetic field distribution presented in figure 2. A lathe is used to decrease the diameter of the shaft in the seal module and pressure chamber to 7.8 mm, creating a seal gap of 100 µm. The ferrofluid used in the setup and experiments is Ferrotec EFH1 and generates a theoretical sealing capacity of 96.2 kPa, which was calculated during the FEM analysis.

Figure 6 presents an overview of the ferrofluid seal module that has been designed and manufactured. The four layers of transparent acrylic sheets are mounted by transparent tape-sheet (3M 7955MP) having a thickness of 127 µm. All acrylic parts have been manufactured using a laser cutter. By using transparent structural material good visibility inside of the ferrofluid rotary seal is enabled. Layer 1 functions as inner shield and creates a shielding channel that stabilises the liquid-ferrofluid interface. Acrylic sheet layer 2 contains a small milled channel of approximately 1 mm depth and width which is used for radial supply of ferrofluid in front of the first seal. The ring magnet is supported by layer 3 and this layer also contains a brass tube connector for the ferrofluid supply hose. Finally, layer 4 functions as outer shield and makes sure ferrofluid of the second seal is directed towards a low intensity region of the magnetic field. The magnetic field intensity plot of figure 3 showed that a layer thickness of 6 mm is sufficient in order to reach the full potential of the sealing capacity of the second ferrofluid seal.

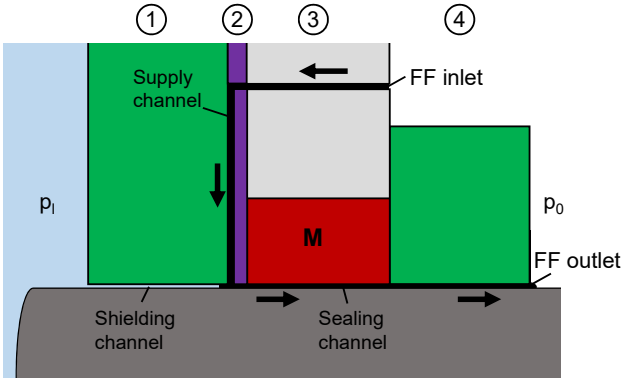

Figure 6: This figure presents a cross-sectional view of the seal module. The seal module consist of 4 different layers of transparent acrylic sheets.

Ferrofluid flows into the seal module via the inlet of layer 3 and enters through a hole in the supply channel of layer 2, which ends just before the first seal. Subsequently ferrofluid travels through the sealing channel to the ferrofluid outlet. Due to gravity the ferrofluid will leak along the surface of the outer shield out of the system. Table 3 presents an overview of width and function of the four layers.

Table 3: This table presents an overview of the transparent acrylic layers used in the sealing module. The layers are connected by 127 µm transfer tape (3M 7955MP).

Layer	Width	Function
1	6 mm	Outer shield
2	2 mm	Supply channel
3	6 mm	Magnet support
4	6 mm	Inner shield

In order to simulate the sealing environment the sealing module is mounted on a pressure chamber

(6082T6 AlMgSi) by non magnetic bolts. Figure 7 presents a cross sectional view of the test setup. The transparent acrylic cover plate enables good visibility inside of the pressure chamber. The total volume of the pressure chamber is approximately 58 ml. The liquid that is stored in the pressure chamber is pressurised by air through the pressure inlet. The shaft is supported by two pillow block ball bearings made of a zinc alloy. The ferrofluid supply hose is connected to the ferrofluid inlet of the seal module.

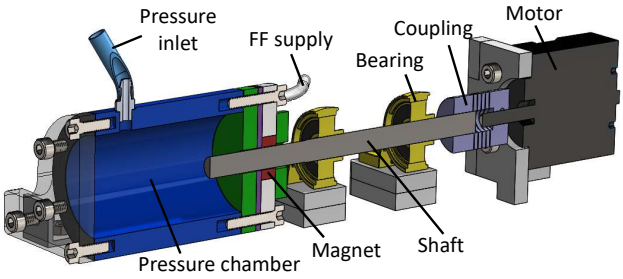

Figure 7: This figure presents a cut through of the test setup. The seal module is mounted on a pressure chamber which simulates the sealing environment. A DC motor drives the ferromagnetic shaft supported by two ball bearings.

In order to perform consistent experiments it is important that the surface speed of the shaft is constant and therefore is velocity controlled. A 24 V brushless DC motor (Trinamic QBL4208-41-04-006) is connected to the shaft by a aluminum flexible motor coupling. The DC motor is supported by an acrylic structure and controlled using a single axis driver module (Trinamic TMCM-1640). A computer with software (TMCL-IDE 3.0) is connected to the driver module in order to provide instructions to the DC motor.

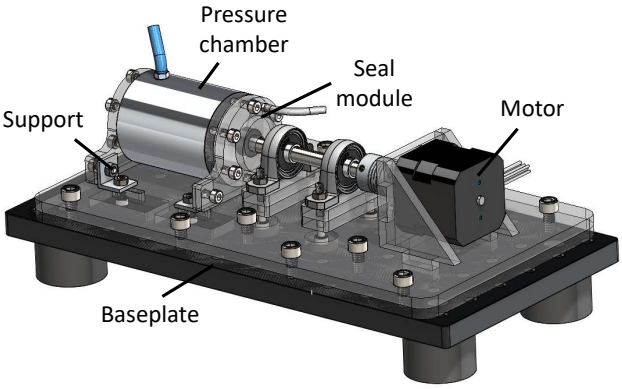

Figure 8: This figure presents a render of the experimental test setup. The setup is mounted on an aluminum breadboard base.

A render of the test setup is presented in figure 8. The pressure chamber is mounted to an acrylic baseplate by supports (6060T66 AlMgSi 0.5). The holes of these supports are slightly larger than the bolts used for mounting, enabling alignment of the seal module around the shaft. Also slots have been made in the acrylic support plate in order to set enable alignment of the sealing module. The base consists of an aluminum breadboard (Thorlabs) with four sorborthane vibration isolaters (Thorlabs ⌀ 38.1 mm). Non magnetic stainless steel bolts are used throughout the system for mounting. The setup has been placed inside of an aluminum drip tray.

A global overview of the experimental test setup including supporting systems is presented in figure 9. The air pressure that is used in order to pressurise the pressure chamber is generated by a compressor and regulator. A needle valve is added for the manual control of the pressure rise. In order to stabilise the pressure a buffer tank having a volume of 2 liters is added. A ball valve is used to shut off the pressure of the pressure chamber after desired sealing pressure is reached. Ferrofluid is rate controlled added to the system by the combination of a syringe pump (WPI SP100iZ) and a 3 ml syringe (HSW soft-ject). The device allows to set the rate and total volume of ferrofluid supply. The syringe and ferrofluid supply hose are connected by a Huer lock connection in order to make refill of the syringe convenient.

The air inlet hose of the pressure chamber is split and connected to a monolithic silicon gauge pressure sensor (MPX4250DP). The sensor measures the pressure inside of the pressure chamber (p_l) relative to the ambient air pressure (p_0). This means that the sealing capacity of the seal ($p_l - p_0$) is directly measured by the pressure sensor. The sensor is connected to a 16 bit analog I/O device (NI USB-6211). Labview 2013 has been used to live display the pressure inside of the pressure chamber and to store the sensor data that has been obtained during the experiments. The pressure is sampled at a frequency of 10 Hz.

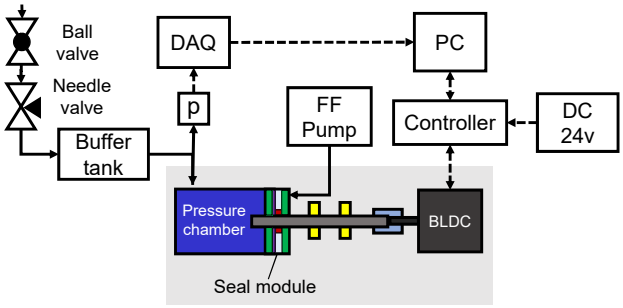

Figure 9: This figure presents a global overview of the experimental test setup and its supporting systems. Continuous arrows represent flows of air or ferrofluid, dotted arrows represent digital signals.

2.7 Experimental procedure

2.7.1 Examination of sealing capacity

The first performance parameter of the ferrofluid sealing system that will be experimentally evaluated is its sealing capacity for a number of different static and dynamic sealing conditions. It is important that the

exact moment of seal failure is obvious. That is why for the experiments evaluating the sealing capacity the buffer tank is removed. The sealing device is prepared for each sealing condition by first transporting ferrofluid through the sealing system. Once the sealing channel is completely filled with ferrofluid the supply is stopped and the seal is considered to be ready. During all experiments that have been performed the alignment between the seal module and shaft will not be changed.

First the static sealing capacity of the system is tested when it seals demineralised water. The sealing capacity is tested 5 times immediately after the test setup is prepared and 3 times 24 hours after the setup is prepared. During this settling time of 24 hours the seal is not pressurised, shaft speed is zero and the ferrofluid replenishment system is not active. These experiments are also conducted for air as sealed medium. The dynamic sealing capcity of the system when demineralised water is sealed is tested at five different shaft speeds, ranging from 500 till 2500 rpm.

In order to obtain the sealing capacity of the system during a certain sealing condition the pressure inside the pressure chamber will be increased until the seal bursts. The rate of pressure increase is manually controlled using the needle valve. The pressure of the pressure chamber is live monitored during the experiments. When the seal bursts during an experiment the needle and ball valve are closed.

2.7.2 Examination of service life

When the static and dynamic sealing capacity of the seal system are determined, the influence of the ferrofluid replenishment system on the service life of the seal can experimentally be examined. Service life of the seal system that seals demineralised water is dependent on shaft speed, sealing pressure and rate and duration of ferrofluid transport through the seal.

The pressure p_l of the demineralised water that is sealed is chosen to be at least higher than the sealing capacity of a single ferrofluid seal (48.1 kPa). By doing so, it is made sure that both ferrofluid seals have to attribute to the sealing capacity of the seal system when ferrofluid is transported through the seals. The upper bound of the sealing pressure is determined by the dynamic sealing capacity of the system at 500 rpm. The closer sealing pressure p_l approaches the dynamic sealing capacity, the faster the seal will degrade and fail after the replenishment system is deactivated. The amount of time required to perform the experiments can be reduced this way. Within this range p_l is set at 55 kPa for the service life experiments ($\pm$90% of its dynamic sealing capacity at 500 rpm).

In order to examine the influence of the ferrofluid replenishment system on the service life of the seal, the ferrofluid replenishment system will be deactivated after different amounts of time. These amounts of time are 10, 30 and 60 minutes. The ferrofluid supply rate is selected to be 2 ml/hr, which theoretically results into a replacement of the ferrofluid in the system around every minute. The experiments are alternated in order to exclude coincidence. Five measurements per duration of ferrofluid replenishment are performed. The preparation of the test setup is the same as with the sealing capacity experiments, only now the ferrofluid transport is not stopped for a certain period of time.

3 Results and discussion

3.1 Static sealing capacity

The static sealing capacities of the seal that have been measured during the four different sealing conditions are listed in table 4. The moments that the seal failed were very obvious, both during the experiments as in the recorded pressure data. The average sealing capacity measured for water (75.9 kPa) and air (69.8 kPa) slightly differ. The larger sealing capacity that has been measured when water was sealed could be due to the fact water has higher viscosity than air and therefore leaks slower through the seal gap. Pressure in the pressure chamber therefore could have had some extra time to rise.

Table 4: This table presents the average sealing capacity that has been measured for four different static sealing conditions. Also the number of experiments per condition is listed.

Static condition	Mean $p_{c,s}$ [kPa]	#
Water	75.9	5
Air	69.8	5
Water (24 hrs)	213	3
Air (24 hrs)	156	3

The static sealing capacity that has been measured is lower than that was predicted by the analytical model and FEM analysis (96.2 kPa). Overestimation of the static sealing capacity could be due to wrong assumptions in the FEM analysis, analytical model or manufacturing errors in the test setup. Alignment of the shaft and the sealing module during the experiments was not perfectly concentric. Due to this misalignment the radial seal gap height h is larger than 100 μm at some locations in the seal system. This results in a lower magnetic field gradient at these weakest spots of the seal, thus lowering the sealing capacity of the system. Also the non uniformity of the coating of the ring magnet could introduce error in the height of the seal gap. Other authors have also reported that an increase in seal gap decreases the sealing capacity of the seal [34].

The FEM analysis did not account for the influence of ferrofluid on the magnetic field distribution in the system. Furthermore were in the analytical model capillary effects neglected, which theoretically could lower the maximum pressure the sealed liquid can reach before the seal system fails. Other research also indicated overestimation of the seal capacity of a ferrofluid seal could be due to capillary effects [35, 6]. However, it is shown that the assumptions made only result into an acceptable small overestimation of the load capacity. This means manufacturing errors are probably the main reason sealing capacity is overestimated.

The average sealing capacity for water and air that was measured after the ferrofluid in the seal system had been able to settle for 24 hours, 213 kPa and 156 kPa respectively, are significantly higher than the sealing capacity that is measured when it was tested immediately after preparation. A phenomenon that could attribute to this rise in seal capacity is the magnetic field gradient instability of the ferrofluid, which was presented in equation 6. This relation learns that magnetic field gradient stability of the ferrofluid depends on among others on particle size. The ferrofluid used in the setup (Ferrotec EFH1) is one of the cheapest on the market today. This could suggest quality of the ferrofluid, in particular its distribution in particle size, is not optimal.

Also a difference in the sealing capacity for water and air after 24 hours settling was observed. The sealing capacity measured after water has been sealed for 24 hours (213 kPa) is larger than the sealing capacity when air is sealed for 24 hours (156 kPa). This implies that the increase in static sealing capacity over time when water was sealed not only can be attributed to the migration of particles to a higher magnetic field intensities.

The magnetic field intensity in the sealing gap and thus the sealing capacity of the seal can further be increased by adding pole pieces on both sides of the ring magnet [15]. Pole pieces consist of ferromagnetic material that concentrate the magnetic field in the seal gap. During this research the usage of pole-pieces is not investigated.

3.2 Dynamic sealing capacity

Figure 10 presents the dynamic sealing capacity of the ferrofluid rotary seal at different shaft speeds ranging from 0 till 2500 rpm. It can be seen that the sealing capacity of the seal drops when the shaft speed increases. An increase in shaft speed from 0 to 500 rpm results in the largest drop of sealing capacity. The exponential function $21.4 \cdot e^{-0.0019n} + 54.3$ can be fitted through the data having coefficient of determination $R^2 = 0.94$.

The decrease in sealing capacity at higher shaft speeds shows similarities with other results found in literature. Szczech and Horak have proposed a mathematical model that can be used to predict the dynamic sealing capacity of a seal [13]. However, the dynamic sealing capacity that is calculated using this model predicts a faster decrease in sealing capacity at high speeds than is measured. The setup that they have used in order to derive their mathematical model did not contain a shield. This could suggest that a shield can also be used to improve dynamic sealing capacity. Further research is required in order to validate this.

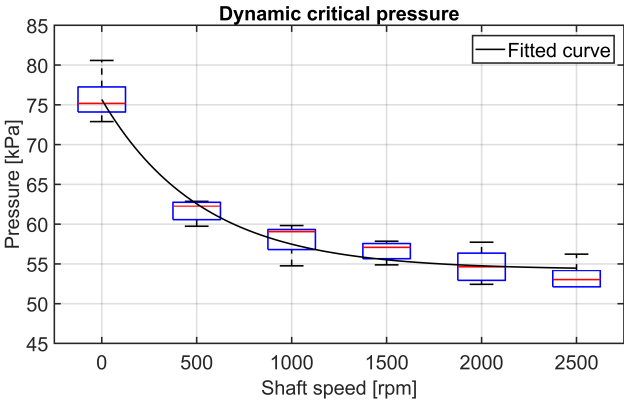

Figure 10: This figure presents boxplots of the measured dynamic sealing capacity of the seal system at different shaft speeds. The fitted line through the data is $21.4 \cdot e^{-0.0019n} + 54.3$.

It is not fully understood why the sealing capacity drops when the shaft speed increases. It is possible that higher inertial and viscous effects result into a faster destabilisation of the ferrofluid flow inside of the seal, which affects the sealing capacity of the system. Also some authors consider the Kelvin-Helmholtz instability that was mentioned in section 2.4 as the main reason the dynamic sealing capacity decreases [18, 13]. However, since the test setup contains a shield, relative velocity between the water that is sealed and ferrofluid of the seal is minimal. Furthermore it is not evident how the pressure of the liquid that is sealed is related to the stability of the interface between the ferrofluid and the liquid.

3.3 Service life

Figure 11 presents the results of the service life experiments on the ferrofluid rotary seal with replenishment system. In the graph 15 measurements of the water pressure inside of the pressure chamber are presented. All measurements start at a liquid pressure p_l of 55 kPa and for each of the measurements a sudden drop in pressure after a period of time can be seen. This drop indicates the moment the seal failed and started to leak water through the sealing channel. When the pressure had dropped sufficiently, the ferrofluid that was left over at the ring magnet was able form a new seal and the pressure inside of the stabilised. It can be seen that during most of the measurements a new seal

was formed at a pressure slightly below 20 kPa. After the seal stabilised the measurements were stopped.

During the measurements presented in figure 11 ferrofluid transport through the seals of 2 ml/hr was either stopped after 10, 30 or 60 minutes. When the ferrofluid supply was stopped after 10 minutes the seal failed within 20 minutes. If the ferrofluid supply was stopped after 30 minutes, service life of the seal increased to approximately 30 to 40 minutes. Finally, if ferrofluid supply was only stopped after 60 minutes, service life ranged from approximately 60 till 80 minutes. The measurement presented in figure 11 show that the ferrofluid rotary seal did not fail while the replenishment system was active.

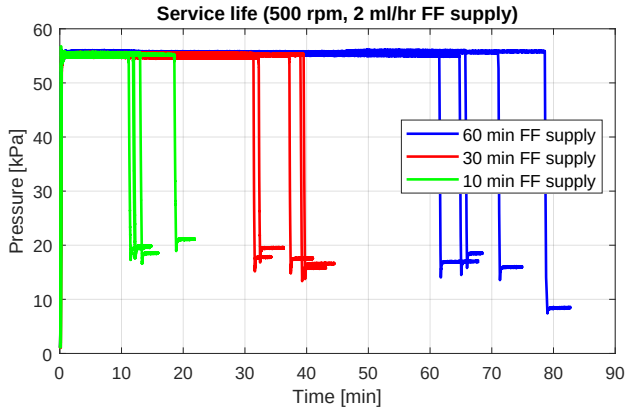

Figure 11: This figure presents the service life of the ferrofluid rotary seal when the ferrofluid replenishment system is deactivated after 10, 30 or 60 minutes. Water pressurised at 55 kPa is sealed at a shaft speed of 500 rpm. The ferrofluid rate is 2 ml/hr.

Because the seal module is transparent and easily accessible it could visually be confirmed that ferrofluid is transported through the seal to the outlet of the seal system while the replenishment system was active. Due to gravity the ferrofluid at the output of the seal leaked along the shield on the base-plate.

The measurements of the pressure in figure 11 show that the moment the seal fails can be controlled by the ferrofluid replenishment system. If it is assumed all supplied ferrofluid is transported through the seal and no mixing occurs, a ferrofluid supply rate of 2 ml/hr results into replacement of the seal volume about every minute. The sealing pressure of 55 kPa during the service life experiments is higher than the sealing capacity of a single ferrofluid seal. This means that while ferrofluid was transported from one seal to another, both seals were able to maintain their sealing capacity.

It can be seen that the original service life of the seal without active ferrofluid replenishment system is short and ranges from a few minutes till 20 minutes. It is expected that the service life of the seal without ferrofluid replenishment was short, since the seal was operating at 90% of its dynamic sealing capacity. It also has been found in literature that service life becomes shorter when the sealing pressure becomes higher [14]. The ferrofluid supply rate that is required in order to prevent failure of the ferrofluid seal is dependent on the degradation rate of the seal. It is expected required supply rate decreases when original service life of the seal is higher at lower sealing pressures.

During ferrofluid transport through the seal no water was observed at the ferrofluid outlet of the seal. However, the composition and properties of the ferrofluid leaving the seal and of the water in the pressure chamber were not investigated in this research.

4 Conclusion

Degradation of the ferrofluid seal when it dynamically seals a liquid decreases its sealing capacity over time and results into premature seal failure when the sealing capacity becomes lower than the operational sealing pressure. In this research it is demonstrated that the service life of a ferrofluid rotary seal that dynamically seals pressurised water can successfully be improved and controlled by implementing a ferrofluid replenishment system into its design.

It has been demonstrated that the degraded ferrofluid of the seals in sealing device can be replaced without losing their sealing capacity. When the ferrofluid seals in the system are completely replaced at a sufficient rate, service life of the seal theoretically can be extended towards infinity. The increase in static sealing capacity over time that was observed during experiments could partially be attributed to the migration of particles through the carrier liquid towards higher magnetic field intensities. Overall, it is believed that the implementation of a ferrofluid replenishment system in ferrofluid rotary seals will pave the way for the development of a new rotary sealing technology for liquids.

References

[1] S. Papell, "Low viscosity magnetic fluid obtained by the colloidal suspension of magnetic particles: Us, 3215572."

[2] R. E. Rosensweig, *Ferrohydrodynamics*. Courier Corporation, 2013.

[3] R. Rosensweig, "Directions in ferrohydrodynamics," *Journal of Applied Physics*, vol. 57, no. 8, pp. 4259–4264, 1985.

[4] C. Scherer and A. M. Figueiredo Neto, "Ferrofluids: properties and applications," *Brazilian Journal of Physics*, vol. 35, no. 3A, pp. 718–727, 2005.

[5] R. Bailey, "Lesser known applications of ferrofluids," *Journal of magnetism and magnetic materials*, vol. 39, no. 1-2, pp. 178–182, 1983.

[6] S. Lampaert, J. Spronck, and R. van Ostayen, "Load and stiffness of a planar ferrofluid pocket bearing," *Proceedings of the Institution of Mechanical Engineers, Part J: Journal of Engineering Tribology*, vol. 232, no. 1, pp. 14–25, 2018.

[7] S. Lampaert, B. Fellinger, J. Spronck, and R. Van Ostayen, "In-plane friction behaviour of a ferrofluid bearing," *Precision Engineering*, vol. 54, pp. 163–170, 2018.

[8] P. Baart, P. Lugt, and B. Prakash, "Review of the lubrication, sealing, and pumping mechanisms in oil-and grease-lubricated radial lip seals," *Proceedings of the Institution of Mechanical Engineers, Part J: Journal of Engineering Tribology*, vol. 223, no. 3, pp. 347–358, 2009.

[9] Z. Szydlo, W. Ochoński, and B. Zachara, "Experiments on magnetic fluid rotary seals operating under vacuum conditions," *Tribotest*, vol. 11, no. 4, pp. 345–354, 2005.

[10] I. Anton, I. De Sabata, L. Vekas, I. Potencz, and E. Suciu, "Magnetic fluid seals: some design problems and applications," *Journal of Magnetism and Magnetic Materials*, vol. 65, no. 2-3, pp. 379–381, 1987.

[11] K. Raj, P. Stahl, and W. Bottenberg, "Magnetic fluid seals for special applications," *ASLE TRANSACTIONS*, vol. 23, no. 4, pp. 422–430, 1980.

[12] K. Raj, B. Moskowitz, and R. Casciari, "Advances in ferrofluid technology," *Journal of magnetism and magnetic materials*, vol. 149, no. 1-2, pp. 174–180, 1995.

[13] M. Szczech and W. Horak, "Tightness testing of rotary ferromagnetic fluid seal working in water environment," *Industrial Lubrication and Tribology*, vol. 67, no. 5, pp. 455–459, 2015.

[14] L. Matuszewski and Z. Szydlo, "Life tests of a rotary single-stage magnetic-fluid seal for shipbuilding applications," *Polish Maritime Research*, vol. 18, no. 2, pp. 51–59, 2011.

[15] T. Liu, Y. Cheng, and Z. Yang, "Design optimization of seal structure for sealing liquid by magnetic fluids," *Journal of Magnetism and Magnetic Materials*, vol. 289, pp. 411–414, 2005.

[16] Y. Mitamura, K. Sekine, M. Asakawa, R. Yozu, S. Kawada, and E. Okamoto, "A durable, non power consumptive, simple seal for rotary blood pumps," *Asaio Journal*, vol. 47, no. 4, pp. 392–396, 2001.

[17] K. Heinz, B. Müller, and S. Nau, "Fluid sealing technology principles and applications," 1998.

[18] J. Kurfess and H. Müller, "Sealing liquids with magnetic liquids," *Journal of Magnetism and Magnetic Materials*, vol. 85, no. 1-3, pp. 246–252, 1990.

[19] Y. Mitamura, T. Yano, W. Nakamura, and E. Okamoto, "A magnetic fluid seal for rotary blood pumps: Behaviors of magnetic fluids in a magnetic fluid seal," *Bio-medical materials and engineering*, vol. 23, no. 1-2, pp. 63–74, 2013.

[20] K. Sekine, Y. Mitamura, S. Murabayashi, I. Nishimura, R. Yozu, and D.-W. Kim, "Development of a magnetic fluid shaft seal for an axial-flow blood pump," *Artificial organs*, vol. 27, no. 10, pp. 892–896, 2003.

[21] Y. Mitamura, S. Takahashi, S. Amari, E. Okamoto, S. Murabayashi, and I. Nishimura, "A magnetic fluid seal for rotary blood pumps: Long-term performance in liquid," *Physics Procedia*, vol. 9, pp. 229–233, 2010.

[22] Y. Mitamura, S. Arioka, D. Sakota, K. Sekine, and M. Azegami, "Application of a magnetic fluid seal to rotary blood pumps," *Journal of Physics: Condensed Matter*, vol. 20, no. 20, p. 204145, 2008.

[23] H. Wang, D. Li, S. Wang, X. He, and S. Zhen, "Effect of seal gap on the seal life when sealing liquids with magnetic fluid," *Revista de la Facultad de Ingenieria*, vol. 31, no. 12, pp. 83–88, 2016.

[24] V. Jarmo, E. Matti, and P. Raimo, "Sealing of liquids with magnetic fluid seals," in *6th Nordic Symposium on Tribology, Szwecja*, pp. 697–702, 1994.

[25] L. Matuszewski and Z. Szydło, "The application of magnetic fluids in sealing nodes designed for operation in difficult conditions and in machines used in sea environment," *Polish Maritime Research*, vol. 15, no. 3, pp. 49–58, 2008.

[26] Z. Szydło and L. Matuszewski, "Experimental research on effectiveness of the magnetic fluid seals for rotary shafts working in water," *Polish Maritime Research*, vol. 14, no. 4, pp. 53–58, 2007.

[27] R. Rosensweig, *Ferrohydrodynamics*. Dover Publications, 5 1998.

[28] R. Perez-Castillejos, J. Plaza, J. Esteve, P. Losantos, M. Acero, C. Cané, and F. Serra-Mestres, "The use of ferrofluids in micromechanics," *Sensors and Actuators A: Physical*, vol. 84, no. 1-2, pp. 176–180, 2000.

[29] V. Polevikov and L. Tobiska, "Influence of diffusion of magnetic particles on stability of a static magnetic fluid seal under the action of external pressure drop," *Communications in Nonlinear Science and Numerical Simulation*, vol. 16, no. 10, pp. 4021–4027, 2011.

[30] D. L. Hujun Wang, "Effect of the seal gap on the seal life when sealing liquids with magnetic fluid," *Revista de la Facultad de Ingenieria U.C.V.*, vol. 31, no. 12, pp. 83–88, 2016.

[31] O. Potma, "Designs for rotary shaft fluid seals in an aqueous environment using ferrofluid," Master's thesis, Delft University of Technology, 2017.

[32] O. Potma, S. Lampaert, and R. van Ostayen, "Method for transport of ferrofluid in a liquid contactless rotational seal," in *Conference report: 17th EDF–Pprime workshop*, 10 2018.

[33] M. Szczech, "Experimental study on the pressure distribution mechanism among stages of the magnetic fluid seal," *IEEE Transactions on Magnetics*, vol. 54, no. 6, pp. 1–7, 2018.

[34] D. C. Li, H. N. Zhang, and Z. L. Zhang, "Study on magnetic fluid static seal of large gap," in *Key Engineering Materials*, vol. 512, pp. 1448–1454, Trans Tech Publ, 2012.

[35] A. Boots, L. Krijgsman, B. de Ruiter, S. Lampaert, and J. Spronck, "Increasing the load capacity of planar ferrofluid bearings by the addition of ferromagnetic material," *Tribology International*, vol. 129, pp. 46–54, 2019.

Chapter 6

Discussion

The main objective of this thesis is to improve the service life of a ferrofluid rotary seal that seals liquids. By doing so a new rotary sealing technology for liquids becomes available that could be implemented in for example the marine industry. In this chapter the results of this research will be discussed in a broad sense. First the most relevant results from the literature study will be discussed and its meaning for the method to accomplish the main objective of this thesis. Subsequently the results of the paper will be discussed and finally some extra results derived from the appendices supporting the paper will be discussed.

6-1 Literature

Literature research learned that ferrofluid rotary seals fail prematurely when they are used for sealing liquids [17, 18, 19, 20, 21]. Service life of the ferrofluid rotary seal that seals liquids can not be predicted and appears to depend on many different variables, among others variables introduced by the design of the seal and its sealing conditions. Analysis of the literature suggests that the failure mechanisms of a ferrofluid rotary can be categorised in instant seal failure and seal failure after a period of operation. The two important phenomena that are responsible for the premature failure of a ferrofluid rotary seal when it is used to seal a liquid are:

1. Instant dynamic failure of the ferrofluid rotary seal due to instability of the interface between the liquid that is sealed and ferrofluid of the seal.
2. Degradation of the ferrofluid seal, which decreases the sealing capacity of the ferrofluid rotary seal over time and results into seal failure when the sealing capacity becomes lower than the required operational sealing pressure.

Many researchers describe the instability of the interface between the liquid that is sealed and the ferrofluid rotary seal by using the Kelvin Helmholtz instability that Rosensweig has derived

for a magnetic and non magnetic fluid which are in relative motion [3, 20, 17, 4]. However, this relation appears to be incomplete for predicting the stability of the seal interface. The derivation assumes that the magnetic field is oriented in the flow direction and therefore stabilises the interface. This is not the case for ferrofluid rotary seals, where the magnetic field is oriented normal to the flow. Another factor that is not taken into account for the stability of the interface is the magnetic field gradient which is present in the seal system. In literature it can be found that an imposed magnetic field gradient at the interface of a magnetic and non-magnetic fluid stabilises the fluid interface [33]. Despite the Kelvin-Helmholtz instability used in literature is not complete, its implication that relative velocities are playing an important role in the dynamic failure mechanism of ferrofluid rotary seals that seal liquids has proved to be very useful. Shielding of the ferrofluid rotary seal appears to be an effective method in order to stabilise the interface between the ferrofluid and liquid that is contained [5, 42, 52], since it decreases the relative velocity between the two fluids. Despite shielding stabilises the flow between the ferrofluid and the liquid sealed and prolongs its service life, failure of the seal is still not prevented due to degradation of the ferrofluid seal.

Degradation of the ferrofluid seal when the ferrofluid rotary seal dynamically seals a liquid is not fully understood. It is found in literature that the magnetic properties of ferrofluid which is stirred in water decreases [22]. It is suggested the existence of shear forces at the interface between the liquid sealed and ferrofluid of the seal could decrease the sealing capacity of the seal over time [24]. Also it has been suggested gradual removal of ferrofluid when it dynamically seals a liquid could occur [23]. However, these theories have not been experimentally validated yet. If seal failure due to interfacial instability is solved by the implementation of a shield structure in the design of the seal, service life of the seal could potentially further be improved by solving the problem of seal degradation.

Despite ferrofluid rotary seals for sealing vacuum and gasses are implemented in industry, limited knowledge on the design principles of such devices is available in literature. This means basic design aspects, for example suitable shaft materials and structural dimensions, should also be investigated. While service life of a ferrofluid rotary seal that seals liquids is the most important aspect for enabling implementation of the technology, environmental impact of the ferrofluid seal could also become crucial. As mentioned before currently used elastomer rotary seals operating in for example ships are reported to leak oil into the marine environment [2]. Increasing environmental regulations forces the industry to apply more sustainable sealing solutions. It has been demonstrated in literature that a single stage ferrofluid rotary seal surrounding a 50 mm shaft was able to seal water for a short period of time ($\pm$20 hrs) [18]. The shaft diameter corresponds to the shaft diameter of small boat or fish cutter. Also it has been demonstrated a ferrofluid seal could successfully be implemented in a small rotary blood which operated at sub-critical pressure for over 275 days [5]. In literature it is found that environmental friendly ferrofluids already are being developed for the decontamination of water [61]. Iron oxide based materials like magnetite are natural occurring minerals and nanoparticles made from these minerals appear to be non toxic [59]. Also iron oxide nanoparticles show many potential in biotechnology, for example in tissue repair and drug delivery [60]. This means that ferrofluids having particles based on iron oxide minerals have the potential to be safely used for ferrofluid rotary seals operating in for example in marine environments or medical devices.

6-2 Paper

The literature review has provided the required knowledge for designing a state of the art ferrofluid rotary seal for liquids and has narrowed down the focus of this research to the problem of ferrofluid seal degradation over time. The paper (chapter 5) presents the design of a new type of ferrofluid rotary seal which implements a ferrofluid replenishment system in order to solve premature seal failure due to degradation. A shield structure is added in order to stabilise the interface between the ferrofluid and the liquid that is sealed. The ferrofluid that is used in the test setup consists of an oil carrier liquid having magnetite nanoparticles. An analytical model and FEM analysis have been used to design the seal and predict its static sealing capacity. The results of the FEM analysis showed that the magnetic field distribution in the sealing device creates two ferrofluid seals, both having approximately the same sealing capacity. The performance of the seal was measured by its static and dynamic sealing capacity and service life when dynamically sealing pressurised water.

The results of the service life experiments showed that the service life of the ferrofluid rotary seal was effectively controlled and prolonged by the replenishment of the ferrofluid in the seal. The seal has not been observed to fail while the ferrofluid replenishment system was active. The original service life of the ferrofluid rotary seal operating without an active ferrofluid replenishment system was in the order of minutes. This short original service life was expected since the sealing pressure of the water was selected to be just below the dynamic critical pressure of the ferrofluid seal. By doing so, the run-time of the experiments could be minimised. Theoretically, the transport rate of the ferrofluid through the seals during the experiments resulted into a replacement of the ferrofluid present in the system every minute. In practice this rate could have been different due to inaccuracies in the calculation of the effective ferrofluid seal volume or ferrofluid loss. Also inefficiencies in the transport of the ferrofluid through the seal due to mixing of the new and degraded ferrofluid seal could lower this replacement rate. When all ferrofluid in the system is replaced, the original service life of the system should be restored. This means that theoretically service life of the seal could be extended infinitely. Since the longest service life experiments with an active ferrofluid replenishment system lasted for one hour, long term experiments are recommended in order to validate this theory.

During the service life experiments the pressure of the water that was sealed was higher than the calculated critical pressure of a single ferrofluid seal present in the seal system. This means that both seals continued to function while ferrofluid was transported from one seal to another. The pressure of the water that has been sealed was not observed to decrease during the service life experiments. This could suggest no or very low leakage of water due to the axial flow of ferrofluid through the seal occurred. Also the ferrofluid leaving the sealing device at the ferrofluid outlet did not show any visible traces of water. However, it has to taken into consideration that the pressure measured in the pressure chamber could be influenced by the increase in water temperature due to fluid friction and small leaks that may have been present in the system.

The analytical model and FEM analysis have overestimated the static sealing capacity by approximately 20 %. This could be due to wrong assumptions made in the analytical model and FEM analysis and by manufacturing errors in the test setup. Most likely misalignment of the shaft and non uniformity of the coating of the ring magnet have resulted in a larger seal gap than that has been assumed in the FEM analysis. During the experiments it was

observed that the static sealing capacity of the system increased over time when shaft speed was zero and the ferrofluid replenishment system was not active. It is believed that this increase in sealing capacity can partly be attributed to the diffusion of the magnetic particles through the carrier liquid to a higher magnetic field intensity region. The ferrofluid becomes non homogeneous and its effective magnetisation is increased. Analysis of the stability of the ferrofluid in the magnetic field gradient of the seal showed that this instability mainly depends on the size of the particles. The quality of the ferrofluid that has been used in the setup is one of the cheapest on the market today. This could indicate that the quality of the ferrofluid, in particular its distribution in particle size, that has been used in the setup was poor. When water was statically sealed instead of air, an extra increase in static sealing capacity over time has been observed. This means that the increase in static sealing capacity over time when water was sealed not only could be attributed to particle diffusion and is not fully understood yet.

The sealing capacity of the device decreased when the shaft speed increased. A mathematical model found in literature showed a similar decrease of sealing capacity. However, this model predicts a faster decrease in sealing capacity at higher speeds than was observed in the experiments. The mathematical model was derived by using an experimental setup which had no shielding structure. This could imply the shield used in the ferrofluid seal setup has influence on the dynamic sealing capacity of the device at higher speeds. Experiments without shield could be performed in order to validate this theory.

6-3 Appendices

The measurements of the sealing pressure in the pressure chamber in order to determine the sealing capacity of the system are presented in appendix B. The measurements show that when the ferrofluid seal fails, the pressure inside of the pressure chamber drops until it stabilises at some point. This means that when the sealing pressure has become sufficient low, the ferrofluid left over at the ring magnet is able to form a new seal. This is the case for both dynamic and static sealing conditions. The finite element analysis presented in appendix C calculates the magnetic field intensities in the sealing device. The results showed that magnetic properties of the shaft have great influence on the the magnetic field distribution in the system. When the shaft is made of a ferromagnetic material the magnetic field distribution generated in the seal gap creates two ferrofluid seals. When the shaft is made of non-magnetic material the difference in magnetic field intensities in the seal system becomes smaller, resulting in a lower sealing capacity of the system. This means a ferromagnetic shaft is preferred in the sealing device, which enables the formation of two independent ferrofluid seals having a high sealing capacity.

Stability of the interface between the water and the ferrofluid of the sealing device is checked using the Kelvin-Helmholtz instability derived by Rosensweig. Despite this equation is not complete, it could give an insight in the sensitivity of some design parameters to the interfacial stability of the sealing device. Calculations made for different values of the height difference between the shielding and sealing channel (h_0) causing a relative velocity shows that the stability criterion is satisfied at low shaft speeds. According to the calculations stability of the interface at 500 rpm is not very sensitive to relative velocities caused by height difference h_0. This suggests manufacturing and alignment errors causing height difference h_0 are less important at low shaft speeds.

Chapter 7

Conclusions and Recommendations

In this research the main objective is to improve the service life of a ferrofluid rotary seal that is used to seal a liquid, enabling application of the sealing technology in industry. This goal is successfully accomplished by the results of the research presented in chapter 5. A new type of ferrofluid rotary seal is developed and presented in the paper, which implements a ferrofluid replenishment system in order to solve premature seal failure. It is experimentally validated that the service life of the device while dynamically sealing water is prolonged and controlled by the ferrofluid replenishment system. The first part of this chapter summarises the most important conclusions of this thesis project. In the second part recommendations, ideas and tips for further research are given.

7-1 General Conclusions

7-1-1 Literature

- Compared to currently used elastomer rotary seals, ferrofluid rotary seals are very interesting due to their simple structure, lack of mechanical contact with the rotating shaft, low friction and ability to hermetically seal.
- The service life of a ferrofluid rotary seal drastically decreases when it is used to seal a liquid instead of a gas or vacuum.
- The two most important phenomena which could cause premature failure of a ferrofluid rotary seal that seals a liquid are:
  - Instability of the liquid-ferrofluid interface, which causes instant seal failure.
  - Degradation of the ferrofluid seal, which decreases the sealing capacity of the rotary seal over time and causes seal failure when the sealing capacity becomes lower than the required operational sealing pressure.
- Degradation of a ferrofluid seal over time that arises when it is used to dynamically seal a liquid is not fully understood. The magnetic properties of the ferrofluid in the seal appear to decrease and it is suggested that ferrofluid could be lost during operation.

- The Kelvin-Helmholtz instability derived by Rosensweig is incomplete for describing the stability of the liquid-ferrofluid interface of a ferrofluid rotary seal. However, its implication that the relative velocity between the two fluids is the main drive causing instabilities was found to be useful.
- A shielding structure that is placed in front of a ferrofluid rotary seal can be used to stabilise the interface between the liquid that is sealed and ferrofluid of the seal by decreasing the relative velocity between the two fluids.
- Environmental friendly ferrofluids having nanoparticles that are based on iron oxide minerals like magnetite are already being developed. These could potentially be used in ferrofluid rotary seals operating in marine environments.

7-1-2 Paper

- Premature failure of the ferrofluid rotary seal that has been designed when it dynamically seals a liquid is caused by the degradation of its ferrofluid seals. The shielding structure prevents failure due to interfacial instability.
- By introducing a ferrofluid replenishment system into the design of the seal premature failure due to degradation of the ferrofluid seal can be prevented by replacing degraded ferrofluid by new ferrofluid.
- The service life of the ferrofluid rotary seal can be controlled and prolonged by the ferrofluid replenishment system. When the replenishment system was deactivated during the service life experiments the seal failed shortly after.
- Both ferrofluid seals in the ferrofluid rotary sealing system continue to function while ferrofluid is transported from one seal to another.
- When the ferrofluid in the seals is fully replaced by the ferrofluid replenishment system at a sufficient rate, service life of the ferrofluid rotary seal theoretically can be extended towards infinity.
- The static sealing capacity of the ferrofluid rotary seal increased over time when it was not operating. This partially could be attributed to the migration of particles through the carrier liquid of the ferrofluid towards higher magnetic field intensities. It is not understood why the sealing capacity increases extra when the seal is in contact with water instead of air.
- The sealing capacity of the ferrofluid rotary seal decreases when the shaft speed increases. At higher shaft speeds the sealing capacity becomes less sensitive to shaft speed.

7-1-3 Appendices

- After the ferrofluid rotary seal fails and the sealing pressure has dropped sufficiently, the ferrofluid left around the magnet is able to form a new seal. This is true for both dynamic and static sealing conditions. This makes it a robust sealing technology.
- The magnetic properties of the shaft are important for the sealing capacity of a rotary ferrofluid seal. A ferromagnetic shaft generates the highest sealing capacity.

- At low shaft speeds of the ferrofluid rotary seal the Kelvin-Helmholtz stability condition derived by Rosensweig is satisfied. The stability appears to be not very sensitive to manufacturing errors causing a height difference (h_0) between the shielding channel and sealing channel at low speeds.

7-2 Recommendations

First some recommendations for important and interesting research subjects regarding ferrofluid rotary sealing technology for sealing liquids are given. Next recommendations are given for improving the experimental test setup that has been built and used during this research and for the design of new test setups. Finally, an overview of interesting potential applications of the sealing technology is presented.

7-2-1 Research

- Model the axial flow of ferrofluid through the seals generated by the replenishment system in order to check for mixing and its replacement efficiency.
- Perform long term service life experiments in order to validate that service life of the seal can be extended as long as desired, theoretically even towards infinity.
- Minimalise the rate of ferrofluid supply to the seal and investigate both continuous and discrete supply.
- Investigate the decrease of sealing capacity of the ferrofluid rotary seal when the shaft speed increases.
- Create more insight in the degradation process of the ferrofluid seal over time.
- Investigate influence of the ferrofluid properties on the service life when liquids are sealed.
- Optimise the sealing capacity of the system by implementing pole pieces in the design of the system.
- Investigate the influence of sea water on the degradation rate of the ferrofluid seal.

7-2-2 Experimental Test Setup

- Implement air bearings into the design of the experimental test setup. By doings so, parameters of the ferrofluid seal can be identified by measuring the current of the motor. Note that this not works when the pressure chamber contains a liquid.
- Use a programmable pump for the supply of ferrofluid, enabling more supply options.
- Investigate further automatisation of the experimental procedures in order to reduce lab time.
- Enable the controlled rise of pressure inside the pressure chamber in order to improve consistency of the experiments.

7-2-3 Potential Applications

- The application of the ferrofluid sealing technology in stern-tube seals for propeller shafts of ships. Currently the lip seals that are used have to be replaced every couple of years which causes downtime of the ship. Also they leak oil into the water. Possibly this can be prevented by implementing the ferrofluid rotary sealing technology.
- Application of the technology in water decontamination systems.
- The application of the ferrofluid rotary seal in hydraulic pumps.
- Application of ferrofluid sealing technology in marine machinery, for example used for dredging.
- Implementation of the sealing technology in medical devices, for example ventricular assist devices used for patients having heart failure.
- General application for the rotary sealing of oils and other liquids in industrial machinery.

Appendix A

Experimental Test Setup

In this appendix additional information on the experimental test setup that been designed and built for the research of the paper is provided.

A-1 Overview Setup

A picture taken of the experimental test setup can be seen in figure A-1.

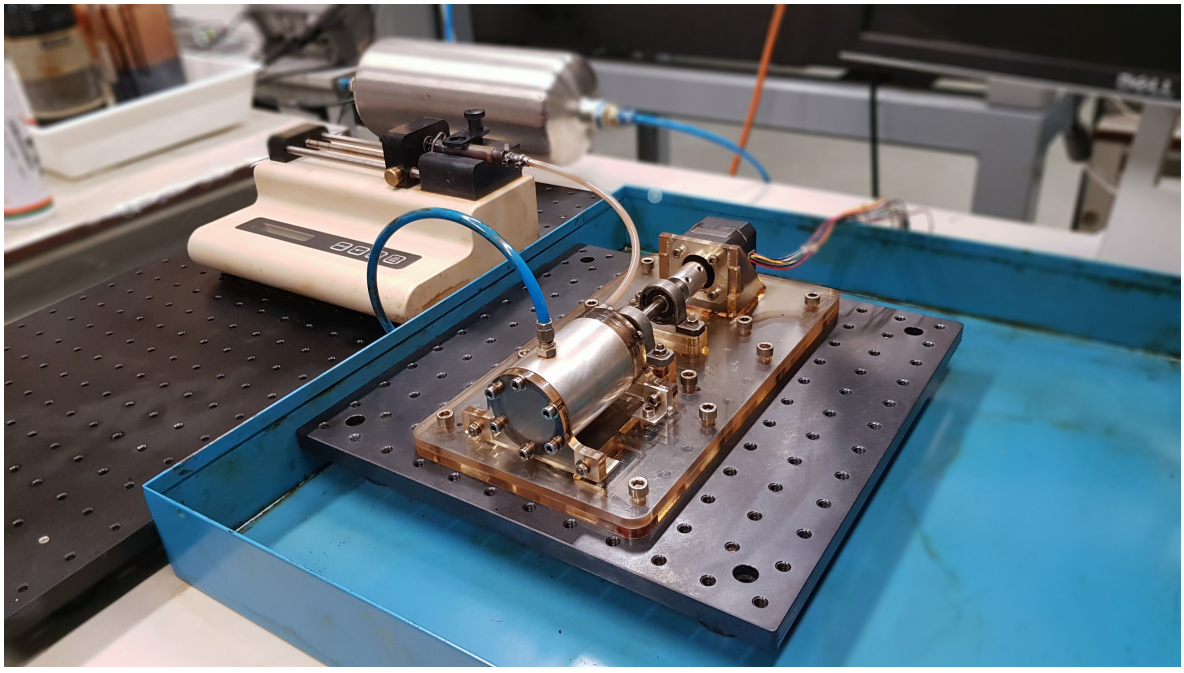

Figure A-1: Picture taken of the experimental test setup. The syringe pump is used to supply ferrofluid to the ferrofluid sealing module that is mounted to the pressure chamber.

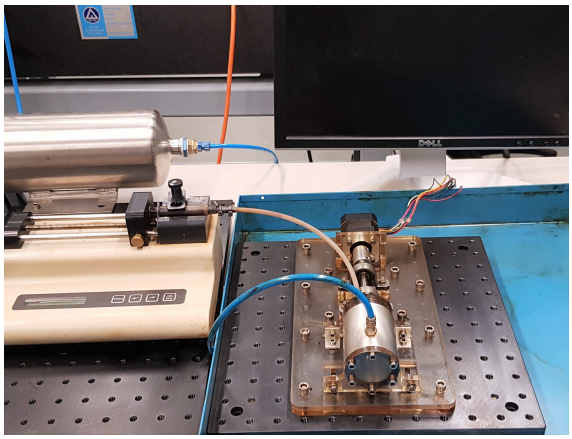

Figure A-2: Photo of the test setup. During the experiments the pressure was live displayed on the monitor.

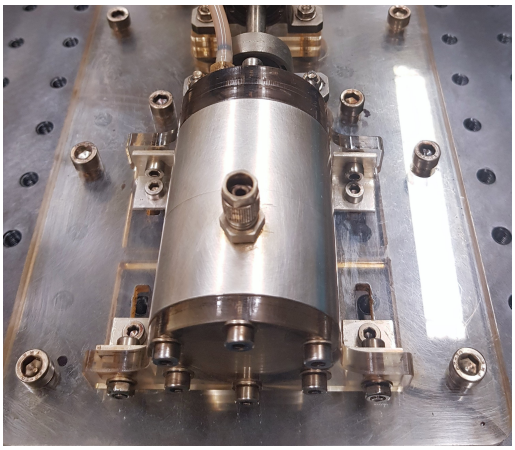

Figure A-3: Photo of the pressure chamber. The pressure inlet is also used to fill the chamber with demineralised water.

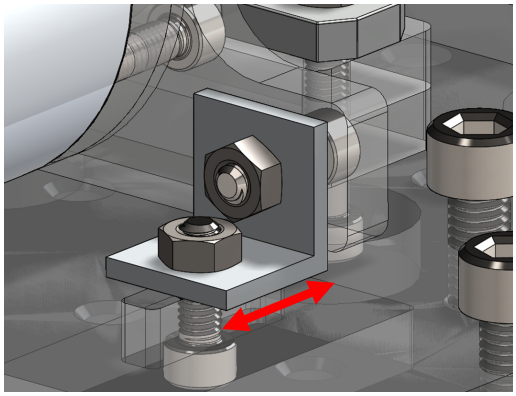

Figure A-4: Drawing of a pressure chamber support. Slots in the base plate enable adjustment of the position of the pressure chamber.

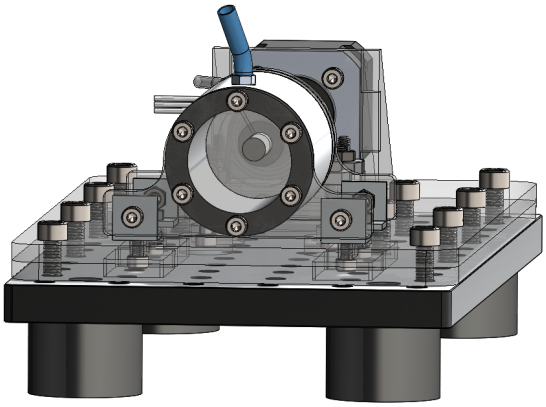

Figure A-5: The transparent acrylic cover plate of the pressure chamber enables visual inspection inside the pressure chamber.

A-2 Motor and Control

In order to test the performance of the ferrofluid rotary sealing system at different shaft speeds a motor for driving the shaft is required. The required peak torque T_p of the motor consists of the sum of the following components:

$$T_p = T_J + T_L + T_F \tag{A-1}$$

where T_J is torque due to inertia, T_L torque due to mechanical load and T_F torque due to friction. The system has no mechanical load and torque due to inertia is low since the acceleration of the shaft can be relatively low. The most important load the motor has to

overcome is generated by the friction of both ball bearings that are supporting the shaft and the fluid friction of the water in the pressure chamber and ferrofluid seal. A 24 volts brushless direct current motor of the company Trinamic (QBL4208-41-04-006) has been selected. Table A-1 presents an overview of the properties of the motor. Figure A-6 presents the torque of the motor versus shaft speed. The motor has an specified operational range of 0 till 4000 rpm and maximum torque of the motor is 6.25 Ncm. The dimensions of the motor are shown in figure A-7.

Table A-1: Properties of the DC motor (Trinamic QBL4208-41-04-006).

Property	Value
Flange	42 mm
Torque	6.25 Ncm
Phase current	1.79 A
Pole count	8
Length	41 mm
Weight	300 g

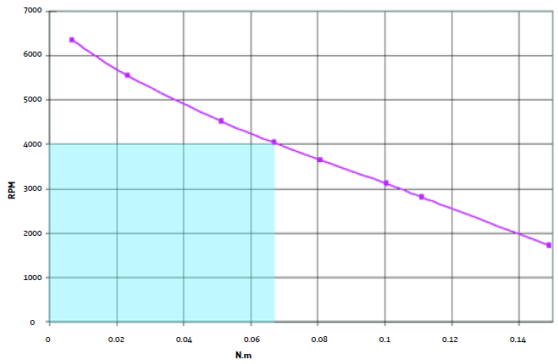

Figure A-6: Torque versus shaft speed of the DC motor used in the experimental test setup.

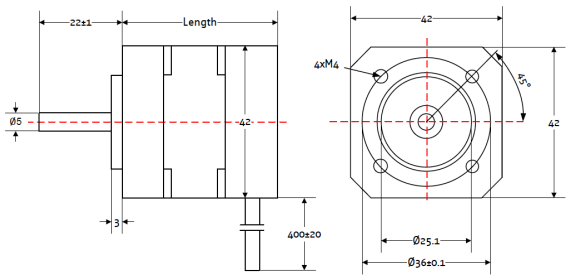

Figure A-7: Dimensions of the DC motor used in the experimental test setup.

In order to generate a constant surface velocity closed loop control of the motor speed is required. The brushless DC motor has hall sensors incorporated that enable feedback control of the motor speed without the need of using an extra encoder. The motor is field oriented controlled (FOC) using the Trinamic TMCM-1640 driver module. Figure A-8 presents an overview of the driver module. This driver module is connected to a computer and operated using Trinamic software IDE3.0. Figure A-8 presents an overview of the connections of the driver module. The power for the motor and driver module is provided by a laboratory power supply.

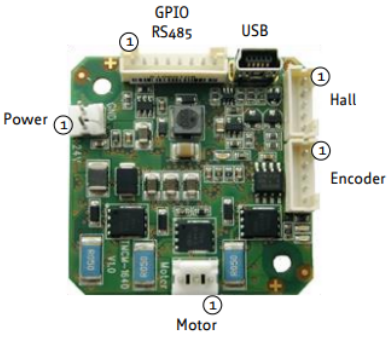

Figure A-8: Overview of the connections of the Trinamic TMCM1640 driver module.

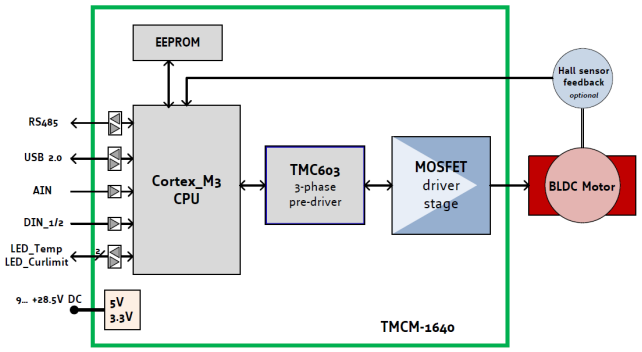

Figure A-9: Control scheme of the TMCM-1640.

A-3 Ferrofluid and Ferrofluid Pump

For the experiments ferrofluid EFH1 from the company ferrotec has been used. Table A-2 gives an overview of the properties of this ferrofluid obtained from the datasheet of Ferrotec. Table A-3 provides information on the composition of the ferrofluid. The precise composition of the mixture is proprietary information.

Table A-2: Ferrotec EFH1 Ferrofluid properties.

Property	SI Units
Saturation Magnetization (M_s)	44 mT
Viscosity at 27°C	6 mPa· s
Density at 25°C	$1.21 \cdot 10^3$ kg/m^3
Pour Point	−94°C
Flash Point	92°C
Initial Magnetic Susceptibility	2.64

Table A-3: Composition of the ferrofluid that is used. The precise composition of the mixture is proprietary information.

Composition	proportion % (by volume)
Iron oxide (magnetite)	3 - 25
Oil Soluble Dispersant	6 - 30
Distillates (Petroleum) Hydrotreated Light	55 - 91

Ferrofluid is rate controlled added to the system by combining a syringe pump (WPI SP100iZ) and a 3 ml syringe (HSW soft-ject). The device allows to set a certain volume and rate which can be used to automatically the supply of ferrofluid to the ferrofluid rotary seal module. The syringe is connected to the ferrofluid supply hose by a Huer lock connection. Outside diameter of this hose is 5 mm.

The syringe pump has the following operational modes:

- Dispense volume mode, in which the pump keeps track of the volume dispensed and automatically stops the pump when a set target volume is reached.

- Run mode, where the pump runs at the selected flow rate until manually stopped.

Figure A-10: The combination of a syringe pump and a syringe is used to supply ferrofluid to the sealing system.

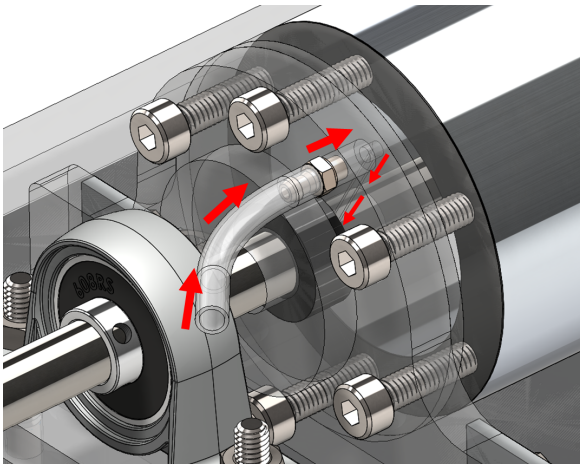

Figure A-11: Zoom in of the ferrofluid supply channel. The red arrows indicate direction of the ferrofluid supply flow.

A-4 Pressure Sensor and DAQ

A monolitic silicon gauge pressure sensor (MPX4250DP) has been used to measure pressure in the pressure chamber relative to atmospheric pressure. The sensor has an operational range of 0 till 250 kPa. Figure A-12 shows a drawing of the pressure sensor and figure A-13 shows the wiring of the sensor.

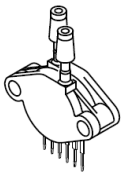

Figure A-12: Drawing of the pressure sensor that has been used (MPX4250DP).

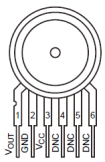

Figure A-13: Wiring of the pressure sensor that has been used (MPX4250DP).

The pressure sensor is connected to a 16 bit data acquisition device (NI USB-6211). For an analog input range of 0 till 5 volts, the resolution of the device is equal to $5/2^{16} \approx 76$ µV. The DAQ device is connected to a computer using an USB cable. Labview 2013 (version 13.0, 32-bit) is used to visualise and store the data of the pressure sensor during the experiments.

A-5 Acrylic parts and Laser-cutting

Most of the structural parts of the experimental test setup consists of 6 and 2 mm transparent acrylic sheets. Figure A-14 gives an overview of the 6 mm thick laser-cut parts. Figure A-15 shows the 2 mm laser-cut part.

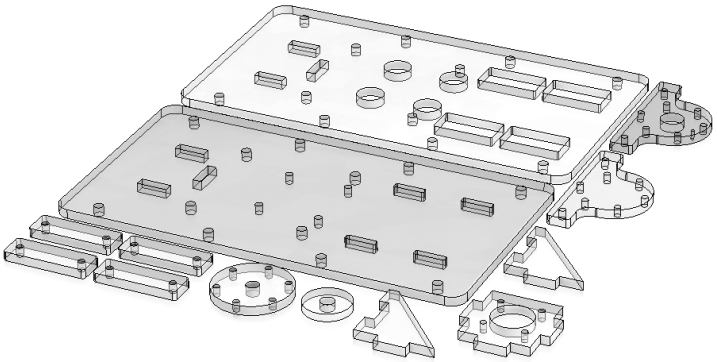

Figure A-14: Required 6 mm acrylic parts for the setup.

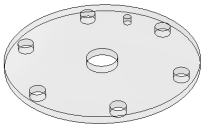

Figure A-15: The supply channel layer of seal module is the only part made of 2 mm acrylic sheet.

A-6 Dimensions of laser-cut parts

Figures A-17 till A-23 show the most important dimensions of the acrylic parts that have been lasercut for the experimental test setup.

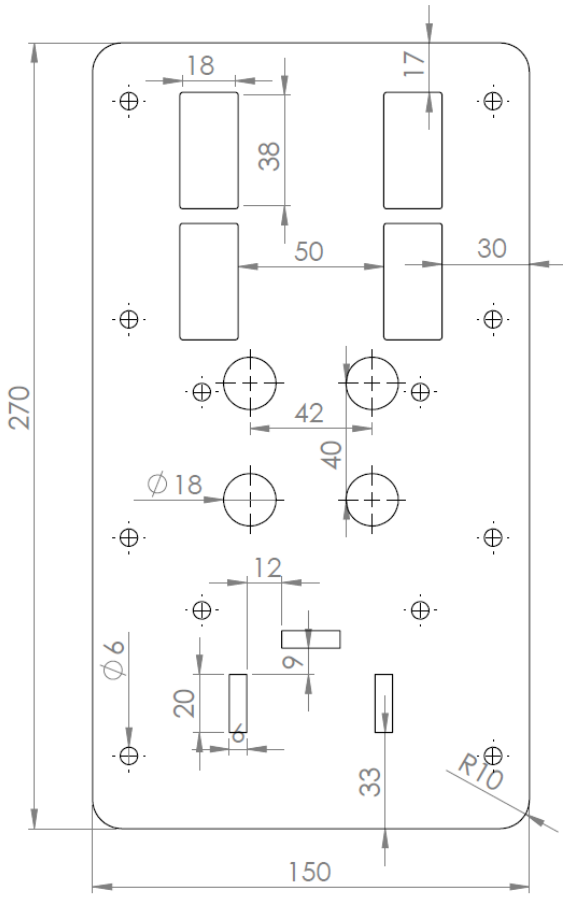

Figure A-16: Drawing of the bottom acrylic baseplate. Dimensions are in millimetres. Thickness of the part is 6 mm.

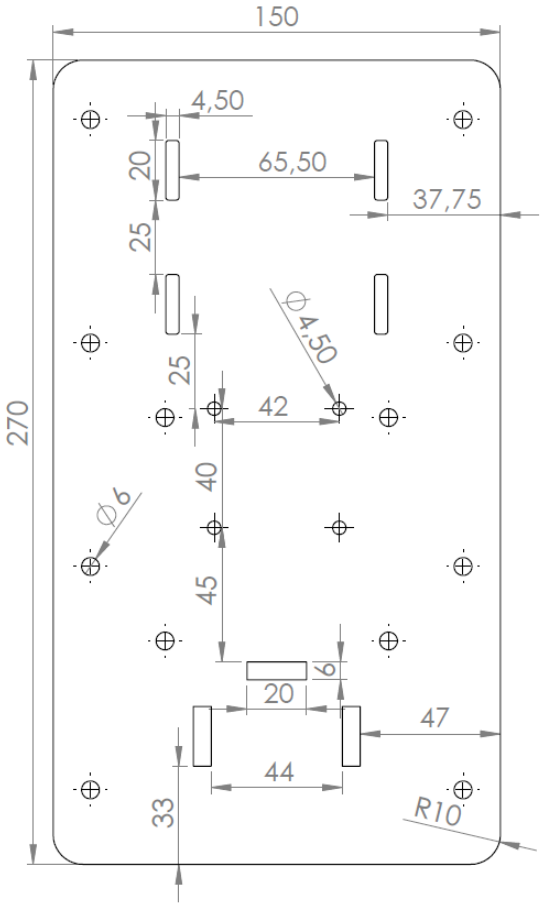

Figure A-17: Drawing of the top acrylic baseplate. Dimensions are in millimetres. Thickness of the part is 6 mm.

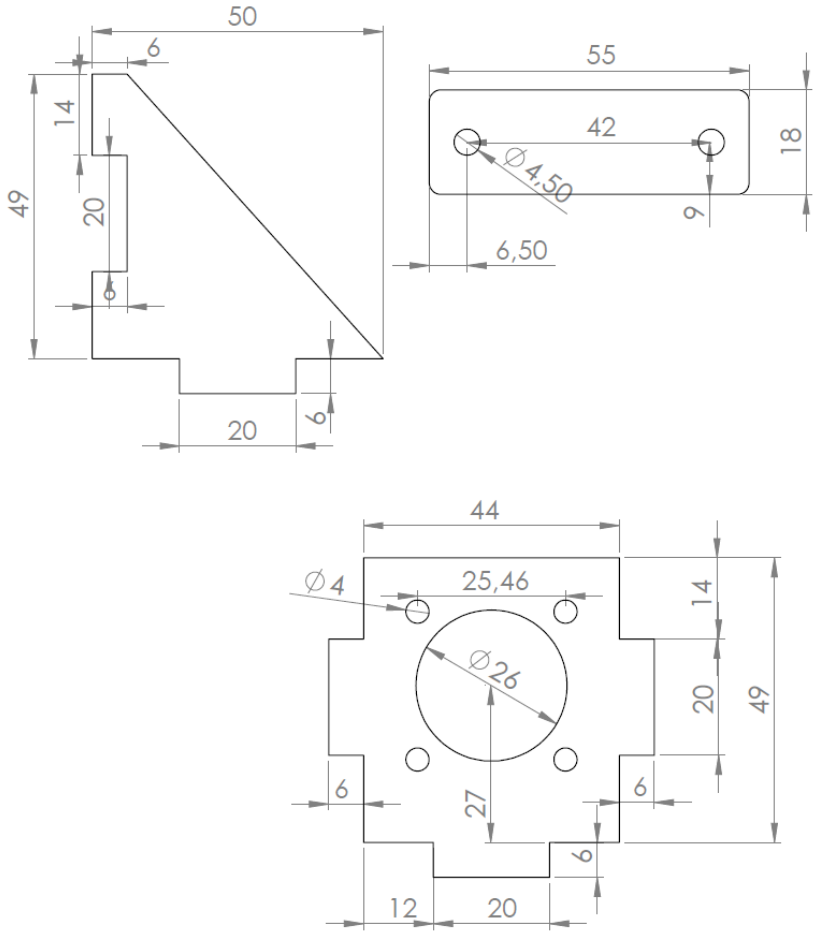

Figure A-18: Drawings of the motor and bearing support parts. Dimensions are in milimetres. Thickness of the parts is 6 mm.

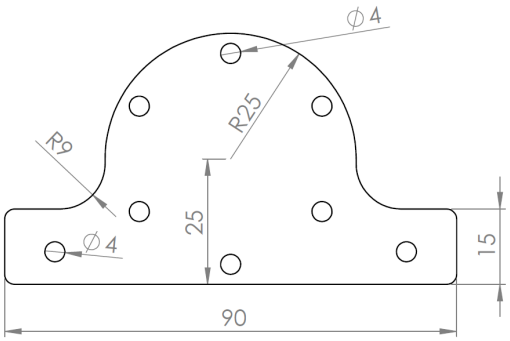

Figure A-19: Drawing of the pressure chamber cover and support. Thickness of the part is 6 mm.

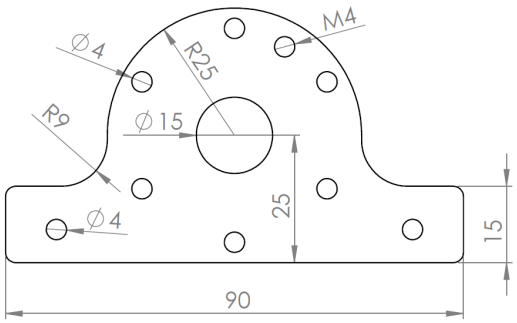

Figure A-20: Drawing of the magnet support layer (6 mm acrylic sheet).

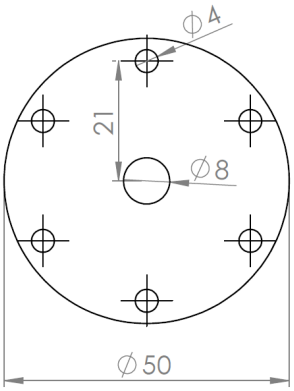

Figure A-21: Drawing of the inside shield (6 mm acrylic sheet).

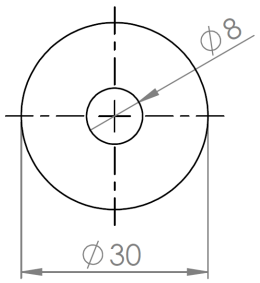

Figure A-22: Drawing of the outside shield (6 mm acrylic sheet).

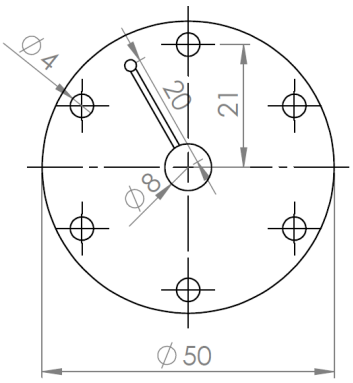

Figure A-23: Drawing of the acrylic layer facilitating the ferrofluid supply channel. Thickness of the layer is 2 mm.

A-7 Dimensions of machined parts

Figures A-24 till A-26 present the parts that have been manufactured using a turning lathe, milling machine or a column drill.

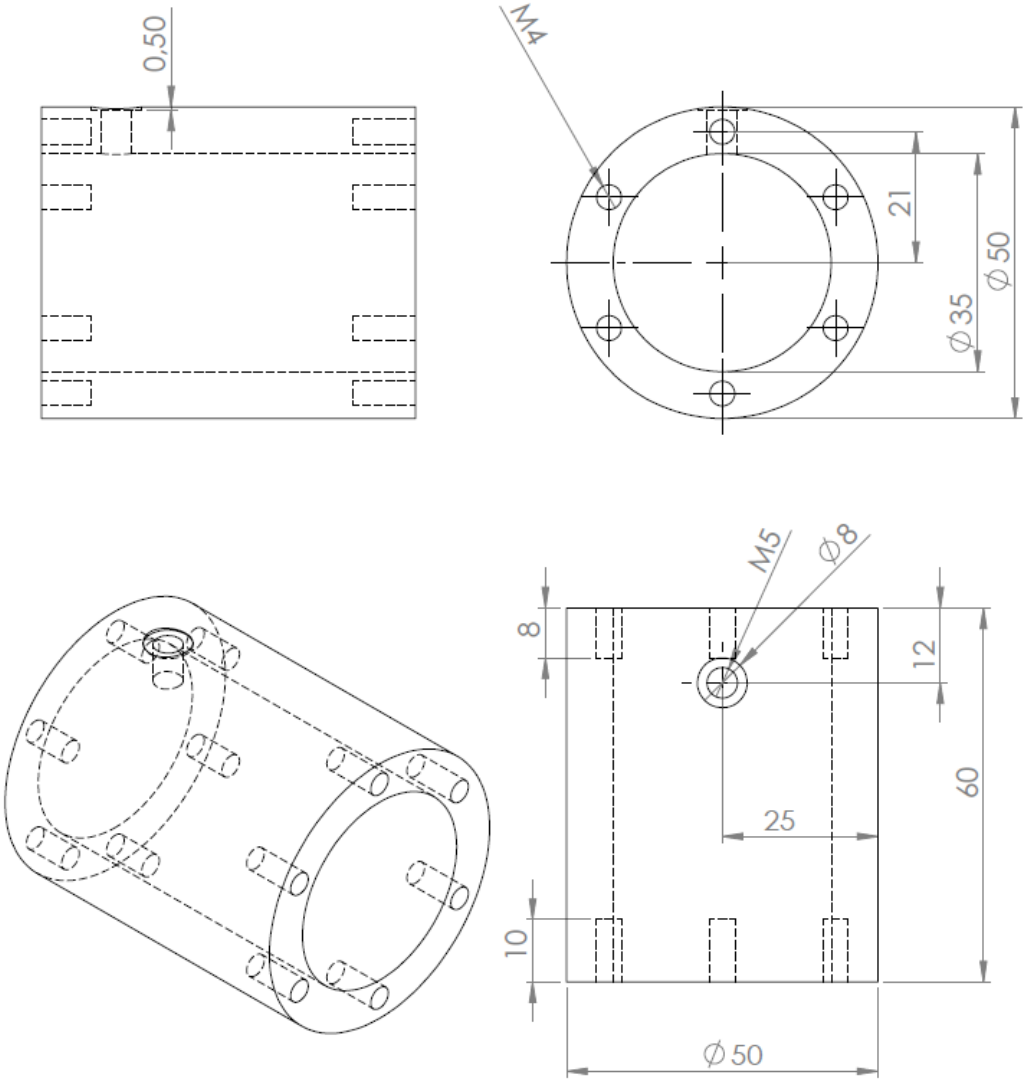

Figure A-24: Drawing of the pressure chamber. The pressure chamber is made of 6082T6 AlMgSi.

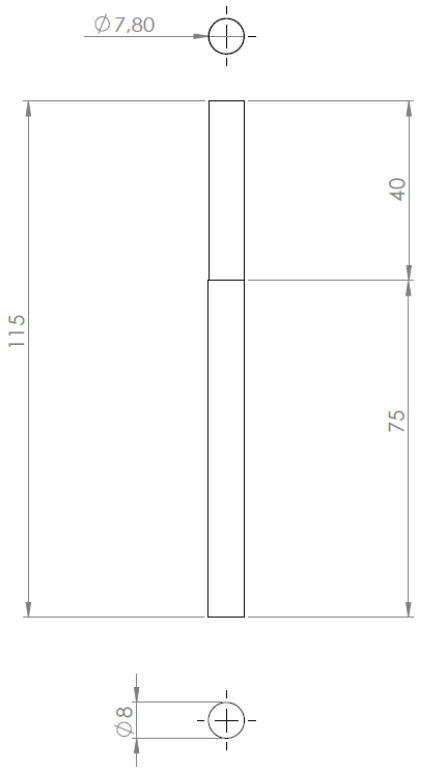

Figure A-25: Drawing of the shaft. The shaft is made of AINSI 430F stainless steel.

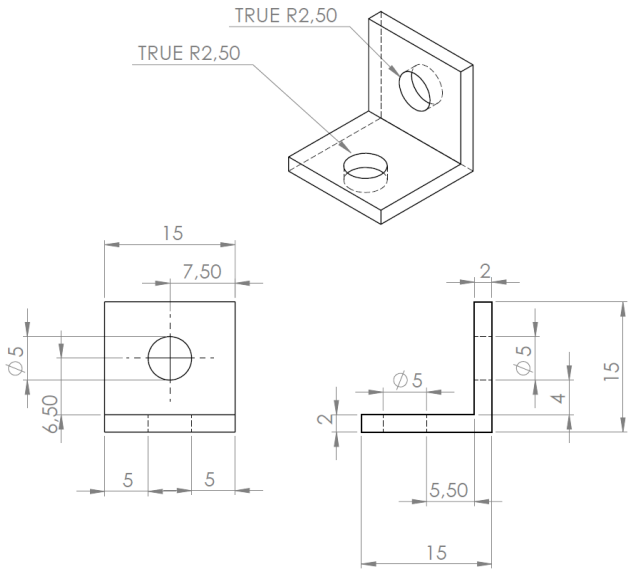

Figure A-26: Drawing of the supports of the pressure chamber. The supports are made of 6060T66 AlMgSi 0,5.

Appendix B

Measurements

This appendix provides the data that has been generated by the experiments done in the paper of chapter 5. The measurements of the pressure inside of the pressure chamber during the static and dynamic sealing capacity experiments and service life experiments are presented.

B-1 Static Sealing Capacity

Figures B-1 and B-2 present the measurements of the pressure inside of the pressure chamber during the static sealing capacity experiments. The capacity of the seal was tested immediately after it was prepared. The red cross indicates the critical pressure of the ferrofluid sealing device and the moment is starts to fail.

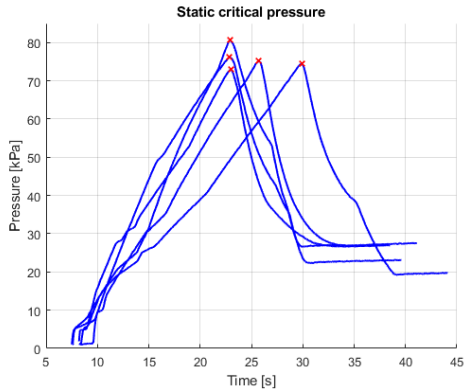

Figure B-1: Critical static pressure when demineralised water was sealed.

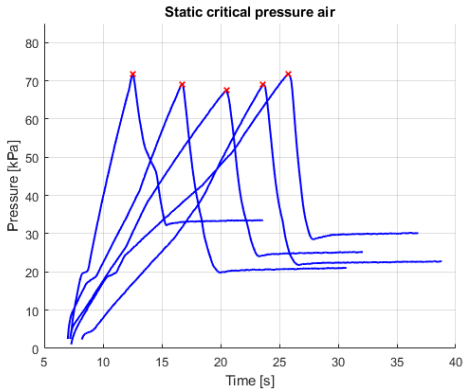

Figure B-2: Critical static pressure when air was sealed.

Figures B-3 and B-4 present the measurements of the critical static pressure of the ferrofluid sealing 24 hours after the seal was prepared. During these 24 hours the seal was not pressurised, the shaft speed was zero and the ferrofluid replenishment system was not active.

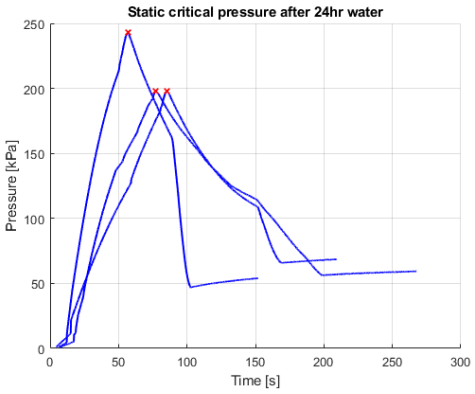

Figure B-3: Critical static pressure when sealing demineralised water after 24 hours of ferrofluid settling time.

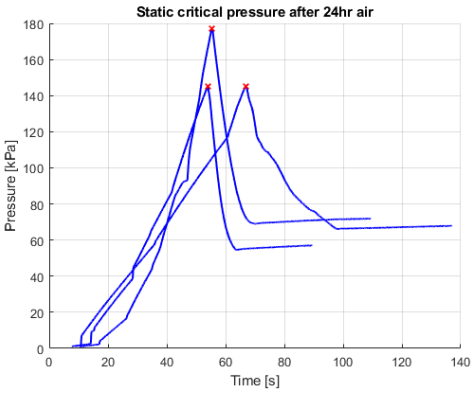

Figure B-4: Critical static pressure when sealing air after 24 hours of ferrofluid settling time.

Table B-1 presents an overview of the static sealing capacity of the seal that has been measured during the experiments.

Table B-1: Static critical pressures [kPa] of the ferrofluid sealing device that are measured for different sealing conditions.

Demi water	Air	Demi water (24hr)	Air (24hr)
80.5830	71.6370	242.8210	145.0760
74.5030	67.4090	197.7230	177.0870
72.8950	69.0860	198.0200	144.9360
75.1840	69.1380		
76.1450	71.6200		

B-2 Dynamic Sealing Capacity

Figure B-5 shows the critical pressures of the ferrofluid sealing that have been measured for different shaft speeds. A curve has been fitted through the data ($21.4 \cdot e^{-0.0019n} + 54.3$) which has coefficient of determination R^2 equal to 0.94. Table B-2 presents an overview of the critical pressures that have been measured during the experiments at shaft speeds ranging from 500 till 2500 rpm.

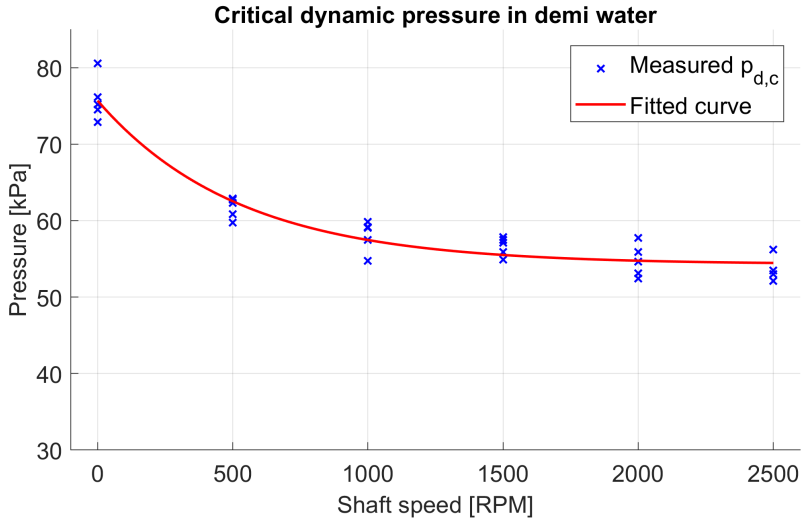

Figure B-5: This plot shows the critical pressures of the ferrofluid sealing device that have been measured for different shaft speeds. A curve ($21.4 \cdot e^{-0.0019n} + 54.3$) is fitted through the data that has $R^2 = 0.94$.

Table B-2: Overview of the critical pressures [kPa] of the ferrofluid sealing device that have been measured for different shaft speeds.

500 rpm	1000 rpm	1500 rpm	2000 rpm	2500 rpm
59.7380	59.1610	57.8510	52.4340	52.1200
62.2890	59.8250	57.0820	57.7280	53.0280
62.7080	59.0560	54.8800	54.6360	53.5000
62.8660	54.7580	55.9110	55.8940	56.2260
60.8390	57.4840	57.4660	53.0980	52.1200

Figures B-6 till B-10 present the measurements of the pressure inside of the pressure chamber which have been used to obtain the sealing capacity of the ferrofluid sealing device for different shaft speeds. The red cross indicates the critical pressure measured and the moment that water start to leak out of the pressure chamber through the seal.

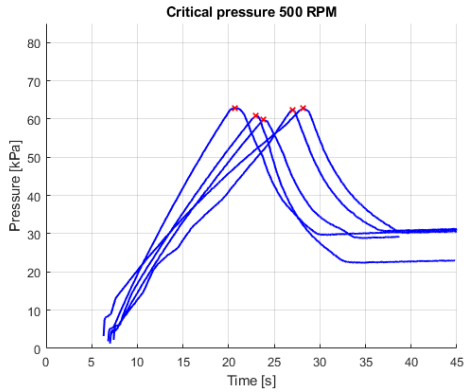

Figure B-6: Critical dynamic pressure at 500 rpm in demineralised water.

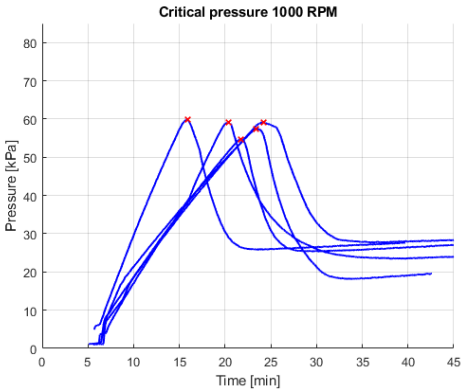

Figure B-7: Critical dynamic pressure at 1000 rpm in demineralised water.

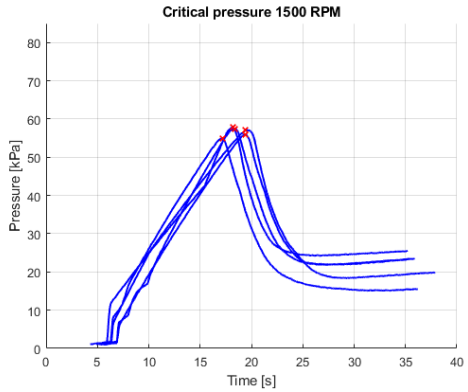

Figure B-8: Critical dynamic pressure at 1500 rpm in demineralised water.

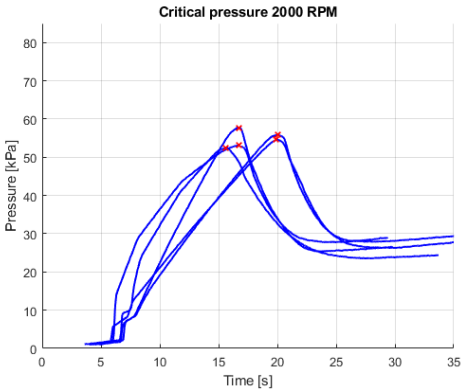

Figure B-9: Critical dynamic pressure at 2000 rpm in demineralised water.

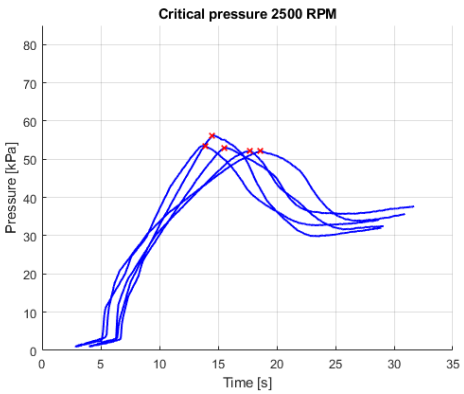

Figure B-10: Critical dynamic pressure at 2500 rpm in demineralised water.

B-3 Service Life

Figure B-11 presents a box-plot of the service life measurements of the ferrofluid sealing system when the supply of ferrofluid (2 ml/hr) was stopped after 10, 30 and 60 minutes.

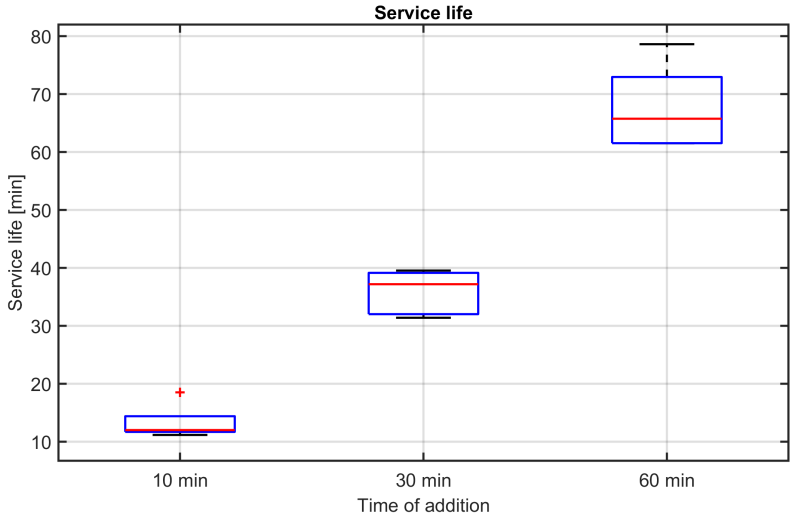

Figure B-11: Boxplots of the service life of the ferrofluid rotary seal system when ferrofluid supply (2 ml/hr) is stopped after 10, 20 and 30 minutes. The shaft speed is 500 rpm and the water pressure is 55 kPa.

Table B-3 presents an overview of the measurements of the service life of the sealing device when supply of ferrofluid (2 ml/hr) is stopped after 10, 30 and 60 minutes.

Table B-3: Service life of the sealing system measured in minutes when supply of ferrofluid (2 ml/hr) is stopped after 10, 30 and 60 minutes. The shaft speed is 500 rpm and demineralised is sealed at 55 kPa.

Stopped after 10 min	Stopped after 30 min	Stopped after 60 min
11.14	31.37	61.49
11.84	32.20	61.51
11.98	37.16	65.73
12.99	38.99	71.05
18.52	39.52	78.59

Appendix C

Calculations Test Setup

In this appendix some additional calculations that were done on the experimental test setup are presented.

C-1 Shaft Material

Shafts that are operating in aqueous environments often are made of stainless steels. Most important groups are austenitic stainless steels, ferritic stainless steels and martensitic stainless steels.

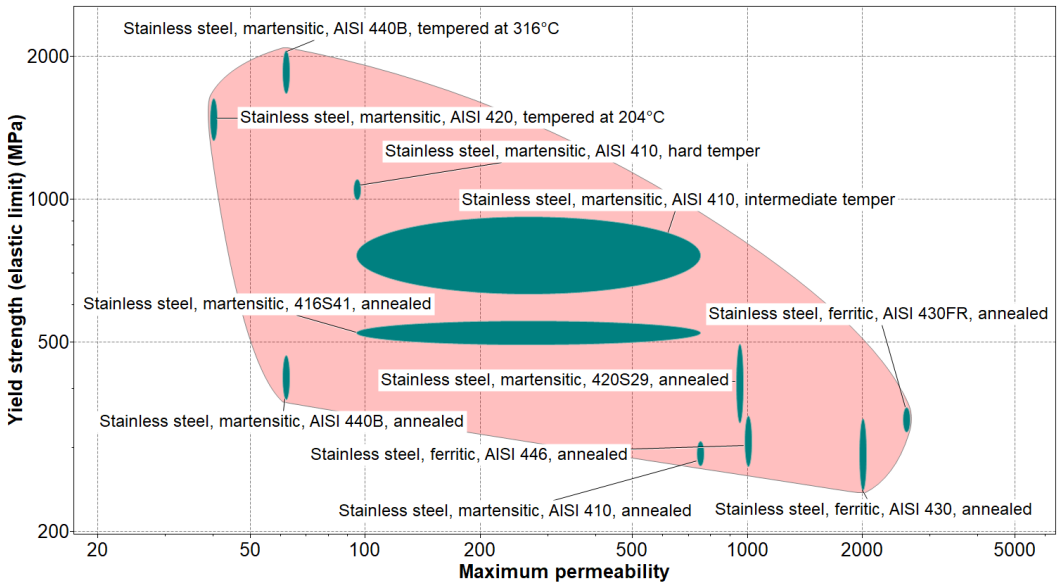

Figure C-1: This figure presents a material plot of martensitic and ferritic stainless steels. Horizontal axis displays magnetic permeability and vertical axis displays Yield strength.

Figure C-1 presents a material plot of stainless steels that has been made using CES Edupack. On the horizontal axis maximum magnetic permeability is displayed and on vertical axis Yield strength. Yield strength of the material is defined as the stress at which the material begins to deform plastically. Ferritic stainless steels appear to have better magnetic properties than martensitic steels. However, yield strength of ferrtic stainless steels also appears to be lower. It can be seen that stainless steel AINSI 430F has the highest magnetic permeability in the plot of figure C-1.

C-2 FEM Analysis

In order to calculate the magnetic field intensities in the sealing device finite element analysis using numerical analysis package COMSOL 5.3 Multiphysics has been done. Figure C-2 presents the magnetic field distribution of the sealing device having a ferromagnetic shaft. The magnetic properties of the shaft are modelled using the BH-curve of stainless steel 430F annealed from the COMSOL material library. Figure C-3 presents the magnetic field distribution when the shaft is made of non-magnetic material having a relative permeability μ_r equal to 1.

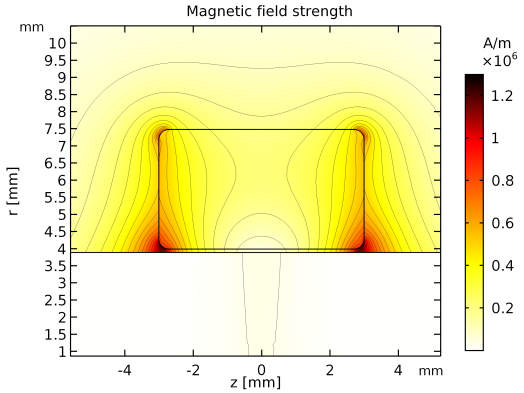

Figure C-2: Magnetic field intensity (H) in the sealing device when the material of the shaft is ferromagnetic stainless steel (AINSI 430F).

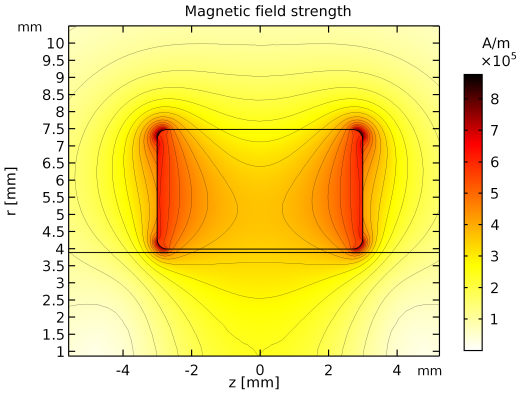

Figure C-3: Magnetic field intensity (H) in the sealing device when the material of the shaft is made of non-magnetic stainless steel ($\mu_r = 1$).

In figures C-4 and C-5 the magnetic field strength evaluated along a line at the top (magnet) and bottom (shaft) of the seal gap for respectively a ferromagnetic and non-magnetic stainless steel shaft is presented. When the shaft is made of ferromagnetic material and enough ferrofluid will be supplied, two seals will be formed in the seal gap. Capacity of the sealing device will be much lower when a non-magnetic stainless steel shaft is used.

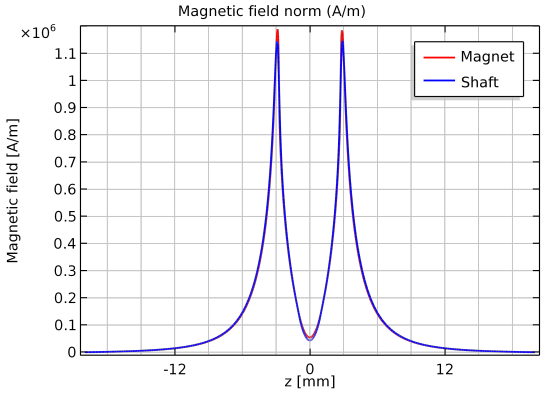

Figure C-4: Magnetic field intensity evaluated at the top (magnet) and bottom (shaft) of the seal gap when the shaft is made of AINSI 430F stainless steel.

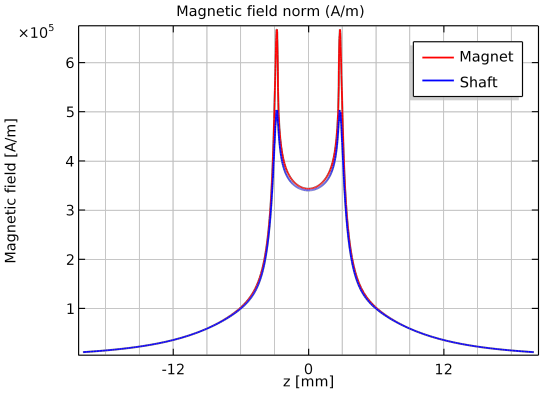

Figure C-5: Magnetic field intensity evaluated at the top (magnet) and bottom (shaft) of the seal gap when the shaft is made of non-magnetic stainless steel ($\mu_r = 1$).

C-3 Flow-Rate Ferrofluid Supply

Equation C-1 can be used to calculate the volume of the ferrofluid in the seal.

$$V_{seal} = \pi \cdot \left((r_s + h)^2 - r_s^2 \right) \cdot w_{seal} \tag{C-1}$$

where r_s is radius of the shaft [m], h height of the seal gap [m] and w_{seal} width of the seal [m]. Replacement rate R of the ferrofluid inside of the sealing device then can be calculated using equation C-2.

$$R = \frac{V_{seal}}{Q_{supply}} \tag{C-2}$$

When uniform transport through the seal and no mixing is assumed, axial velocity of the ferrofluid through the seals can be calculated using equation C-3.

$$v_{ff,axial} = \frac{Q_{supply}}{\pi \cdot ((r_s + h)^2 - r_s^2)} \tag{C-3}$$

C-4 Critical Dynamic Pressure

Equation C-4 shows the mathematical model that has been proposed by Sczcech and Horak for calculating the critical dynamic pressure as function of the static critical pressure $p_{c,static}$, surface speed v_s and ferrofluid density ρ_{ff} [17].

$$p_{crit}(v_s, p_{c,s}, \rho_{ff}) = 0.75 \cdot p_{c,s} \cdot e^{-v_s \cdot (1.96 - \rho_{ff}))} + 0.25 \cdot p_{c,static} \tag{C-4}$$

The surface speed can be calculated using equation C-5. Shaft radius of the test setup r_s is equal to 3.9 mm. Density of the ferrofluid (Ferrotec EFH1) is equal to $1.21 \cdot 10^3$ kg/m^3.

$$v_s = \frac{\pi n}{30} r_s \tag{C-5}$$

Applying this model to te ferrofluid used in the test setup (ferrotec EFH1) and the measured critical static pressure $p_{c,s}$ (75.9 kPa) the predicted dynamic critical pressure according to the model of Sczcech and Horak can be calculated. Curve fitting that has been performed on the data of the critical dynamic pressure experiments results into the relation presented into C-6. The exponential relation obtained has coefficient of determination $R^2 = 0.94$. Figure C-6 shows a plot of the critical dynamic pressure that has been measured and that has predicted using the mathematical model of Sczcech and Horak.

$$p_{c,d} = 21.3997 \cdot e^{-0.0019 \cdot n} + 54.2803 \tag{C-6}$$

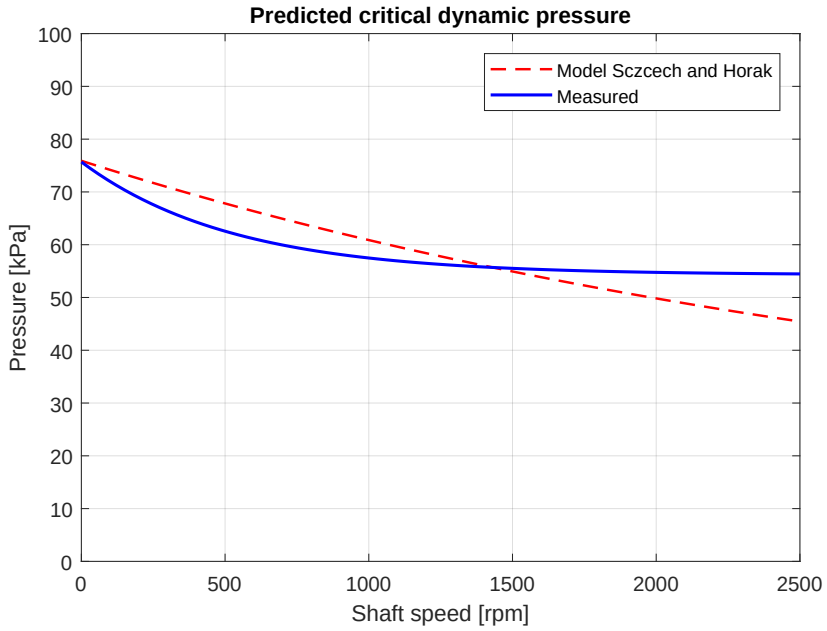

Figure C-6: Critical dynamic pressure of the experimental test setup that has been measured during the experiments and that is predicted using the mathematical model proposed by Sczcech and Horak [17].

C-5 Kelvin-Helmholtz Instability

Equation C-7 presents the Kelvin-Helmholtz instability derived by Rosensweig for the stability of the interface between ferrofluid and another liquid [27].

$$(v_{ff} - v_l)^2 > \frac{\rho_{ff} + \rho_l}{\rho_{ff}\rho_l} \left(2[g(\rho_{ff} - \rho_l)\sigma_{l-ff}]^{1/2} + \frac{(\mu_l - \mu_{ff})^2 H^2}{\mu_l + \mu_{ff}} \right) \tag{C-7}$$

Magnetic field H in equation C-7 is defined collinear with the flow direction. Since magnetic field H in the sealing device is perpendicular to the flow direction, it is equal to zero. Equation C-7 can be simplified as following:

$$(v_{ff} - v_l)^2 > \frac{\rho_{ff} + \rho_l}{\rho_{ff}\rho_l} \left(2[g(\rho_{ff} - \rho_l)\sigma_{l-ff}]^{1/2}\right) \tag{C-8}$$

The velocity difference between the two fluids can be calculated using equation C-9, which also has been elaborated in chapters 3 and 5.

$$v_{ff} - v_l = \frac{h_0}{h_0 + h} v_s \quad , \quad v_s = \frac{\pi n}{30} r_s \tag{C-9}$$

Substituting equation C-9 into the stability condition of equation C-8 results into following relation:

$$\left(\frac{h_0}{h_0 + h} \cdot \frac{\pi n}{30} r_s\right)^2 > 2\frac{\rho_{ff} + \rho_l}{\rho_{ff}\rho_l} \left(g(\rho_{ff} - \rho_l)\sigma_{l-ff}\right)^{1/2} \tag{C-10}$$

The density of the ferrofluid used in the sealing device ρ_{ff} (Ferrotec EFH1) is $1.21 \cdot 10^3$ kg/m^3. Density of the demineralised water sealed ρ_l is equal to $0.997 \cdot 10^3$ kg/m^3. Gravitational constant g is equal to 9.81 m/s^2. The radius of the shaft r_s is equal to 3.9 mm and seal gap h is equal to 100 µm. The surface tension σ_{l-ff} between ferrofluid and water is selected to be 50 mN/m, which is based on the interfacial surface tension between the magnetic liquid and water used in [3].

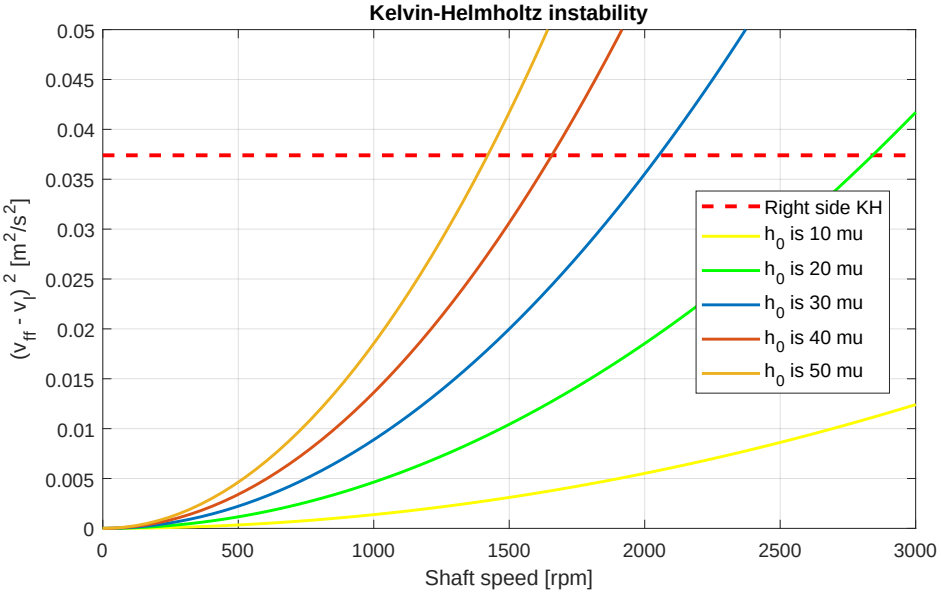

Figure C-7: This figure presents the Kelvin-Helmholtz stability criterion derived by Rosensweig calculated for different values of h_0. When $(v_{ff} - v_l)^2$ becomes larger than the red dotted horizontal line, the interface becomes unstable according to the instability criterion [27].

Figure C-7 presents a plot of the Kelvin-Helmholtz instability criterion for different values of height difference h_0. The right side of the Kelvin-Helmholtz instability presented in equation C-10 is indicated by the red dotted horizontal line. According to the stability criterion the interface between both liquids becomes unstable when the velocity difference squared $(v_{ff} - v_l)^2$ becomes larger than the right side of the Kelvin-Helmholtz equation. However, literature research learned this equation appears to be incomplete for describing the total stability of the interface.

Appendix D

Datasheets

D-1 Flow-Rates Syringe Pump

Table D-1: Flowrates of the SP100i Syringe pump.

Syringe size	Minimum	Maximum
10 µl	0.2 µl/h	126 µl/h
25 µl	0.2 µl/h	318 µl/h
50 µl	0.2 µl/h	625 µl/h
100 µl	0.2 µl/h	1274 µl/h
250 µl	2.0 µl/h	3164 µl/h
500 µl	4.0 µl/h	6359 µl/h
1 ml	0.02 ml/h	12.7 ml/h
2.5 ml	0.02 ml/h	31.7 ml/h
3 ml	0.03 ml/h	44.9 ml/h
5 ml	0.05 ml/h	87.0 ml/h
10 ml	0.2 ml/h	125 ml/h
20 ml	0.2 ml/h	219 ml/h
30 ml	0.2 ml/h	282 ml/h
50/60 ml	0.3 ml/h	426 ml/h

D-2 Syringe Diameters

Henke-Sass, Wolf GmbH
Keltenstrasse 1 · 78532 Tuttlingen · Germany

To whom it may concern

Henke-Sass, Wolf GmbH

Keltenstrasse 1
78532 Tuttlingen · Germany
Telefon: +49 7462 9466-137
Telefax: +49 7462 9466-5137
heiko.schwoerer@henkesasswolf.de
www.henkesasswolf.de

Tuttlingen, 05.09.2017

Inner diameter / Outer diameter - disposable syringes

Item / Artikel:	Inner diameter (mm):	Outer diameter (mm):
HSW NORM-JECT® 1 ML, LDS, Luer Slip	4,7	6,39
HSW NORM-JECT® 2 ML / 3 ML, Luer Slip and Luer Lock	9,7	10,8
HSW NORM-JECT® 5 ML (6 ML), Luer Slip and Luer Lock	12,5	13,7
HSW NORM-JECT® 10 ML (12 ML), Luer Slip and Luer Lock	15,9	17,3
HSW NORM-JECT® 20 ML (24 ML), Luer Slip and Luer Lock	20,1	21,6
HSW NORM-JECT® 30 ML, Luer Slip and Luer Lock	22,6	24,1
HSW NORM-JECT® 50 ML (60 ML), Luer Slip and Luer Lock	29,0	30,9

HSW SOFT-JECT® 1 ML, Luer Slip	4,7	6,39
HSW SOFT-JECT® 1 ML, LDS, Luer Slip and Luer Lock	4,7	6,4
HSW SOFT-JECT® 2 ML / 3 ML, Luer Slip and Luer Lock	9,7	10,8
HSW SOFT-JECT® 5 ML, Luer Slip and Luer Lock	12,5	13,7
HSW SOFT-JECT® 10 ML (12 ML), Luer Slip and Luer Lock	15,9	17,3
HSW SOFT-JECT® 20 ML, Luer Slip and Luer Lock	20,1	21,6
HSW SOFT-JECT® 30 ML, Luer Slip and Luer Lock	22,0	24,0
HSW SOFT-JECT® 50 ML (60 ML), Luer Slip	27,75	30,5
HSW SOFT-JECT® 50 ML (60 ML), Luer Lock (BD)	26,6	29,1
HSW SOFT-JECT® 50 ML (60 ML), Catheter	27,8	30,45

D-3 Annular Magnet

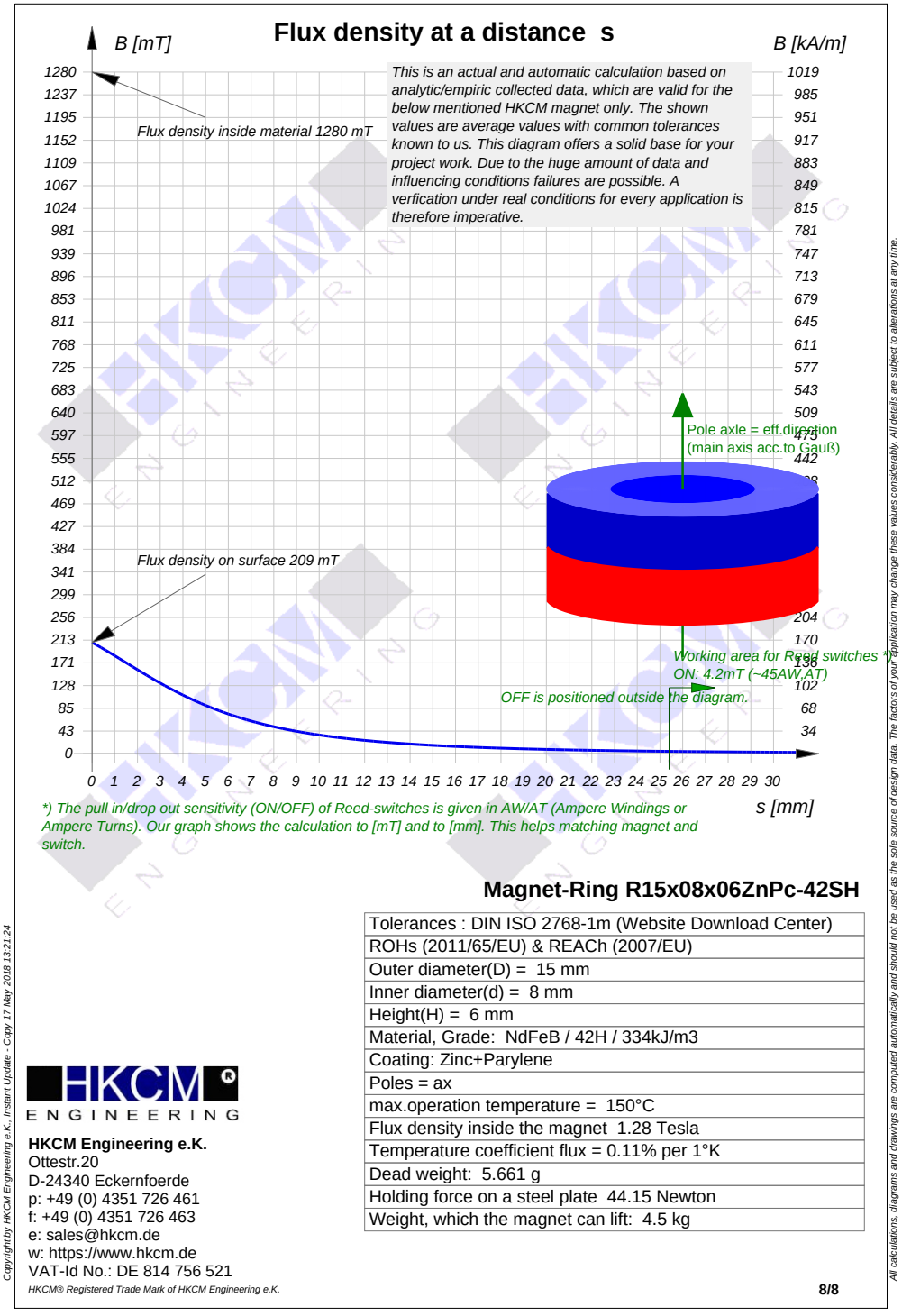

Figure D-1: Datasheet of the annular magnet that has been used in the experimental test setup.

D-4 Pressure Sensor

Rating	Symbol	Value	Unit
Maximum pressure (P1 > P2)	P_{MAX}	1000	kPa
Storage temperature	T_{STG}	–40 to +125	°C
Operating temperature	T_A	–40 to +125	°C

Figure D-2: Maximum ratings of the pressure sensor (MPX4250DP).

Symbol	Characteristic	Min	Typ	Max	Unit
P_{OP}	Pressure range[1]	0	—	250	kPa
V_{CC}	Supply voltage[2]	4.85	5.1	5.35	Vdc
I_o	Supply current	—	7.0	10	mAdc
V_{off}	Minimum pressure offset[3] (0 °C to 85 °C)	0.139	0.204	0.269	Vdc
V_{FSO}	Full scale output[4] (0 °C to 85 °C)	4.844	4.909	4.974	Vdc
V_{FSS}	Full scale span[5] (0 °C to 85 °C)	—	4.705	—	Vdc
—	Accuracy[6] (0 °C to 85 °C)	—	—	±1.4	$\%V_{FSS}$
ΔV/ΔP	Sensitivity	—	18.8	—-	mV/kPa
t_R	Response time[7]	—	1.0	—-	ms
I_{o+}	Output source current at full scale output	—	0.1	—-	mAdc

Figure D-3: Operating characteristics of the pressure sensor (MPX4250DP).

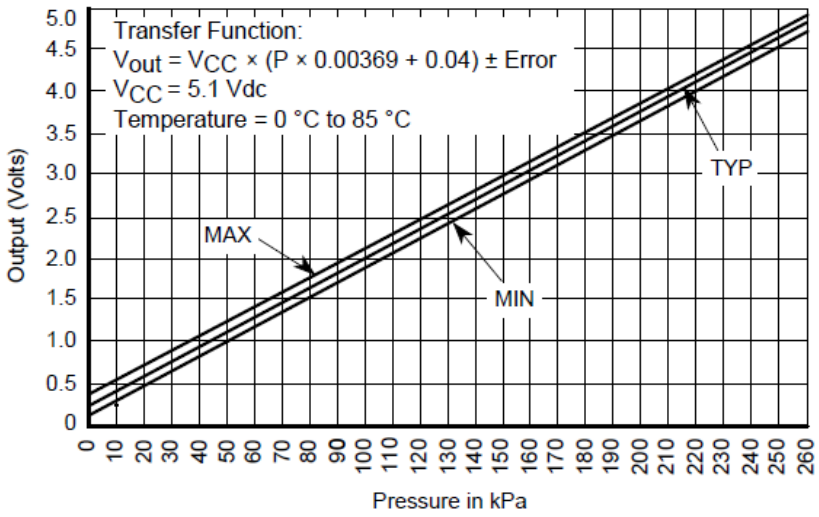

Figure D-4: Transfer function of the pressure sensor (MPX4250DP).

D-5 DAQ Device

NI USB-621*x* Specifications

Specifications listed below are typical at 25 °C unless otherwise noted.

Analog Input

Number of channels
- USB-6210/6211/6215 ..... 8 differential or 16 single ended
- USB-6218 ..... 16 differential or 32 single ended

ADC resolution ..... 16 bits

DNL ..... No missing codes guaranteed

INL ..... Refer to the *AI Absolute Accuracy Table*

Sampling rate
- Maximum ..... 250 KS/s (aggregate)
- Minimum ..... 0 S/s
- Timing accuracy ..... 50 ppm of sample rate
- Timing resolution ..... 50 ns

Input coupling ..... DC

Input range ..... ±10 V, ±5 V, ±1 V, ±0.2 V

Maximum working voltage for analog inputs (signal + common mode) ..... ±10.4 V of AI GND

CMRR (DC to 60 Hz) ..... 100 dB

Input impedance
- Device on
  - AI+ to AI GND ..... >10 GΩ in parallel with 100 pF
  - AI– to AI GND ..... >10 GΩ in parallel with 100 pF
- Device off
  - AI+ to AI GND ..... 1200 Ω
  - AI– to AI GND ..... 1200 Ω

Input bias current ..... ±100 pA

Crosstalk (at 100 kHz)
- Adjacent channels ..... –75 dB
- Non-adjacent channels ..... –90 dB

Small signal bandwidth (–3 dB) ..... 450 kHz

Input FIFO size ..... 4,095 samples

Scan list memory ..... 4,095 entries

Data transfers ..... USB Signal Stream, programmed I/O

Overvoltage protection (AI <0..31>, AI SENSE)
- Device on ..... ±30 V for up to two AI pins
- Device off ..... ±20 V for up to two AI pins

Input current during overvoltage condition ..... ±20 mA max/AI pin

Settling Time for Multichannel Measurements

Accuracy, full scale step, all ranges
- ±90 ppm of step (±6 LSB) ..... 4 µs convert interval
- ±30 ppm of step (±2 LSB) ..... 5 µs convert interval
- ±15 ppm of step (±1 LSB) ..... 7 µs convert interval

NATIONAL INSTRUMENTS™

Figure D-5: Analog input specifications.

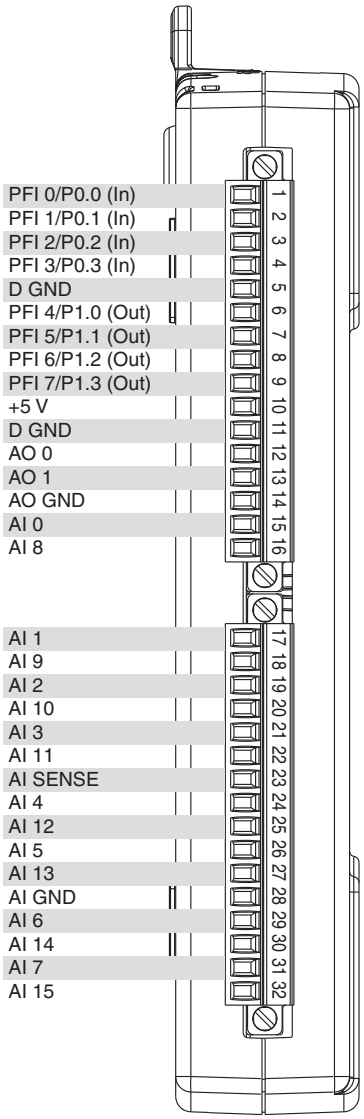

Figure D-6: Pinout of the DAQ device (National Instruments USB-6211).

Bibliography

[1] P. Baart, P. Lugt, and B. Prakash, "Review of the lubrication, sealing, and pumping mechanisms in oil-and grease-lubricated radial lip seals," *Proceedings of the Institution of Mechanical Engineers, Part J: Journal of Engineering Tribology*, vol. 223, no. 3, pp. 347–358, 2009.

[2] G. J. G. of Experts on the Scientific Aspects of Marine Environmental Protection, *Estimates of Oil Entering the Marine Environment from Sea-Based Activities*. International Maritime Organization, 2007.

[3] J. Kurfess and H. Müller, "Sealing liquids with magnetic liquids," *Journal of Magnetism and Magnetic Materials*, vol. 85, no. 1-3, pp. 246–252, 1990.

[4] O. Potma, "Designs for rotary shaft fluid seals in an aqueous environment using ferrofluid," Master's thesis, Delft University of Technology, 2017.

[5] Y. Mitamura, S. Takahashi, S. Amari, E. Okamoto, S. Murabayashi, and I. Nishimura, "A magnetic fluid seal for rotary blood pumps: Long-term performance in liquid," *Physics Procedia*, vol. 9, pp. 229–233, 2010.

[6] S. Papell, "Low viscosity magnetic fluid obtained by the colloidal suspension of magnetic particles: Us, 3215572."

[7] R. E. Rosensweig, *Ferrohydrodynamics*. Courier Corporation, 2013.

[8] R. Rosensweig, "Directions in ferrohydrodynamics," *Journal of Applied Physics*, vol. 57, no. 8, pp. 4259–4264, 1985.

[9] C. Scherer and A. M. Figueiredo Neto, "Ferrofluids: properties and applications," *Brazilian Journal of Physics*, vol. 35, no. 3A, pp. 718–727, 2005.

[10] R. Bailey, "Lesser known applications of ferrofluids," *Journal of magnetism and magnetic materials*, vol. 39, no. 1-2, pp. 178–182, 1983.

[11] A. Boots, L. Krijgsman, B. de Ruiter, S. Lampaert, and J. Spronck, "Increasing the load capacity of planar ferrofluid bearings by the addition of ferromagnetic material," *Tribology International*, vol. 129, pp. 46–54, 2019.

[12] S. Lampaert, J. Spronck, and R. van Ostayen, "Load and stiffness of a planar ferrofluid pocket bearing," *Proceedings of the Institution of Mechanical Engineers, Part J: Journal of Engineering Tribology*, vol. 232, no. 1, pp. 14–25, 2018.

[13] Z. Szydlo, W. Ochoński, and B. Zachara, "Experiments on magnetic fluid rotary seals operating under vacuum conditions," *Tribotest*, vol. 11, no. 4, pp. 345–354, 2005.

[14] I. Anton, I. De Sabata, L. Vekas, I. Potencz, and E. Suciu, "Magnetic fluid seals: some design problems and applications," *Journal of Magnetism and Magnetic Materials*, vol. 65, no. 2-3, pp. 379–381, 1987.

[15] K. Raj, P. Stahl, and W. Bottenberg, "Magnetic fluid seals for special applications," *ASLE TRANSACTIONS*, vol. 23, no. 4, pp. 422–430, 1980.

[16] K. Raj, B. Moskowitz, and R. Casciari, "Advances in ferrofluid technology," *Journal of magnetism and magnetic materials*, vol. 149, no. 1-2, pp. 174–180, 1995.

[17] M. Szczech and W. Horak, "Tightness testing of rotary ferromagnetic fluid seal working in water environment," *Industrial Lubrication and Tribology*, vol. 67, no. 5, pp. 455–459, 2015.

[18] L. Matuszewski and Z. Szydlo, "Life tests of a rotary single-stage magnetic-fluid seal for shipbuilding applications," *Polish Maritime Research*, vol. 18, no. 2, pp. 51–59, 2011.

[19] T. Liu, Y. Cheng, and Z. Yang, "Design optimization of seal structure for sealing liquid by magnetic fluids," *Journal of Magnetism and Magnetic Materials*, vol. 289, pp. 411–414, 2005.

[20] Y. Mitamura, K. Sekine, M. Asakawa, R. Yozu, S. Kawada, and E. Okamoto, "A durable, non power consumptive, simple seal for rotary blood pumps," *Asaio Journal*, vol. 47, no. 4, pp. 392–396, 2001.

[21] K. Heinz, B. Müller, and S. Nau, "Fluid sealing technology principles and applications," 1998.

[22] Y. Mitamura, S. Arioka, D. Sakota, K. Sekine, and M. Azegami, "Application of a magnetic fluid seal to rotary blood pumps," *Journal of Physics: Condensed Matter*, vol. 20, no. 20, p. 204145, 2008.

[23] V. Jarmo, E. Matti, and P. Raimo, "Sealing of liquids with magnetic fluid seals," in *6th Nordic Symposium on Tribology, Szwecja*, pp. 697–702, 1994.

[24] H. Wang, D. Li, S. Wang, X. He, and S. Zhen, "Effect of seal gap on the seal life when sealing liquids with magnetic fluid," *Revista de la Facultad de Ingenieria*, vol. 31, no. 12, pp. 83–88, 2016.

[25] L. Matuszewski and Z. Szydło, "The application of magnetic fluids in sealing nodes designed for operation in difficult conditions and in machines used in sea environment," *Polish Maritime Research*, vol. 15, no. 3, pp. 49–58, 2008.

[26] Z. Szydło and L. Matuszewski, "Experimental research on effectiveness of the magnetic fluid seals for rotary shafts working in water," *Polish Maritime Research*, vol. 14, no. 4, pp. 53–58, 2007.

[27] R. Rosensweig, *Ferrohydrodynamics*. Dover Publications, 5 1998.

[28] Z. Wang, C. Holm, and H. W. Müller, "Molecular dynamics study on the equilibrium magnetization properties and structure of ferrofluids," *Physical Review E*, vol. 66, no. 2, p. 021405, 2002.

[29] B. Huke and M. Lücke, "Magnetization of ferrofluids with dipolar interactions: A born-mayer expansion," *Physical Review E*, vol. 62, no. 5, p. 6875, 2000.

[30] M. Lopez-Lopez, F. Nogueras-Lara, L. Rodriguez-Arco, N. Guigo, N. Sbirrazzuoli, A. Y. Zubarev, S. Lacis, and P. Kuzhir, "Kinetics of doublet formation in bicomponent magnetic suspensions: The role of the magnetic permeability anisotropy," *Physical Review E*, vol. 96, no. 6, p. 062604, 2017.

[31] M. Cowley and R. E. Rosensweig, "The interfacial stability of a ferromagnetic fluid," *Journal of Fluid mechanics*, vol. 30, no. 4, pp. 671–688, 1967.

[32] M. Petit, A. Kedous-Lebouc, Y. Avenas, M. Tawk, and E. Artega, "Calculation and analysis of local magnetic forces in ferrofluids," *Przeglad Elektrotechniczny (Electrical Review)*, vol. 87, no. 115, p. 119, 2011.

[33] R. E. Rosensweig, "Magnetic fluids," *Annual review of fluid mechanics*, vol. 19, no. 1, pp. 437–461, 1987.

[34] G. S. Park and S. H. Park, "Determination of the curvature of the magnetic fluid under the external forces," *IEEE transactions on magnetics*, vol. 38, no. 2, pp. 957–960, 2002.

[35] R. Perez-Castillejos, J. Plaza, J. Esteve, P. Losantos, M. Acero, C. Cané, and F. Serra-Mestres, "The use of ferrofluids in micromechanics," *Sensors and Actuators A: Physical*, vol. 84, no. 1-2, pp. 176–180, 2000.

[36] M. Perry and T. Jones, "Hydrostatic loading of magnetic liquid seals," *IEEE Transactions on magnetics*, vol. 12, no. 6, pp. 798–800, 1976.

[37] D. C. Li, H. N. Zhang, and Z. L. Zhang, "Study on magnetic fluid static seal of large gap," in *Key Engineering Materials*, vol. 512, pp. 1448–1454, Trans Tech Publ, 2012.

[38] R. Ravaud, G. Lemarquand, and V. Lemarquand, "Mechanical properties of ferrofluid applications: centering effect and capacity of a seal," *Tribology International*, vol. 43, no. 1, pp. 76–82, 2010.

[39] Z. Jibin and L. Yongping, "Numerical calculations for ferrofluid seals," *IEEE transactions on magnetics*, vol. 28, no. 6, pp. 3367–3371, 1992.

[40] M. Szczęch, "Experimental study on the pressure distribution mechanism among stages of the magnetic fluid seal," *IEEE Transactions on Magnetics*, vol. 54, no. 6, pp. 1–7, 2018.

[41] V. Polevikov and L. Tobiska, "Influence of diffusion of magnetic particles on stability of a static magnetic fluid seal under the action of external pressure drop," *Communications in Nonlinear Science and Numerical Simulation*, vol. 16, no. 10, pp. 4021–4027, 2011.

[42] Y. Mitamura, T. Yano, W. Nakamura, and E. Okamoto, "A magnetic fluid seal for rotary blood pumps: Behaviors of magnetic fluids in a magnetic fluid seal," *Bio-medical materials and engineering*, vol. 23, no. 1-2, pp. 63–74, 2013.

[43] D. L. Hujun Wang, "Effect of the seal gap on the seal life when sealing liquids with magnetic fluid," *Revista de la Facultad de Ingenieria U.C.V.*, vol. 31, no. 12, pp. 83–88, 2016.

[44] J. Bonvouloir, "Experimental study of high speed sealing capability of single stage ferrofluidic seals," *Journal of tribology*, vol. 119, 1997.

[45] J. Singh and R. Bajaj, "Parametric modulation in the taylor–couette ferrofluid flow," *Fluid dynamics research*, vol. 40, no. 10, p. 737, 2008.

[46] P. J. Stiles and M. Kagan, "The influence of particle diffusion on couette–taylor instability of a radially magnetized ferrofluid," *Journal of colloid and interface science*, vol. 179, no. 2, pp. 628–630, 1996.

[47] P. Stiles and P. Blennerhassett, "Stability of cylindrical couette flow of a radially magnetized ferrofluid in a radial temperature gradient," *Journal of magnetism and magnetic materials*, vol. 122, no. 1-3, pp. 207–209, 1993.

[48] M. Niklas, "Influence of magnetic fields on taylor vortex formation in magnetic fluids," *Zeitschrift für Physik B Condensed Matter*, vol. 68, no. 4, pp. 493–501, 1987.

[49] H. Kikura, M. Aritomi, and Y. Takeda, "Velocity measurement on taylor–couette flow of a magnetic fluid with small aspect ratio," *Journal of magnetism and magnetic materials*, vol. 289, pp. 342–345, 2005.

[50] H. Kikura, Y. Takeda, and F. Durst, "Velocity profile measurement of the taylor vortex flow of a magnetic fluid using the ultrasonic doppler method," *Experiments in Fluids*, vol. 26, no. 3, pp. 208–214, 1999.

[51] M. Reindl and S. Odenbach, "Influence of a homogeneous axial magnetic field on taylor–couette flow of ferrofluids with low particle–particle interaction," *Experiments in Fluids*, vol. 50, no. 2, pp. 375–384, 2011.

[52] K. Sekine, Y. Mitamura, S. Murabayashi, I. Nishimura, R. Yozu, and D.-W. Kim, "Development of a magnetic fluid shaft seal for an axial-flow blood pump," *Artificial organs*, vol. 27, no. 10, pp. 892–896, 2003.

[53] H. Wang, D. Li, X. He, and Z. Li, "Performance of the ferrofluid seal with gas isolation device for sealing liquids," *International Journal of Applied Electromagnetics and Mechanics*, no. Preprint, pp. 1–16, 2018.

[54] W. Ochonski, "New designs of magnetic fluid exclusion seals for rolling bearings," *Industrial Lubrication and Tribology*, vol. 57, no. 3, pp. 107–115, 2005.

[55] J. R. Melcher, "Field-coupled surface waves. comparative study of surface-coupled electrohydrodynamic and magnetohydrodynamic systems," 1963.

[56] L. D. Flansburg and N. Hershkowitz, "Magnetism in austenitic stainless steels," *Journal of Applied Physics*, vol. 41, no. 10, pp. 4082–4086, 1970.

[57] O. V. Kharissova, H. R. Dias, B. I. Kharisov, B. O. Pérez, and V. M. J. Pérez, "The greener synthesis of nanoparticles," *Trends in biotechnology*, vol. 31, no. 4, pp. 240–248, 2013.

[58] B. A. Bolto, "Magnetic particle technology for wastewater treatment," *Waste management*, vol. 10, no. 1, pp. 11–21, 1990.

[59] P. Xu, G. M. Zeng, D. L. Huang, C. L. Feng, S. Hu, M. H. Zhao, C. Lai, Z. Wei, C. Huang, G. X. Xie, *et al.*, "Use of iron oxide nanomaterials in wastewater treatment: a review," *Science of the total environment*, vol. 424, pp. 1–10, 2012.

[60] A. K. Gupta and M. Gupta, "Synthesis and surface engineering of iron oxide nanoparticles for biomedical applications," *biomaterials*, vol. 26, no. 18, pp. 3995–4021, 2005.

[61] C. Nadejde, M. Neamtu, and D. Creanga, "Environment-friendly magnetic fluids for wastewater remediation-synthesis and characterization," *Acta Phys. Pol. A*, vol. 2, no. 127, pp. 647–649, 2015.

[62] C.-L. Chun and J.-W. Park, "Oil spill remediation using magnetic separation," *Journal of environmental engineering*, vol. 127, no. 5, pp. 443–449, 2001.

[63] A. Atta, H. Al-Lohedan, and S. Al-Hussain, "Functionalization of magnetite nanoparticles as oil spill collector," *International journal of molecular sciences*, vol. 16, no. 4, pp. 6911–6931, 2015.

[64] L. Matuszewski, "Multi-stage magnetic-fluid seals for operating in water–life test procedure, test stand and research results: Part i life test procedure, test stand and instrumentation," *Polish Maritime Research*, vol. 19, no. 4, pp. 62–70, 2012.

[65] L. Matuszewski, "Multi-stage magnetic-fluid seals for operating in water–life test procedure, test stand and research results," *Polish Maritime Research*, vol. 20, no. 1, pp. 39–47, 2013.

[66] H. Tamama, Y. Ozawa, J. Miyazaki, H. Ito, and T. Kinoshita, "Device for sealing a propeller shaft against invasion of sea water," Mar. 13 1984. US Patent 4,436,313.

[67] Y. Mitamura, S. Takahashi, S. Amari, E. Okamoto, S. Murabayashi, and I. Nishimura, "A magnetic fluid seal for rotary blood pumps: effects of seal structure on long-term performance in liquid," *Journal of Artificial Organs*, vol. 14, no. 1, pp. 23–30, 2011.

[68] F. D. Ezekiel, "Magnetic liquid shaft sealing," Oct. 6 1981. US Patent 4,293,137.

[69] R. Moskowitz, P. Stahl, and W. R. Reed, "Dynamic lip seal using ferrofluids as sealant/lubricant," Oct. 23 1979. US Patent 4,171,818.

[70] R. Ehmsen, U. Fruedenberg, F. Heck, and R. Vogt, "Ferrofluid seal for a shaft," Mar. 3 1992. US Patent 5,092,611.

[71] K. Raj and R. Casciari, "Single-pole-piece ferrofluid seal apparatus and exclusion seal system," Oct. 4 1983. US Patent 4,407,508.

[72] H. L. Gowda and K. Raj, "Ferrofluid linear seal apparatus," Mar. 5 1985. US Patent 4,502,700.

[73] K. Raj and R. Casciari, "Bearing assembly with integrated ferrofluid seal," Sept. 8 1987. US Patent 4,692,826.